UNIVERSITY OF SOUTHAMPTON

FACULTY OF SCIENCE

DEPARTMENT OF PHYSICS

A DIGITAL LASER SLOPEMETER

by

Grant James Crossingham

A thesis submitted for the degree of Doctor of Philosophy

April 2000

UNIVERSITY OF SOUTHAMPTON

ABSTRACT

FACULTY OF SCIENCE

PHYSICS

Doctor of Philosophy

A DIGITAL LASER SLOPEMETER

by Grant James Crossingham

This thesis is concerned with the design of a new ocean going instrument to measure the local sea surface profile. The motivation behind this project was the need to investigate oceanographic features that have been observed using imaging radar aboard aircraft and satellites. The measurements made with this instrument will further the understanding of the processes involved in radar backscatter from the ocean surface and will enable further analysis of ocean phenomena detected using imaging radars. With an improved understanding of these processes it will be possible to analyse quantitatively satellite images generated from around the globe. This will allow global environmental monitoring which could lead to improved weather forecasting, pollution control such as oil slick monitoring and surface and subsurface operations.

It is believed that radar signals having a wavelength of 10 to 300mm are backscattered from waves on the ocean surface of similar length. Earlier attempts to measure waves including those designed to measure millimetric waves are critically reviewed and an account of the evolution of the design of a new instrument to measure these small waves is presented. This new instrument has been tested in the laboratory, which has demonstrated that a repeatable wave slope measurement accuracy of $\pm 0.56°$ has been achieved in static tests. Dynamic tests made using a wave tank have generated a wave slope profile, clearly showing 10mm wavelengths present on the surface.

The new Digital Slopemeter is designed to measure the small-scale sea surface roughness for wavelengths in the range 10mm to 224mm. This instrument uses two grids of wavelength shifting fibres to digitally record the slope of a refracted laser beam. The laser beam is rapidly scanned over the sea surface to ensure that the profile of the surface is effectively stationary over a length of 224mm. The wave slope is sampled at 3.5mm intervals along each scan, allowing 7mm wavelengths to be resolved. This efficient measurement of the sea surface roughness enables a real-time display of the data collected. The design of the instrument permits it to be deployed from the bow of a research vessel in moderate seas. This instrument is therefore simple and flexible to deploy.

Contents

Acknowledgements

I would like to thank my Mum and Dad for their continuous support for everything I have ever achieved. Thankyou!

Dr David Ramsden has provide support, guidance and a continuous flow of ideas throughout the period of this project and I am thankful for all his help. Without his support this project would not of been completed successfully. I'd also like to thank members of the TLS project team, Dr Harbie Ghataure, and Prof Ian Robinson for there help and guidance during of my PhD. Special thanks must go to John Willoughby for hours of discussions concerning the project and life in general and for putting up with me in the office while I have been writing up this thesis. I would also like to thank him and Luisa Morales Rueda for there friendship and for proof reading my thesis! I would also like to thank everyone in the detector physics group with whom I have spent many hour both working with.

I would like to thank Graham Chadwick for his help and friendship while I have been at Southampton. I would also like thank him and Rob Evans for joining me on a cycle from Lands End to John O'Groats in appalling conditions. In fact I would like to thank all my friends in the Department of Physics and Astronomy who have made my time at Southampton great fun. Special thanks must go to the members of the Xtreme Division of the Astronomy Group, Ian Jupp, Anthony Lawson, Graham Chadwick and Rob Evans, for joining in many events including a parachute jumps, hang gliding, cycling and wind surfing. Special thanks to Ian Jupp for suffering the cold Solent waters on many wind surfing days and to Helen Jupp for feeding me when I was a poor student.

I would like to thank all my friends in the Hang gliding Community that have helped me stay sane during the period of my PhD, especially those in the Sky Surfing Club and Southampton University Club. Finally I would like to thank everybody who has contributed to the completion of my work at Southampton.

Chapter 1
Introduction

1.1. Thesis Outline

This thesis is concerned with the development of an instrument designed to be deployed on the bow of a research vessel to measure the sea surface roughness. The aim is to provide information on the shape of the sea surface for wavelengths between 10 and 300mm. The significance of this range of wavelengths will become clear during this chapter which outlines the scientific motivation for the development of this instrument. Chapter 2 presents a critical review of some previous attempts to measure the sea surface and discusses the limitations of these instruments. A critical review of the Towed Laser Slopemeter, which was designed and deployed by the University of Southampton, is present in chapter 3. The author was involved in severl deployments of this instrument. This provided invaluable experience for the development of the new Digital Slopemeter. The remainder of the work related to the development of this Digital Slopemeter, with the exception of the real-time software, is original research carried out by the author. Chapter 4 describes the problem associated with measuring a sea surface wave spectrum and introduces a possible solution, which involves a submersed laser scanning system design. The design of a new detector that allows the concepts developed in chapter 4 to be implemented follows in chapter 5. The readout and control electronics required from the new instrument are described in chapter 6, and chapter 7 describes the mechanical aspects of the system and presents the results demonstrating the initial performance of the detector. The affect of the wave curvature on the laser beam diameter is investigated in chapter 8 and results showing a measured wave slope profile of the water surface in a wave tank are presented. Also presented in this chapter are the preliminary laboratory measurements of small-scale water waves. Finally, chapter 9 suggests further work that is required before the initial deployments of the instrument at sea and provides a description of additional instrumentation that would be required in a field operation.

1.2. Motivation for Research

Measurements of ocean currents, depths, temperatures and wild life where often made by ships on navigational voyages [McConnell, 1981]. However, it has become increasingly important to understand the ocean surface whose energy, ships and ocean structures have to withstand. For over 150 years, ships navigating the oceans have been reporting wave heights they have encountered [Kinsman, 1965, P9-22]. However it is only in the past half a century that more comprehensive studies have been made. The incentive for this has been an interest in the predicting and understanding the nature of ocean waves, by off shore operations such as the oil industry and the Navy [Verboom 1980, Pitt et. al. 1980, Russell 1963]. It is also important to be able to predict waves for coastal protection. In these cases it is the larger amplitude waves that carry the majority of the energy that are of most interest. However, the transfer of energy from the wind to the ocean surface is via much shorter waves with millimetre wavelengths.

The roughness of the ocean surface depends primarily on the wind. When a wind starts blowing over a completely calm sea the friction between the air and the sea generates very small capillary waves with millimetre wavelengths that are relatively quick to react to changes in wind velocity. The restoring force for these waves is primarily the water surface tension and they soon abate with a decline in the wind speed. As the wind continues to blow, energy from these waves is transferred to longer wavelengths [Kinsman, 1965, P6-22]. When the wavelengths become greater than a few centimetres the dominant restoring force is gravity and these waves are then known as gravity waves. Once the wind abates these waves may continue for some time and large gravity waves can travel vast distances before breaking on a coastline or any other structure in their path. If the wind continues to blow, more and more energy is transferred to the sea surface and eventually the energy of the waves is dissipated through breaking. This often occurs when the waves become too steep causing the tops of the waves to collapse which is also aided by the wind blowing the tops of the waves off. This complex wind water interaction is not well understood because of its non-linear nature. In an attempt to understand this process it is imperative that these capillary waves are measured with respect to the wind speed and longer ocean waves.

The main incentive, however, for measuring the small-scale surface roughness was the use of remote sensing instruments to study the ocean surface. Radar uses electromagnetic waves scattered off the sea surface to generate an image. It is generally assumed that the mechanism involved in the backscatter of radar from the sea-surface is resonant Bragg scattering, as shown in Figure 1. 1 [Macdonald 1963, Vesecky et. al. 1982, Robinson I. 1985]. This implies that microwave radiation will be scattered from ocean waves of similar wavelength to that of the light used, which is generally between 10mm and 300mm (30GHz to 1GHz). The backscatter of

radiation from the sea surface was first noticed during the Second World War as it caused noise in the radar signal. Consequently, its study was motivated by the military. Initially ground based radars were used to retrieve information about sea surface [Macdonald 1963]. However, when radar instruments were flown on satellites, large areas of the sea surface could be imaged in a relatively short time. The first satellite specifically designed for oceanographic use was SEASAT. This was launched in 1978 and was active for only 100 days but in this short time it returned a sufficient amount of radar data to show the usefulness of satellite oceanography.

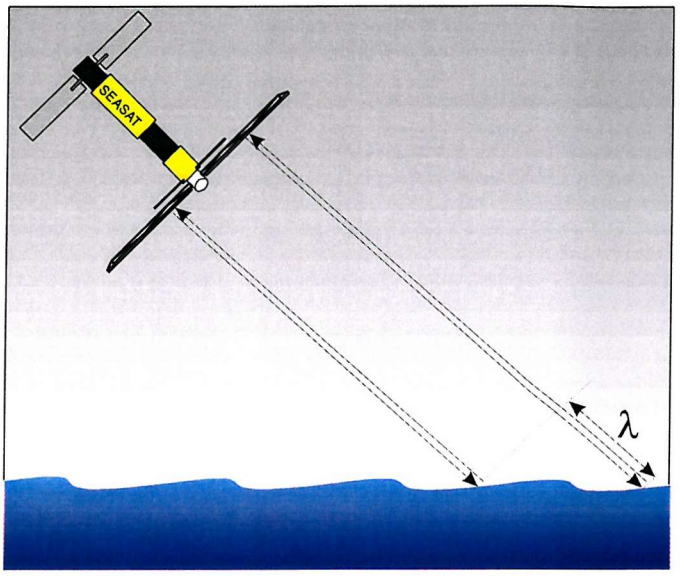

Figure 1. 1. A simplified view of Bragg scattering by the sea surface.

From the images returned from the synthetic aperture radar (SAR) aboard SEASAT it was clear that the waves from which the radar was being scattered where modulated by a great many ocean processes. Features such as swell waves, internal waves (Figure 1. 2), surface slicks (Figure 1. 3), surface currents (Figure 1. 4), wind and rain (Figure 1. 5), and bottom topography (Figure 1. 6) can clearly be seen. Swell waves and internal waves affect surface and subsurface operations. Consequently, it would be useful if a quantitative measure of these waves could be provided over a global scale. The Norwegian Pollution Control Authority used both satellite and airborne SARs to monitor pollution off the coast of Norway [Pedersen et. al.]. At low wind speeds, false alarms may be caused by natural oil seepage leaking from the seabed. At high wind speeds slicks may have no additional affect on the surface because waves modulated by the slick are already saturated in their intensity by the strong winds. So again a quantitative measure of the surface roughness from satellite images would be useful. The identification of surface currents has various applications, such as associating surface current eddies with regions that have a high abundance of fish larvae [ASF]. It has also been used to track the movement of the Gulfstream,

which may affect both fisheries and shipping, in addition to the European weather [Vesecky et. al. 1982]. The modulation of the surface roughness by the interaction of ocean currents with the bottom topography may allow bathymetry mapping of coastal zones by satellite SAR [Gommenginger C. 1998]. The radar backscatter is affected by wind driven waves, consequently, there is a correlation between the wind speed and the intensity of this backscatter. In Figure 1. 5 gust fronts from a storm can clearly be identified [Melsheimer C. et al. 1998].

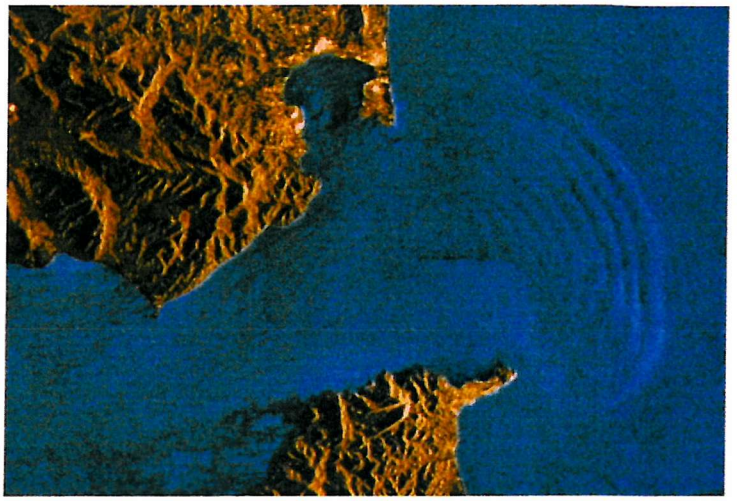

Figure 1. 2. ERS-1 SAR image of the Strait of Gibraltar showing internal waves propagating into the Mediterranean. These waves have been generate by the flow of water from the Atlantic Ocean into the Mediterranean ocean.

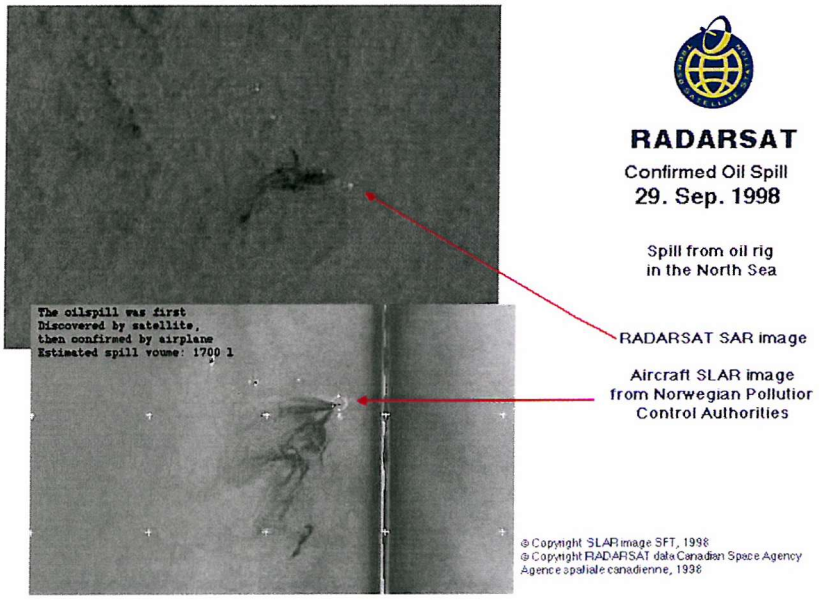

Figure 1. 3. An oilslick observed by SAR instruments in the North Sea. [Tromso Satellite Station AS, Tromso, Norway]

Figure 1. 4. Image showing a surface current eddy in the Bering Sea, which is a region of high abundance of walleye pollock larvae. [ASF ERS-1 SAR: Image 20994200]

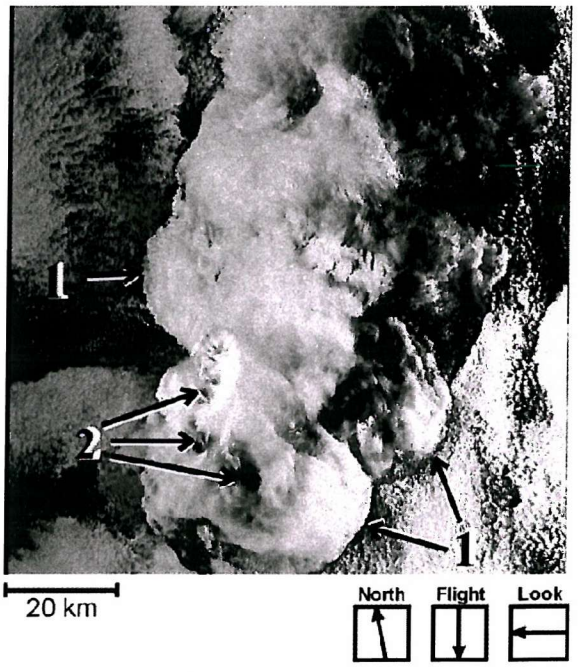

Figure 1. 5. SAR image of the Gulf of Thailand during a rain storm [Melsheimer C. et al. 1998]. (1) Gust fronts that are caused by building cumulus nimbus cloud have caused an increase in sea surface roughness. (2) Precipitation from these clouds damping out the waves that are scattering the radar.

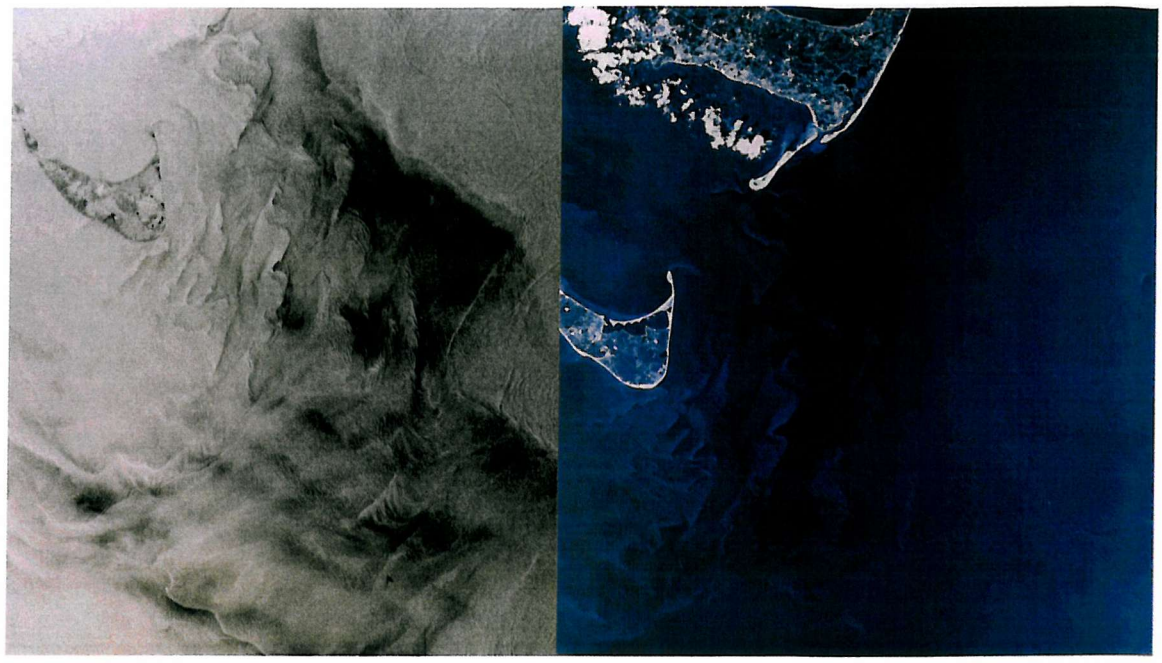

Figure 1. 6. (*Left*) Seasat L-band SAR image of the ocean near Nantucket Island, showing bathymetric signatures, upwelling, and internal waves. (*Right*) Skylab photograph of the same region made several years before, showing white shoal regions that match the bathymetry and SAR backscatter variations very accurately. [From NASA Technical Memorandum 4679]

There was also a scatterometer aboard SEASAT, which is an instrument specifically design to estimate the wind speeds and directions from the radar backscatter [Jones et. al. 1982]. This instrument is ideal for monitoring surface winds globally in order to aid weather predictions and for monitoring wave conditions. This is useful in planning marine operations, such as fishing, rescue operations, oil rig operations and navel exercises. An example of the data collected by NSCAT, a scatterometer aboard the Japan's Advanced Earth Observing Satellite (ADEOS-II) that flew in 1996, is shown in Figure 1. 7. This image shows the surface wind velocity in the vicinity of Typhoon Violet superimposed on an infrared image of the cloud formation in the area.

It is clear that satellite SAR images and wind measurements by the Scatterometers are of great use and have consequently been deployed on various other satellites since SEASATs operation. Radar also has the advantage that it can be used day or night regardless of cloud cover. This has provided an incentive to obtain a much greater understanding of how the radar interacts with the sea-surface which in turn required a better understanding of the sea-surface itself. It is therefore

imperative that detailed in-situ measurements are made, not only to increase the understanding of radar backscatter but also to study further the ocean processes that have been observed.

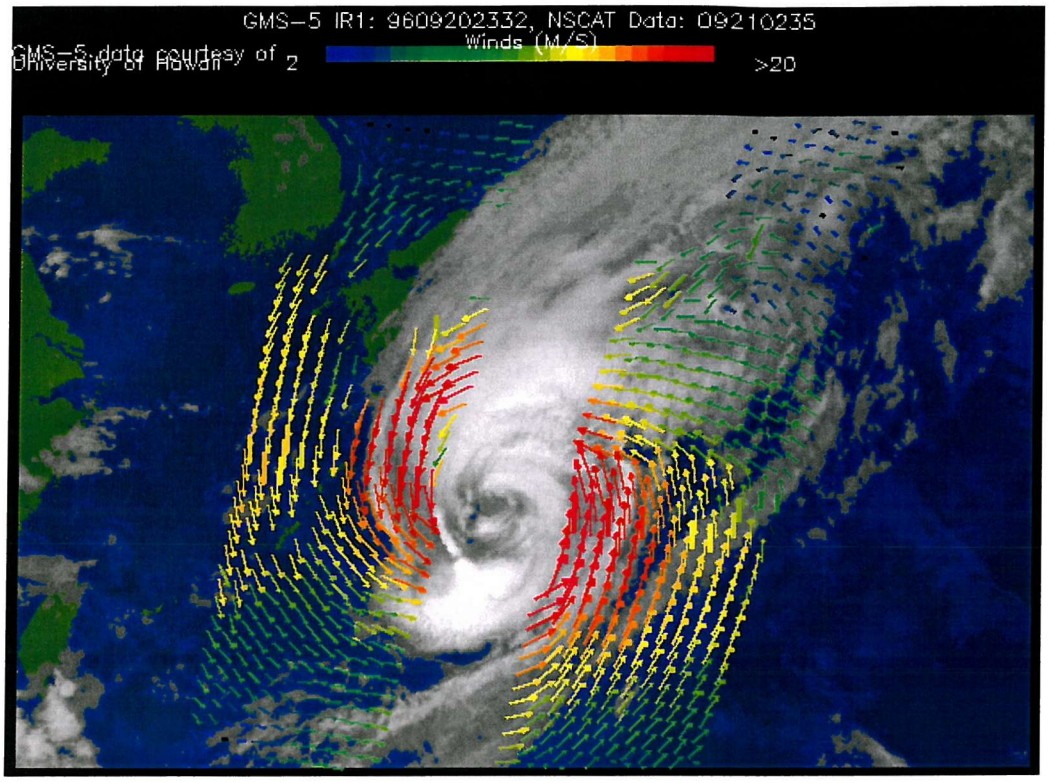

Figure 1. 7. The surface wind velocity in the vicinity of Typhoon Violet measure by NSCAT superimposed onto an infrared cloud cover image. [Winds, Scatterometry, JPL and NASA web site]

Chapter 2
Techniques for Measuring Ocean Waves

2.1 Introduction

This chapter provides a brief description of techniques that have been used to measure the sea surface roughness. It also discusses the need for further instrument developments in order to measure wavelengths in the range 10mm to 300mm. The ocean has a complex surface consisting of many different length waves each with different velocities and phases so that the surface changes in both space and time. In order to measure any particular range of wavelengths, an area large enough to include the longest waves of interest must be studied and this area must be sampled with fine enough resolution to record the shortest waves of interest. Alternatively, the frequency at which waves pass a point can be studied, although maintaining an instrument stationary relative to a mass of water on which the waves are travelling is difficult. Several different types of instrument have been designed to measure waves on a water surface. This chapter will consider whether these techniques could be applied to the wavelength range of interest.

2.2. Measuring Techniques

In general, instruments are designed to measure either the wave height or the wave slope of the sea surface. Both these measurements will be considered and the techniques that have been deployed to make them. Instruments for measuring the sea surface can be broadly separated into two, those that disturb the surface while making a measurement and those that do not. If small waves are to be measured, it is preferable to use a technique that does not disturb the surface in the process. However we shall consider all the possible techniques here, starting with those that disturb the surface while making the measurement.

2.2.1. Invasive Techniques

Perhaps the simplest of methods that can be used to measure wave heights involves placing electrodes at regular intervals on a staff placed vertically in the water. When each electrode is submersed, the water completes a circuit between the electrode and a wire that runs parallel to the staff. This will indicate the level of the water up the staff. This method was used by Russell [1963] to investigate the forces exerted on offshore structures by ocean waves. The advantage of this measurement technique is that is can measure very large wave heights. On certain off shore structures the staff described by Russell [1963] was up to 18m long. The distance between the electrodes on the staff was a few tens of centimetres, which limits the wave height resolution. To measure smaller waves the distance between the electrodes would have to be reduced and to ensure the waves being measured are not significantly distorted, the overall dimensions of the staff would have to be reduced as well.

A better instrument for measuring smaller waves would be a wire wave gauge. These can measure the position of the water continuously along their length and have a width of less than 1mm. They use the changes in the electrical characteristics of the wire when their submersed length varies, to determine the height of the water surface. Several different circuits have been used for this purpose, two of which are shown in Figure 2. 1. Circuit a) is a bare resistive wire that is part of a circuit in which a constant oscillating current signal is passed. The ground of the circuit is placed in the water so that the conductive length of the wire depends on the height of the water level. As the water level moves up the wire its resistance length decreases and consequently so does the amplitude of the oscillating voltage across it [Farmer 1963, Lobemeier 1981].

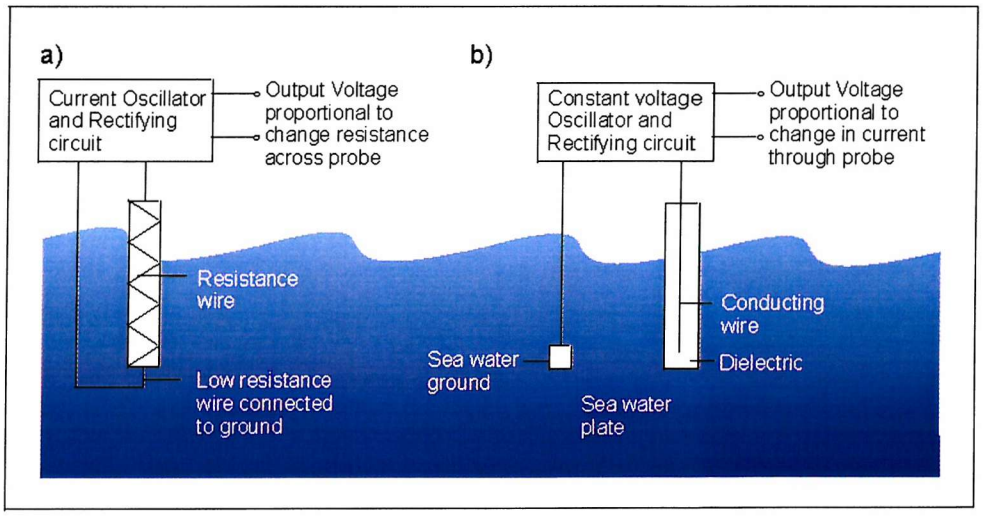

Figure 2. 1. Two types of wire wave-gauge, a) a resistive wire probe, b) a capacitive wire probe [Kinsman 1965].

The second circuit, Figure 2. 1 b), consists of a wire surrounded by a dielectric which again is partly submerged into the sea. The seawater and the wire are isolated by the dielectric so they act as a capacitor whose value depends on the height of the water surface. A square oscillating constant voltage signal is passed through the circuit. As the capacitance of the probe changes the current that flows changes. This current is then converted into a voltage using a transformer and rectifying circuit and this voltage is proportional to the height of the water surface up the probe [Mcgoldrick 1971].

These probes have to pass through the surface of the wave and in doing so distort the surface being measured. This results in the probes having a minimum wavelength resolution. Sturm et al [1973] suggested two effects that limited the frequency response of a wire wave-gauge. The first is the wetting characteristic of the probe, which prevents the probe from responding rapidly to changes in water level. The second effect is the meniscus that forms around the probe. This increases the effective diameter of the probe and reduces the probes sensitivity to small wavelengths. Sturm et al [1973] measured the wave height of sinusoidal waves generated in a wave tank. The wave heights were also inferred from the wave slopes that were measured by a laser slopemeter. In addition, the amplitude of this wave was accurately measured to verify that the laser slopemeter was reading correctly. Using theses two instruments, capillary waves were measured. The results showed that for wavelengths less than 7cm, the wave amplitudes measured by the wire probe were less than 90% of those measured by the laser slopemeter and they decreased further with decreasing wavelength. Lange et. al. [1982] has also shown that a wire probe does not measure waves with the same sensitivity as a laser slopemeter. They assumed the linear dispersion relationship for the waves in order to calculate the wave heights from the measured wave slopes so that they could compare them with the wave heights measured with the wire probe. Hence this was not a comparison of purely experimentally acquired data.

A comprehensive comparison was performed by Liu et al [1982]. The performance of different diameter wire wave gauges was compared with a laboratory based optical instrument that used a camera to measure the height of the water surface directly, as opposed to inferring it from a measurement of the wave slope. The camera imaged the position of the laser beam spot on the air-water interface. This instrument required calibrating so that the position of the spot could be related to an accurately known surface height. With this instrument, Liu et al [1982], showed that surface height was significantly distorted for wave height frequencies > 7Hz. This corresponds to approximately a 2cm wave. Previously, Lobemeier [1981] had claimed that his wire wave gauge could measure waves with an amplitude frequency of at least 50Hz. The waves that were measured by Liu et al [1982] were wind driven and it has been suggested that Lobemeier's [1981] claim was most probably due to the idealistic conditions under which his

probe was tested. Due to the presence of the meniscus that forms around the probe, it appears there is a inherent limit to the wavelength that it is possible to measure with a wire wave gauge.

2.2.2. Non-invasive Non-optical Techniques

It is possible to measure the height of a wave by measuring the pressure fluctuation below the water surface [Tucker 1963, Barber 1956]. As waves on the surface pass over a sensor placed on the seabed, the pressure that is recorded will increase with increasing water height. The pressure fluctuation caused by the wave decreases exponentially with the depth of the sensor [Tucker 1956]. Therefore, in order to make a measurement, the heights of the waves must be comparable to the depth of the sensor below the surface. This type of device will therefore only generate good results in shallow water and even then the pressure changes caused by the small wave amplitudes will be insignificant compared to those of the larger ones. Tucker [1956] describes a pressure sensor deployed on a boat to measure wave heights in open water. This sensor has been used by The Institute of Oceanographic Sciences to study waves around the coast of the United Kingdom [Pitt et. al. 1980]. It was a practical, low cost instrument, although deployments where limited to available ships such as the light ships that are permanently moored. Waves are reflected from the boat causing this instrument to have a limited wave height sensitivity. This effect was largely removed for large waves by placing pressure sensors on opposite sides of the vessel. As an alternative to Tuckers method of deploying the pressure sensors, placing the pressure sensor on a submerged vehicle might be considered. However, to ensure that the surface is not affected significantly, the submersible would have to be at a depth of at least 5 times it's outer dimensions, which greatly reduces the effectiveness of the sensor [Allmendinger E. E. 1990].

Munk suggested the use of an array of upward facing echo sounders mounted to the upper surface of a submarine to detect the height of the sea surface above it [Macovsky et al., 1963]. The Hydrographic Office used this technique to measure the power spectra of surface waves [De Leonibus 1963]. This technique was limited in wave amplitude resolution to the nearest 30cm because of the finite ultrasonic pulse angle used, of 3 degrees. This generates a footprint on the surface of approximately 160cm that effectively averages the surface height over this area. Therefore, neither pressure sensors nor echo sounders can be used to measure small-scale surface roughness although they are useful for larger scale wave monitoring purposes.

In fact recording the amplitude of a wave is not an ideal method of recording small amplitude waves, because on the ocean surface these waves may be riding on much larger amplitude waves. This consequently requires an instrument with a large amplitude range. Alternatively,

the slope of the sea surface may be measured using light and in principle the wave slopes that are measured from any wavelength wave would lie in a similar range.

2.2.3. Optical Reflection Techniques

As light passes the air-sea interface, the change in refractive index causes it to either reflect or refract to a degree that depends on the wave slope at that point. Therefore, measurement techniques may be divided into those that use reflection and those that use refraction.

The main advantage with any reflection technique is that the instrument can be kept above the sea surface. Therefore, the reflected light can be detected without the surface being disturbed. Although, the sea surface is a specula reflector of light, other processes also take place such as, transmission and scattering of light within the ocean. Stilwell Photograghy probably suffers from the most problems and is therefore the least convincing technique [Stilwell 1969]. It demonstrates many of the problems associated with making measurements of the sea surface shape using reflection. This method was first described by Stilwell in 1969, who used it to analyse a photograph taken from a bridge across the Anacostia River in Washington. If the sea is evenly illuminated by a homogenous extended light source then light will be reflected from all points on the surface. The intensity of the reflected light will depend on the coefficient of reflection that varies with the surface slope. If the surface is viewed from above it is not possible to determine whether the wave slope is positive or negative from the intensity of the reflected light alone. This is not the case if the sea surface is viewed from an angle, more light is reflected in the direction of the camera if the surface is sloped towards it. However, the wave direction still cannot completely be determined unambiguously for all directions. For example, the intensity of light reflected towards the camera from a wave, with its crests and troughs aligned parallel to the viewing angle, would be identical for both positive and negative wave slopes. Waves travelling towards or away from the camera would have a coefficient of reflection that varies continuously, although not linearly. In fact the brightness of light reflected from slopes that fall away from the camera can be up 50 times less than from slopes that fall towards the camera [Jahne et al. 1992].

In addition to this highly non-linear change, the reflection intensity will also depend on variations in the sky illumination. Even on a completely overcast day there will be variation in light levels across the sky and it is exceedingly difficult to generate an artificial extended light source, especially when larger areas of the sea have to be illuminated. Both the light that has been transmitted into the sea and scattered back towards the surface, and the light that has had multiple reflections will increase the intensity of light emitted towards the camera. Therefore,

there are several inherent sources of error in this technique of measuring the shape of the sea surface.

Churnside et al., [1995] have suggested a method for measuring the sea surface slope using light backscattered from particles that are suspended in the water. The transmission of light through the air-water interface depends on the angle that the light is incident with the surface. The ratio of light polarised in two orthogonal directions may be related to the surface slope regardless of the intensity of the incident light. However, this method suffers from the same sort of problems as Stilwell photography, with an added limitation. The image of the surface with the two separate polarisations must be taken before the surface moves significantly, consequently the speed of the CCD camera used, limits the waves that can be effectively viewed. It is, therefore, unlikely that this technique would be used at sea where the wavelength range can not be limited.

By illuminating the sea surface with a point light source specula reflections from the sea surface can be used to determine the wave slope at the point where the reflection occurs. Information about the intensity of the light reflected is not required and therefore the problems associated with this are not encountered with this technique. Provided the position of the point source and the camera are known, the angle of each facet reflecting can be ascertained, as shown in Figure 2. 2. This technique is known a glitter photography and was first reported on by Cox and Munk in 1954 using the sun as the point source [Cox and Munk 1954].

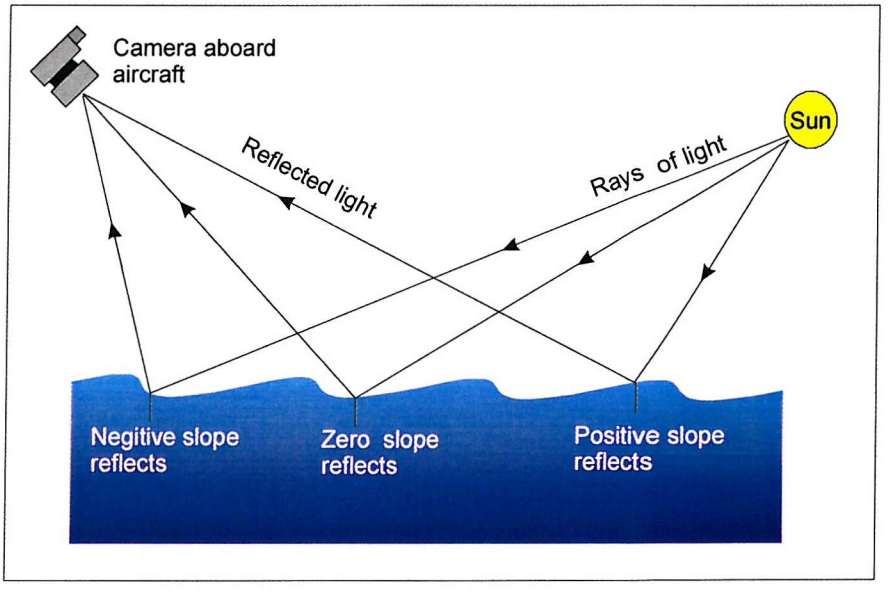

Figure 2. 2. The geometry used for sun glitter photography.

This technique will generate wave slope probability distributions from an area of the sea surface. A large area of the surface must be used or alternatively several photographs of a smaller areas

in order to obtain good statistics. An example of one such probability distribution generated by Cox and Munk is shown in Figure 2. 3. This data was generated from photographs of the sun's reflection off a large area of the sea surface near Monterey California, taken from an aircraft. The study conducted by Cox and Munk [1954] still remains an authoritative guide to sea surface roughness statistics due to the lack of inherent errors in the technique.

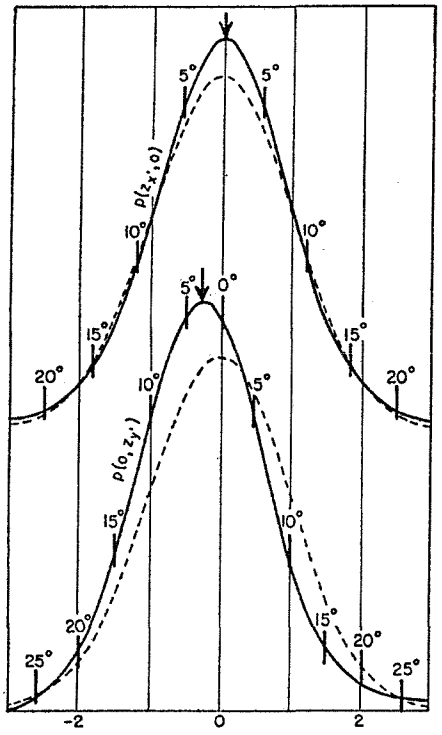

Figure 2. 3. The typical shape of a wave-slope probability distribution in a cross wind direction (*Top*) and in the same direction as the wind (*Bottom*) generated using Glitter photography by Cox and Munk [1954]. The solid line is the measured data and the dotted line is a Gaussian fit of equal mean squared wave slope component.

Shaw et al. [1996] deployed an instrument which measures the glitter from a small area of the sea surface so that the finer wave structure can be studied. This instrument is similar to one used previously in a wave tank by Wu [1971]. It measures the number of times a laser beam is reflected back from the sea surface towards a detector. By scanning the instrument through a range of angles, and counting the number of reflections obtained from each angle, wave slope statistics can be built up. This instrument uses a much more direct method of measuring specula reflection from the sea surface than that of Cox and Munk [1954]. This instrument was deployed in 1995 from floating platform moored of the Oregon coast. It generated results that

where similar to those of Cox and Munk [1954]. However, in order to study the sea surface in more detail the shape of the surface must be measured, which can not be achieved with these types of instruments.

It is possible to determine the height of a surface using stereophotography. This technique has been used by a number of investigators to retrieve wave height information from the sea surface using the parallax between two photographs taken simultaneously [Cote et al. 1960, Dobson 1970, Shemdin et al. 1988, Shemdin, Tran and Wu 1988, Waas et al. 1992]. The height of the surface can be determined by viewing the sea surface from two different angles and measuring the change in position of particular features between the two views, as shown from the geometry in Figure 2. 4.

In order to determine the height of the sea surface, corresponding points on the two images must be identified. However, when the sea surface is viewed from different directions, different facets on the sea surface reflect the light towards the camera. Therefore, features on the surface will be viewed differently in the two photographs. This has meant that stereophotography is very difficult to use on the sea surface. In the past it was also considered difficult to resolve waves over a large range of wavelengths [Jahne et al. 1992]. However, with modern CCD cameras this is now less of an issue as an image can consist of thousands by thousands of pixels as opposed to hundreds.

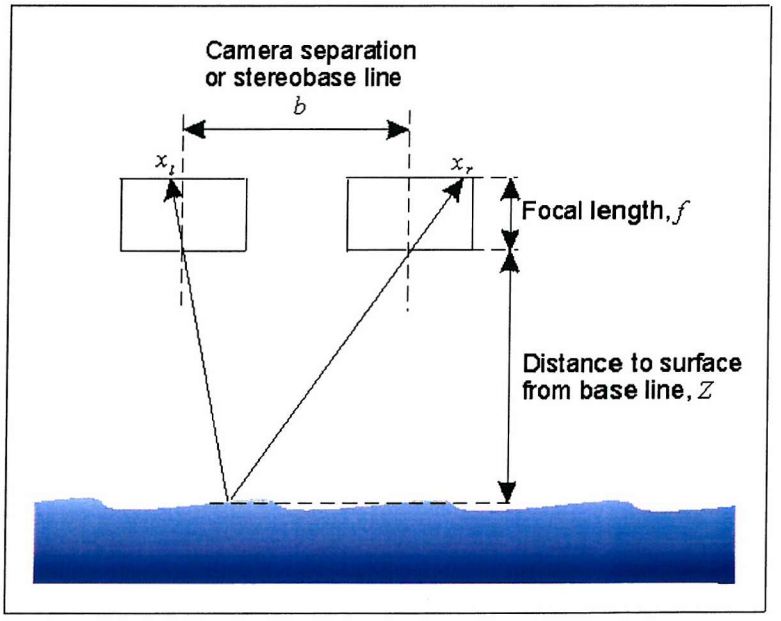

Figure 2. 4. The geometry used for stereophotography of a surface.

More recently Waas et al. [1992] has developed an instrument that uses both stereo imaging and glint imaging that solves the problem of identifying corresponding points. It involved the use of two CCD cameras that viewed the surface through polarising filters. Each camera only images light from one of two polarised point light sources that are illuminating the surface. This allowed the relative orientation of the light source and camera to be identical for both views, so that each camera views a particular facet of the sea surface with exactly the same illumination. Therefore, each light source generates a glitter pattern from the same facets on the surface. By determining the corresponding glint reflections, the height of the surface at those points can be determined. This allowed the height of larger waves over about 10cm in length to be measured. The glitter coverage and the resolution of the camera limited these height measurements. In addition to this measurement, the zero slope probability can be determined by counting the number of specula reflections occurring in the image. From this measurement the mean square slope can be estimated for these smaller waves. Therefore, information about both long and short waves can be obtained which allows their interactions to be studied. However, this technique does not provide continuous coverage over the surface and misses much information about the complete structure of the surface. It also will not record any data if the small waves causing the specula reflection are not present.

Ideally the sea surface should be mapped to give a detailed wave profile and clearly this has not been possible using reflection techniques.

2.2.4. Optical Refraction Techniques

Wave slopes are generally quite small and therefore the majority of the light incident perpendicular to the mean sea surface passes straight through, refracting according to the local surface slope. This refraction angle may be used to determine the slope of the surface. Cox [1958] first used the refraction of light to measure waves in a wind-wave tank. The experimental arrangement that he used is shown in Figure 2. 5. A diffuse light source was placed beneath a glass plate window in the bottom of the wave tank. Inside the wave tank, above the window, was placed a hollow wedge filled with inky water. The wedge was constructed so that the intensity of light that passed through it, varied linearly from one end of the wedge where it was virtually zero, to the other end where almost all the light passed through. A telescope was then focused onto a point on the water surface in the tank. The intensity of the light viewed by the telescope depended on where, on the wedge, the light had originated. This in turn determined the degree of refraction of the light at the water surface. This technique generates a single point measurement of the wave slope. More recently, the experiment has been adapted so

that a 2 dimensional representation of one component of the wave slope could be recorded by replacing the telescope with a CCD camera [Keller et al., 1983 and Jahne et al., 1990].

The main difficulty with this method is that the intensity of light is not solely dependent on its origin on the wedge. The depth of the water can also affect the intensity and measurements made on the crest of a long wave will be different from those made in the trough of the wave. Cox estimated that for high wind velocities over the wave tank, there was as much as ± 20% change in the intensity scale caused by changes in depth. In the open sea, the waves can be considerably larger than those in the wave tank, so this method is not ideal for deployment at sea.

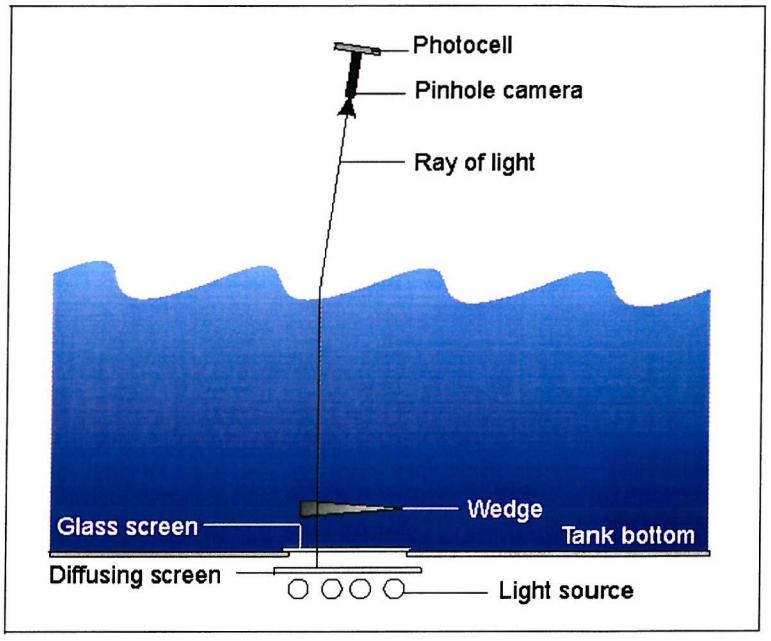

Figure 2. 5. The experimental arrangement used to measure the wave slope of wind driven waves.

In 1969, Prettyman and Cermak [1969] reported on an instrument consisting of a laser that was held approximately 3 meters above the sea surface so that the beam shone directly downwards. Below the surface and directly below the laser, a detector that consisted of a ground glass screen and a high-speed video camera was placed. The camera recorded the position that the laser was refracted to on the glass screen. This position could then be related to the wave slope provided that the height of the sea surface was also recorded. It was intended that the height of the surface would be measured using a laser, by recording the time between a light pulse being emitted and being received after reflecting from the sea surface. It was reported that this feature was not operational and so the height was assumed to remain at a constant distance of 3m from the laser. This caused an error of between 10% and 20% in the wave slopes measured.

It is apparent from this experiment that, in order to measure the slope of the sea surface accurately using a laser detector, it would be convenient to design a detector that does not require the height of the surface in order to make the measurement. Tober et al. [1973] reported on a similar instrument to that used by Prettyman and Cermak [1969] which used a lens to record the position of the laser beam once it had been refracted. The position of the laser beam on the focal plane of the lens is only dependent on the direction that the beam enters the lens from, as shown in Figure 2. 6. Consequently the position of the beam on the focal plane of the lens in uniquely related to the wave slope. To determine the beam position on the focal plane of the lens, graded filters were used as shown in Figure 2. 7. The position at which the beam passes through the filters varies its intensity. The photo-multiplier tube then measures this intensity which can be related to the slope of the laser beam.

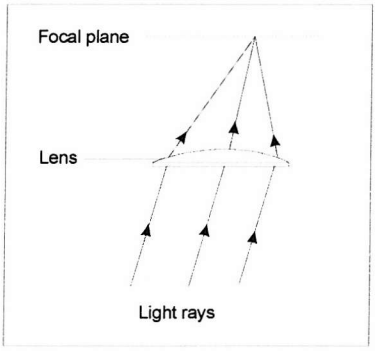

Figure 2. 6. The position of a laser beam on the focal plane of a lens is only dependent on the slope of the laser.

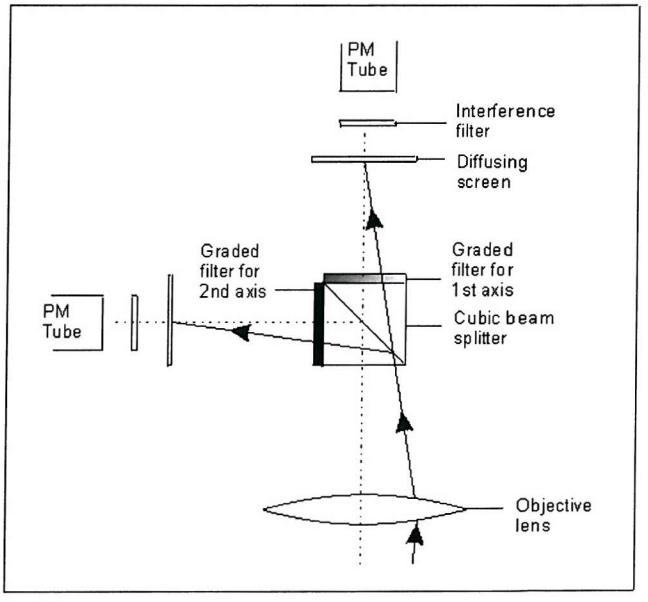

Figure 2. 7. The components of the beam position detector designed by Tober et al.

The laser beam detector designed be Tober et. al. [1973] used the same principal as that used by Cox [1958], consequently, the intensities of the beam also varied with the wave height. This was not important for the measurements that Tober et al. [1973] performed in a wave tank but as before would become important for the larger waves that would be encountered at sea. A similar instrument was deployed by Tang et al [1983] and later by Hwang et al. [1988] in the TOWARD experiment. To reduce the dependence of the instrument on wave height, it was deployed from an ocean platform on the wave follower shown in Figure 2. 8. The wave follower kept the detector at approximately the same height above the sea surface by measuring the position of the surface using a capacitance wire wave-gauge and moving the instrument accordingly. Alternatively, to avoid the height dependence of the detector, the graded filters and photo-multiplier tubes were replaced by one-dimensional position sensitive devices that in principle did not depend on the light intensity [Scott et al, 1974]. This detector measured the wave slope regardless of the wave height.

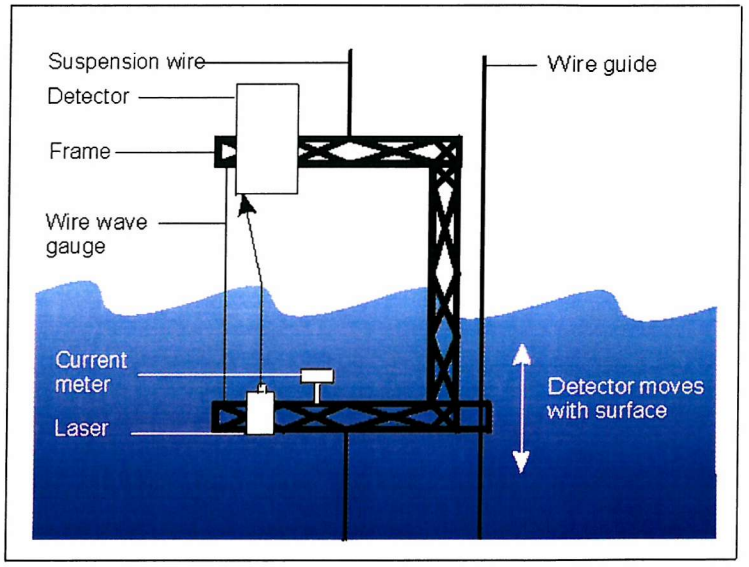

Figure 2. 8. The wave follower used by Hwang et al. to deploy a laser slopemeter instrument.

Palm et al. [1977] reported on an instrument based on this design that used a position sensitive photodiode to record the position of the laser beam on a frosted screen at the focus length of a 300mm lens. The instrument was also deployed at sea using a wave follower to ensure that the range of wave slopes measured remained constant. A calibration process was required in order to determine which position on the frosted screen corresponded with which wave-slope. Palm et al. [1977] reported that the calibration of the instrument was dependent on the temperature and could vary by as much as 20% for a variation in temperature of 3°C. These variations were attributed to the position sensing electronics. The accuracy of the detector was also found to be

dependent on the intensity of the scattered light. Changes in the scattered light were attributed to the attenuation of the laser beam as it passed through the sea and on the scattering properties of the frosted screen. A report by Ghataure et al. [1992] investigated how a frosted screen scattered light with the aim of using a similar technique. However, this investigation revealed that the light from the screen was scattered preferentially in a forward direction within a 5° cone angle. This would have caused large variations in the intensity of light falling on the camera lens making this method difficult to use because of the large dynamic range required to cover the variation in light intensity.

The optical refraction techniques that have been described so far can be used to measure the slope of the sea surface at a single point in time and space. However, using a single point measurement only allows the frequency at which waves passed the instrument to be measured. In order to record the correct frequency of a wave the instrument must be stationary relative to the water that the wave is moving through.

If the instrument is moored, even in the absence of tidal currents, passing swell waves will cause the water, through which the small scale waves are travelling, to circulate and therefore move relative to a fixed instrument [Kinsman 1965 P133, Atakturk et. al. 1987]. To combat this problem the instrument can be allowed to drift along with the motion of the water. In this case the bobbing motion of the drifting instrument could be damped relative to the wave motion.

Longgeut-Higgins et al [1983] deployed a resistive wire wave-gauge on a floating pole structure as part of the MARSEN research program to measure breaking waves. The instrument used is shown in Figure 2. 9. The main buoyancy of this instrument is below the sea surface where it is not affected significantly by the waves being measured. However, the pole would still tend to follow the motion of the longer wavelengths, which therefore cannot be measured. In this experiment only discontinuities in wave height were of interest, as they indicate the presence of a breaking wave, so this deployment method was appropriate.

Alternatively, the motion of the floating instrument as it moves over the waves could be measured. This motion can then be removed from the recorded wave data. Longuett-Higgins et al [1963], used the motion of a buoy floating on the sea surface to record long wavelength waves with frequencies less than 0.6Hz as shown in Figure 2. 10. This method involved using a combination of x and y gyroscopes and an accelerometer in order to ascertain the buoy's inclination and change in height respectively. This instrument had a limited frequency response due to the relatively large dimension of the buoy. However, this type of device may be used to ascertain the inclination of an instrument at sea that is designed to measure smaller waves [Stolte 1994, Li et. al. 1992].

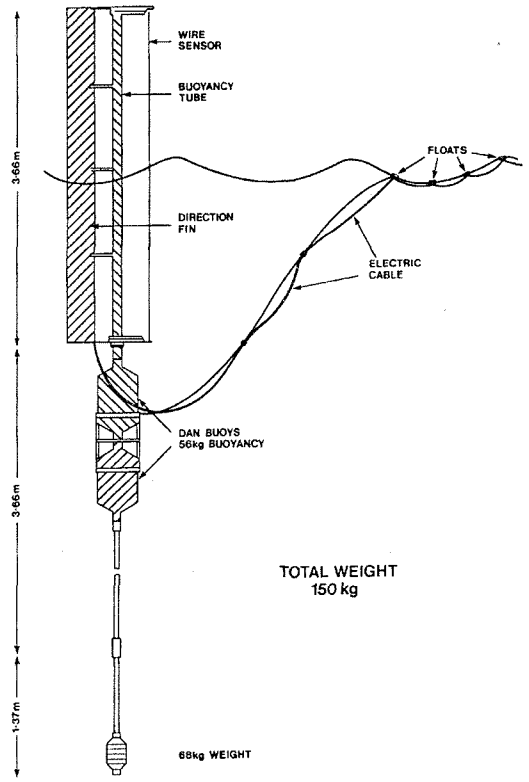

Figure 2. 9. A wire wave-gauge deployed on a floating pole to measure jumps in sea level.

Even if care is put into deploying these probes, waves will still be reflected by the supporting structure as it passes through the water. These waves will consequently interfere with the measurements made by the instrument. A laser slopemeter could be deployed up stream of a fixed platform, with a sufficient tidal flow to ensure that the waves reflected from the platform do not reach the measurement area. However, this limits the deployment times available. Several investigators [Lee et al., 1992, Li et al., 1992 and Martinsen et al., 1992] have deployed laser slopemeters from the front of a moving vessel so that the waves that are generated by the vessel and instrument fall behind and are not measured. If single point measurements are made then neither the shape of the wave nor their frequency can be accurately measured. However, by scanning the laser over the sea surface at high speed, the shape of a virtually stationary sea surface can be mapped. From this slope profile a wave spectrum may be generated.

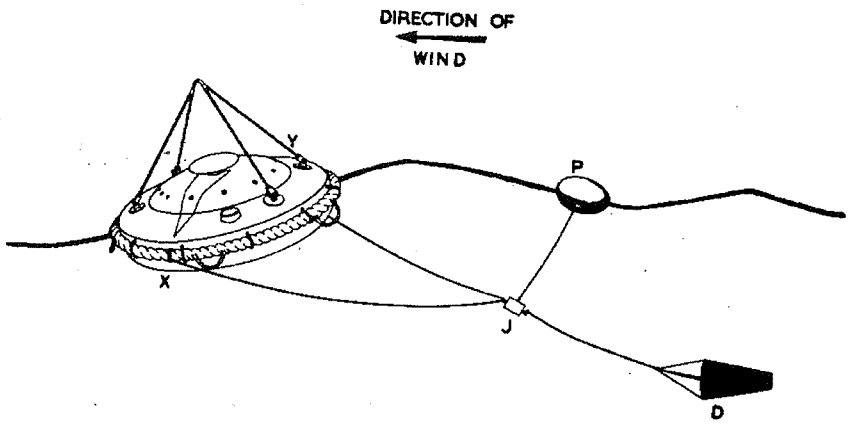

Figure 2. 10. A buoy designed to measure gravity waves.

A scanning instrument was built by TRW and deployed in 1987, [Lee et al. 1992]. Their detector required three wire wave-gauges to measure the sea surface height. The three wire gauges did not record the height of the surface at the point where the slope was being measured therefore this height was inferred from the three measurements. The scanner system that was used with this instrument meant that the position of the laser beam on the surface was dependent on the surface height. Therefore the recovery of the wave slopes and their positions was relatively complex.

Both Li et al. [1992] and Martinsen et al. [1992] used a scanning system with a detector that did not require surface height measurements. Both of these instruments used a similar scanning system. The unit was designed to generate a parallel displacement scan, so that the laser beam is always parallel to the optical axis of the instrument. With this type of scan, the position of the laser beam on the surface is not dependent on the height of the surface. Placing a scanner at the focal point of a lens generates this parallel displacement scan. The size of the scan is limited by the size of the lens used, therefore, Li et al. [1992] and Martinsen et al. [1992] have only scanned areas of 81 x 81mm and 100 x 100mm respectively.

They also developed similar detectors that used a screen placed at the focal length of a lens, in the same way as the instrument designed by Tober et al [1973]. The position of the beam on the screen was then recorded using a position sensitive detector as shown in Figure 2. 11. Li et al. [1992] used a fresnel lens which is significantly lighter than a spherical lens. However, this detector had poor resolution near the centre of the lens because of the finite distance between each of the circular segments of the lens. The majority of wave slopes on the sea surface will be small, as shown in Figure 2. 3, therefore a large proportion of the measurements will fall in this region of the lens.

Both of these devices were deployed on a catamaran and could measure wave slopes in excess of 30°. However, to achieve this wave range the detectors had to be relatively close to the sea surface. This would have limited greatly the sea conditions that the instruments could be deployed in and would have been much more likely to cause interferences with the wind above the surface. It would become impractical, difficult and expensive to manufacture a much larger lens to allow the detector to be placed further from the surface. The scanner unit used by Martinsen et al. [1992] was only 40cm below the mean sea surface and consequently, would have interfered with the sea surface itself. It is likely that this would have been the case for Li et al. [1992] although the dimensions of their unit were not reported. Despite these problems the instruments described by Li et al. [1992] and Martinsen et al. [1992], are in principle suitable for measuring small-scale sea surface roughness.

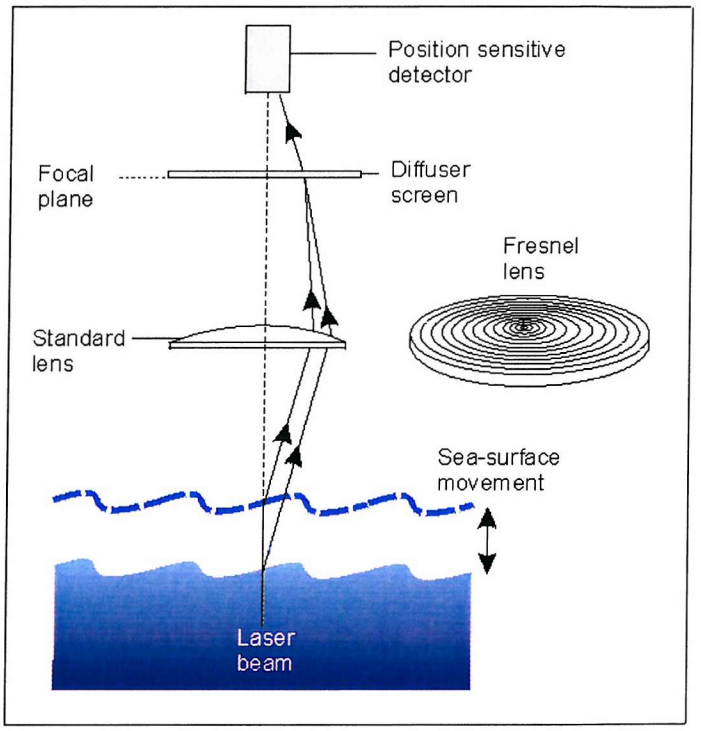

Figure 2. 11. A diagram of a scanning laser slopemeter using a lens to detect the laser beam. Shown on the right is a fresnel lens that was used by Li et al. [1992].

2.3. Conclusion

In order to measure the small-scale sea surface roughness the best approach is to use an optical method that does not require invasive probes. A laser slopemeter that does not require the measurement of the sea surface height is ideal for recording the local surface slope. However, unless the laser is scanned across the surface it is not possible to record spectral information about the surface roughness. Scanning laser slopemeters, although in principle can measure small-scale surface roughness, are severely limited by their size and proximity to the sea surface. In the light of the measuring techniques discussed in this chapter it is clear that the further development of an instrument suitable for measuring small-scale waves effectively at sea is required. In the next chapter the Towed Laser Slopemeter designed by the University of Southampton to address some of these problems is described. After this review the remainder of this thesis describes the design and construction of the new Digital Laser Slopemeter that was developed using the knowledge and experience gained during the design and deployments of the Towed Laser Slopemeter.

Chapter 3

A Critical Review of the Towed Laser Slopemeter

3.1. Introduction

This chapter provides a critical review of the design and operation of the Towed Laser Slopemeter (TLS). In November 1991 the University of Southampton proposed to the DRA a possible method for measuring the short-scale surface roughness on the ocean surface, based on the use of a towed laser slopemeter. The main objective of this instrument was to measure waves on a scale of 1cm to 1m, so that the modulation of these waves by internal waves could be studied and correlated with radar backscatter signals from the same area of sea.

This chapter includes observations based on the operational experience gained by the author during deployments of this instrument in the Solent and in the North Sea from February to September 1996. This review indicates those areas in which the basic TLS instrument design, deployment and data analysis techniques could be improved further.

The Towed Laser slopemeter was deployed on a small catamaran which was towed parallel to a larger manned vessel in such a way to avoid the towing vessel's wake. The instrument was mounted on the bow of the catamaran between its hulls so that the area of the sea that was being measured was not significantly disturbed by the catamaran's bow wave.

The first deployment of this instrument was carried out in September 1994 in Loch Linnhe under the direction of the DRA. From these trials many useful lessons were learnt, regarding the design and deployment of the instrument. During the following year, the instrument was completely refurbished and several aspects of the design were modified. In particular, the analogue electronics were improved in order to reduce the noise that was limiting the quality of the data collected.

It was at this time that the author joined the TLS team, with the specific task of identifying areas that required improvement in the design of the TLS instrument. The refurbished TLS instrument was next deployed in February 1996, in the Solent, in order to assess the improvements made

before it was deployed in the North sea off the coast of Holland in April, as part of the CSTAR experiment (Coastal Sediment Transport Assessment using SAR imaging). This was followed by a further week-long trial in the Solent, in August 1996, with the aim of evaluating the instrument's performance at sea. During these deployments of the instrument, valuable experience was gained and possible improvements to the method of deployment where identified.

This chapter describes the principles of the original TLS instrument and the main areas for improvement that were identified during and after the sea trials both in the North Sea and in the Solent.

3.2. The Towed Laser Slopemeter Principle

A laser slopemeter measures the refraction of a collimated laser beam by the water surface. It therefore, consists of two main components, a laser and a laser beam detector. The laser can either be placed above or below the water surface and the refraction by the air-sea interface, for these two cases, is shown in Figure 3. 1. In order to determine the most suitable geometry for the detector, both cases were considered.

For both cases shown in Figure 3. 1 the angle that the light makes with the surface normal both above the water (θ_a), and below the water (θ_w) can be related to the wave slope (θ_s) and the beam slope (θ_b). It can be seen that $\theta_a = \theta_s$ and $\theta_w = \theta_s - \theta_b$ in Figure 3. 1a) and $\theta_w = \theta_s$ and $\theta_a = \theta_s + \theta_b$ in Figure 3. 1b). Combining these relationships with Snell's Law which in this case is,

$$n_w \sin\theta_w = n_a \sin\theta_a$$

where n_w and n_a are the refractive index of water and air, a relationship between the wave slope and the beam slopes can be generated. The resulting relationships derived for the beam passing from the air to the water is,

$$\theta_b = \theta_s - \sin^{-1}\left(\frac{n_a}{n_w}\sin\theta_s\right) \tag{3. 1}$$

and for the beam passing from the water to the air is,

$$\theta_b = \sin^{-1}\left(\frac{n_a}{n_w}\sin\theta_s\right) - \theta_s \tag{3. 2}$$

Both of these relationships are plotted in Figure 3. 2.

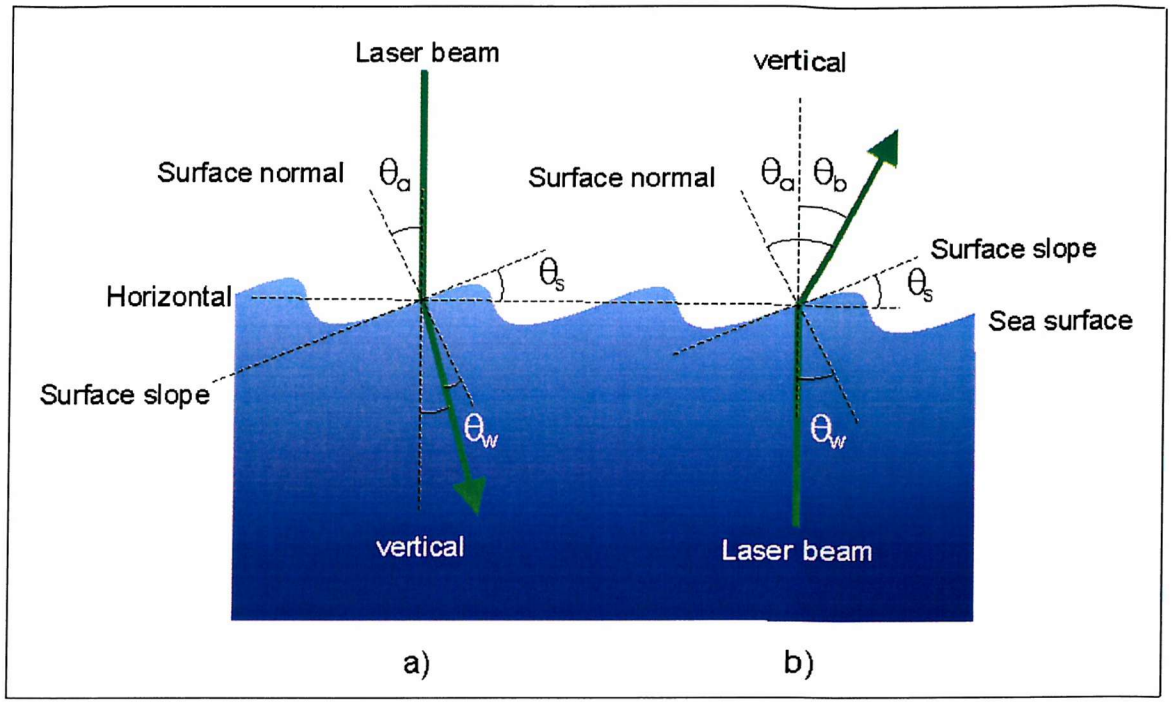

Figure 3. 1. The refraction of light by the sea surface as light passes through the surface from a) above the water and from b) below the water.

The refractive indices of water and air are n_w = 1.33 and n_a, = 1, therefore, the angle of the laser beam to the surface normal in air is greater than that in the water as shown in Figure 3. 1. Therefore if the detector is placed below the surface it would have smaller dimensions than one, that measures the same range of slopes, placed above the surface. In fact the detector above the surface can only measure wave slopes up to 48° before total internal reflection occurs at the air-sea interface, as shown in Figure 3. 2. However, the detector is considerably larger than the laser and the instrument will experience greater forces if the detector is moving through the water. This would necessitate the need for a strong and heavy supporting structure, making the instrument more difficult to deploy. For this reason, the detector was mounted above the surface and the laser source below. The two arrangements described here are discussed in a paper by Bernd et al. [1992].

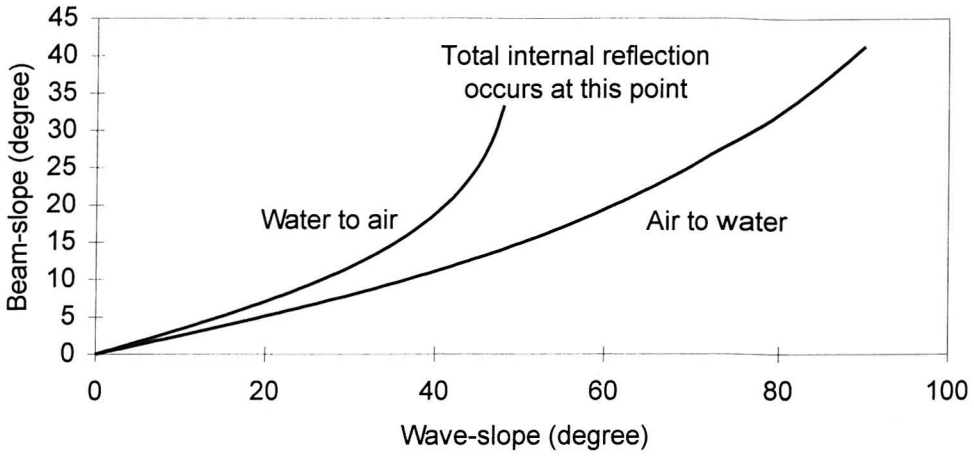

Figure 3. 2. The relationship between the beam slope angle and the wave slope angle for the case of light passing from air to water and for water to air.

In the case of the TLS, the method that was used to measure the slope of the laser beam involved recording the beams position at two points along its path. In this way, no matter where the sea surface is relative to the detector, the slope of the laser beam can be determined. Once the beam slope has been measured, the absolute value of the wave slope can be calculated provided the inclination of the detector is known. To the author's knowledge this principle, illustrated in Figure 3. 3, had not previously been tried.

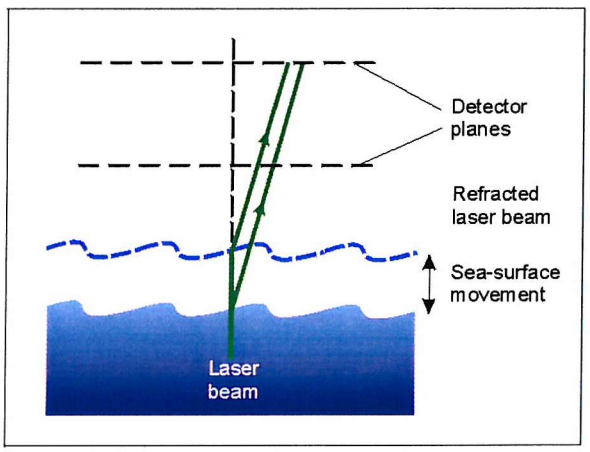

Figure 3. 3. The TLS slopemeter concept.

The TLS detector used two plastic screens, placed 330mm apart and doped with a wavelength shifting dye that absorbs the incident laser light. The laser light is then re-emitted at a shifted wavelength and some of this light is trapped within these screens. The trapped light propagates

by total internal reflection to the edges of the screens where it is detected using six photodiodes placed around their circumference, as shown in Figure 3. 4. The HeCd laser that was used, emits light at a wavelength of 442nm, this corresponds to the absorption band of the dye NE172 [NE Technology] that was used in the detector screens. A plot of the absorption and emission spectrum of NE172 is shown in Figure 3. 5 along with the 442nm line produced by a HeCd laser.

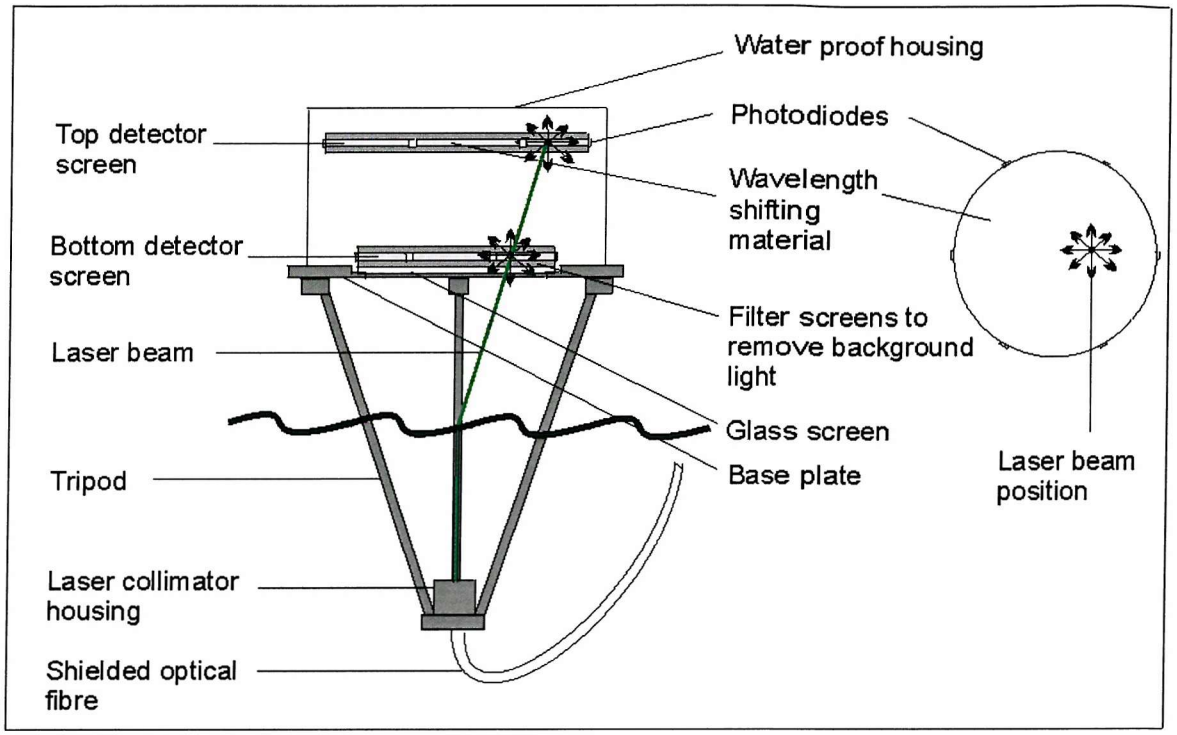

Figure 3. 4. The laser-slopemeter construction.

The lowest screen of the detector was designed to absorb approximately 50% of the incident light energy. The light that is not absorbed by the first screen passes to the second screen where it is completely absorbed. The photodiodes around the circumference of the two screens produced analogue signals that depended on the position of the laser beam on the screens. To provide a reference so that the laser signal can be recovered from the background light, the laser was modulated at a frequency of 10kHz, using an opto-acoustic modulator. This allowed the signal to be recovered using a phase sensitive detector. The stages in the signal processing are shown in Figure 3. 6.

The low pass filter in Figure 3. 6, has a cut-off frequency of 100Hz so that only waves with frequencies less than this can be measured. After this filter, the diode signals are sampled at a rate of 250Hz and then digitised by a 16-bit analogue to digital converter. This sampling rate allows the 100Hz waves passed by the filter to be easily resolved. The final stage of processing was achieved using a microprocessor. This was on board the catamaran and organises the data

for telemetry, in a RS232 format, to the towing vessel. On this vessel the data was then logged onto two PCs, generating two data sets. This was necessary to allow data that may have been lost in the telemetry from one of the data sets to be recovered from the other.

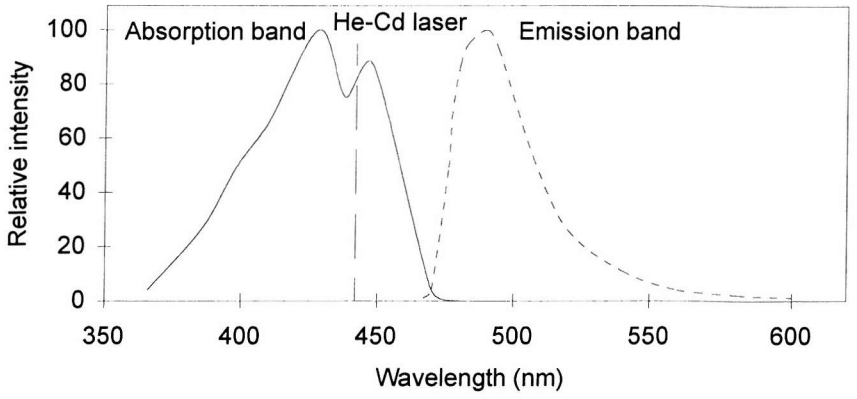

Figure 3. 5. Absorption and emission spectra of NE172 fluorescent light guides.

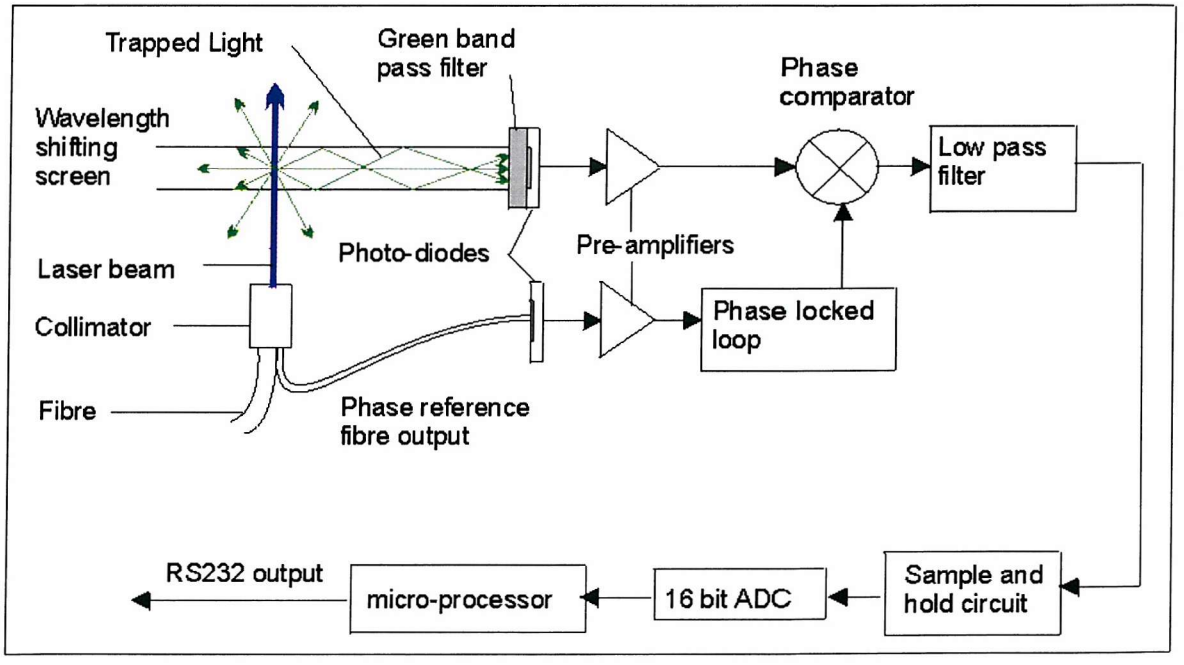

Figure 3. 6. The signal processing of the photodiodes signals on board the catamaran.

The light from the laser was coupled to a 30m length of optical fibre and the output from this fibre was then collimated to form a beam. The end of the fibre was then attached to a tripod

mounted rigidly to the laser beam detector as shown in Figure 3. 4. When the TLS was in operation, the end of the fibre was approximately 500mm below the mean sea level with the beam pointing upwards towards the detector.

The size of the detector was chosen to allow wave slopes of up to ±45° to be measured. This corresponds to beam slopes of up to ±26°. The resolution for the wave slope was chosen to be 1°, which requires the beam angle resolution to be 0.33°. A discussion on the dimensions of the detector is given in section 3.4.1 of Lee's thesis [1995].

3.2.1. Sampling of the sea surface

In order to avoid measuring waves that have been created by the presence of the instrument or the deploying research vessel, measurements were made while the catamaran was being towed to one side of the research vessel. The minimum speed at which the research vessel could still be manoeuvred was approximately 2knots corresponding to ~1ms^{-1}. The sampling frequency for the TLS was chosen assuming that the speeds of the waves were negligible in comparison to the speed at which the instrument was being towed. A 10mm wavelength moving past the instrument at 1ms^{-1}, would take 10ms to pass. Therefore, a 10mm wave would be observed by the instrument as a wave with a frequency of 100Hz. To resolve this wave it must be sampled at a frequency of at least 200Hz. The signal processing electronics was designed to record waves with a frequency up to 100Hz, which were then sampled at 250Hz [Lee 1995].

The diameter of the laser beam at the air-sea interface was chosen to be 2mm. This choice was made for two reasons. Firstly, it is difficult to produce a beam, with a smaller diameter, at the required distance from the end of the fibre. The second is that the finite diameter of the beam effectively acts as a filter to very small-scale surface waves. This is because the beam is only refracted by waves that are significantly larger than the beam diameter as shown in Figure 3. 7. Cox [1958] investigated this phenomenon, the result was that a 2mm beam would respond to a 6.8mm wave with only a 10% error in the measurement of the refracted beam relative to a point source of light.

During the initial stages in the development of the TLS, it was anticipated that all the processing of the data could be performed in real-time. This would have allowed the wave slope data to be displayed while the slopemeter was being deployed. However, as the design of the TLS progressed, it became clear that the detector screen's response was non-linear and could not be easily modelled. Consequently, a large amount of post processing of the data was required to

recover the positions of the laser beam on the screens. In view of the time constraint on the development program of this instrument, real time processing was therefore abandoned.

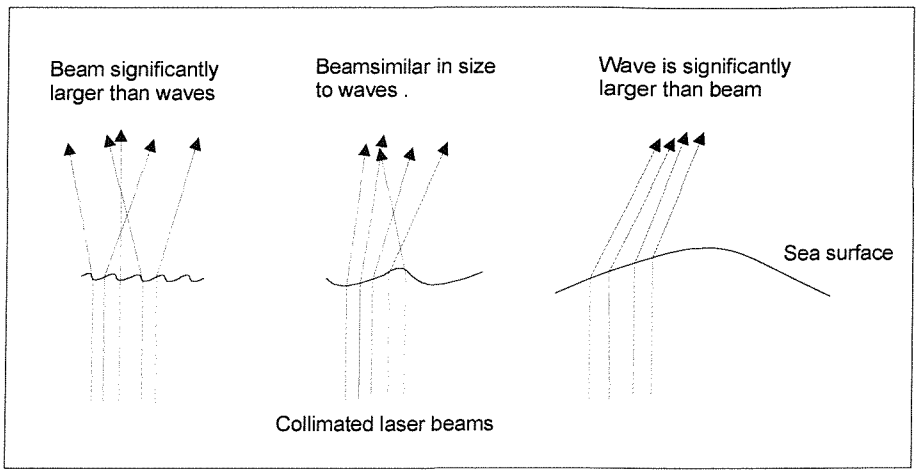

Figure 3. 7. The refraction of a finite diameter laser beam at the sea surface, showing the coherent refraction of the beam only for waves considerably longer than its diameter.

3.2.2. Processing and Calibration

The process of reconstructing the wave slopes from signals generated by the 12 photodiodes around the two screens, was performed in software written by Lee [1995]. This process involved relating the photodiode signals to a unique beam position on each screen using a look-up table that had been previously generated by a calibration of the instrument. Once the position of the beam had been identified on the two screens the beam slope and therefore the wave slope may be calculated. This process was carried out entirely in software, run on two Sun workstations in the laboratory.

Before each trial in which the instrument was used, the look-up table was generated by completing a detailed calibration of the detector screens. This was achieved by directing the laser beam to hundreds of positions on a 5mm grid on each screen using a two axis rotary table. At each position, the signals measured by the photodiodes were recorded. This process took several hours to complete and had to be performed at the beginning, and end, of each trial to ensure that the instrument was working correctly.

3.2.3. Supporting Instrumentation

In addition to the Towed Laser Slopemeter, several other instruments were deployed during the sea trial in 1996. A description of the full complement of instruments that were operated during these deployments and the supporting equipment required to run them is summarised below:

- **The Laser Slopemeter** - This recorded information of on the sea surface roughness. This instrument required two PCs and a tape drive to record the data.

- **An Inertial Motion Unit (IMU)** - This recorded information about the motion of the catamaran. It incorporated accelerometers to measure the acceleration along 3 orthogonal axes and a 3-axis inclination sensor to measure the pitch, roll and yaw of the instrument. The data that it provided was used to correct for the motion of the catamaran. This instrument was mounted close to the laser slopemeter on the catamaran.

- **A Differential Global Positioning System (DGPS)** - This recorded the longitude, latitude and track of the vessel with a precision of a few meters.

- **An Echo Sounder** - This recorded information about the bottom topography. This instrument required a dedicated PC to record the depth of the seabed as the instrument passes over it.

- **A Weather Station** - This recorded the air temperature and pressure, the wind speed and direction and the incident solar radiation. This instrument also required a dedicated PC to record the data that it provided.

3.2.4. Method of Deployment

A modified Catapult catamaran having an increased hull spacing of 2.5m was used to deploy the laser slopemeter. The aim of this modification was to make the catamaran more stable and to ensure that the bow wake formed by the hulls did not cross the measurement area when the catamaran was being towed. Whilst measurements were being made, the catamaran was towed off the starboard side of the research vessel so that the wake of this vessel did not interfere with the catamaran. To keep the number of cables passing between the vessels to a minimum, only the laser slopemeter and the IMU were deployed on the catamaran. The other instruments were deployed on the towing vessel, as shown in Figure 3. 8.

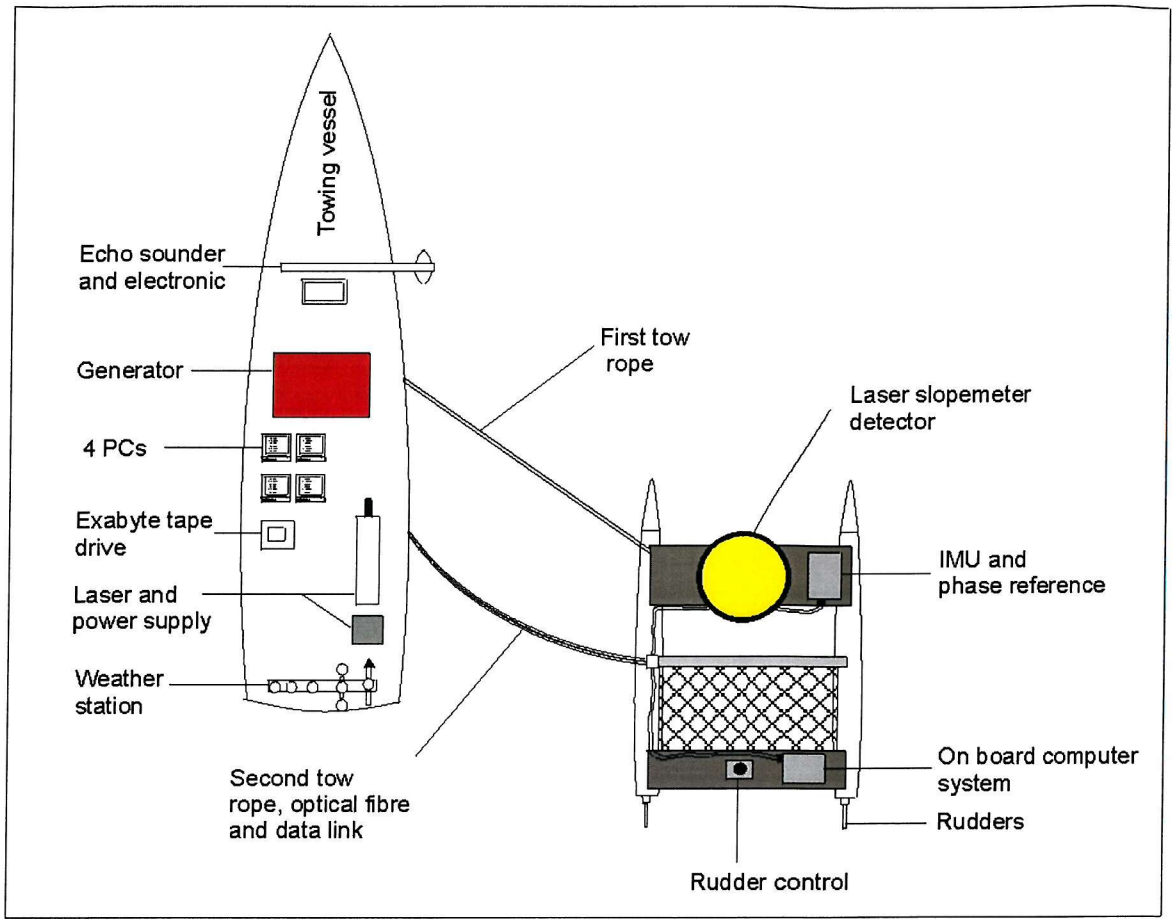

Figure 3. 8. Operational arrangement used in the deployment of the Towed Laser Slopemeter.

The TLS was designed to be towed at about $1ms^{-1}$ whilst taking measurements. However, there was often a need to move the instrument at speed to the region where the measurements were to be made. In Solent waters, the *Willventure* was used to deploy the TLS. This vessel was too small to lift the catamaran out of the water, therefore, to reach the deployment area the catamaran was towed at about 12knots as shown in Figure 3. 9. While the catamaran was being towed at this speed the telemetry cable and optical fibre were removed. Therefore, to deploy the TLS, the catamaran had to be bought along side the *Willventure* and the connections made by a diver, as shown in Figure 3. 10. This was a difficult manoeuvre if the sea conditions increased to a force 3 or more, during a deployment.

Figure 3. 9. The catamaran being towed by the *Willventre* to the deployment area.

During the CSTAR experiment in the North Sea a second method of deploying the catamaran was used. A much larger vessel was hired so that the catamaran could be brought on board for the transit to the deployment area that was approximately 50km off shore. However, a diver was still required to attach the telemetry cable and the optical fibre once the catamaran had been lowered into the water. This method of deployment was much safer because the instrument would only be lowered into the water if the sea conditions were suitable. However, it was found that the larger vessel produced a large bow wave, so the catamaran had to be towed much further from the towing vessel. Even then, on occasions the bow wave interfered with both the catamaran and the measurement area.

Figure 3. 10. The attachment of the optical fibre, data link cable and the wiping of the detector screen by a diver.

3.3. Scientific Data Obtained by the TLS

Some of the most interesting data that has been collected by the TLS during its deployment in the C-STAR experiment in the North Sea off the coast of Holland in April 1996 is presented here. The aim of this experiment was to investigate the modulation of the surface roughness due to the ocean current flowing over sand dunes on the seabed. These sand dunes are situated about 50km off the coast of Holland in about 25 meters of water and where about 5m meters high with a distance of about 40 meters between each crest. At certain states of the tide, when the water flow is greatest over the dunes, a modulation of the surface waves can be seen with the naked

eye. The aim was to measure these waves with the TLS instrument, a drifting buoy wire wave gauge [Stolte, 1994], and an airborne SAR.

A comparison of the data collected from the echo sounder, the Towed Laser Slopemeter and the airborne SAR, has shown that an increase in the sea surface roughness occurs close to the peak of the submerged sand dunes. A study of this correlation has been presented by Gommenginger et al. [1998]. However the main results can clearly be seen from Figure 3. 11. The top two plots in Figure 3. 11 show a mean wave slope power spectral densities in the frequency range 2-6Hz, for waves slope components in a northerly direction and in a easterly direction measured using the Towed Laser Slopemeter. The scale in these two plots is a $\log_{10}$ scale. The TLS was travelling at a average speed of $1.5ms^{-1}$ in this trial, therefore this frequency range corresponded to ocean wavelengths around 50cm. These wavelengths are expected to be responsible for the backscatter of P-band radar that uses electromagnetic wavelengths of around 50cm. The third plot in Figure 3. 11 shows the P-band radar backscatter coefficient profile. The forth plot shows the change in bottom depth in the same period of time as the above plots and the final plot shows the wind speed while the data was being collected. There is a definite correlation in the maximums and the minimums between the easterly wave slopes, radar backscatter and depth. The circles in these plots show similar positions in time. The arrow on the forth plot shows the direction of the tidal flow. As might be expected that as the water approaches the restriction caused by the sand dunes, it speeds up which effectively stretched the surface waves thus reducing the spectral density and consequently the radar backscatter coefficient. Similarly, immediately after the sand dunes, there is a reduction in water velocity and the spectral density increases.

It is, therefore, clear that the wave slopes that are measured by the Towed Laser Slopemeter correlate to the position of the sand dunes and that the instrument has been a useful tool in this experiment. Willoughby [1998] has made further correlation of the data obtained on this trial.

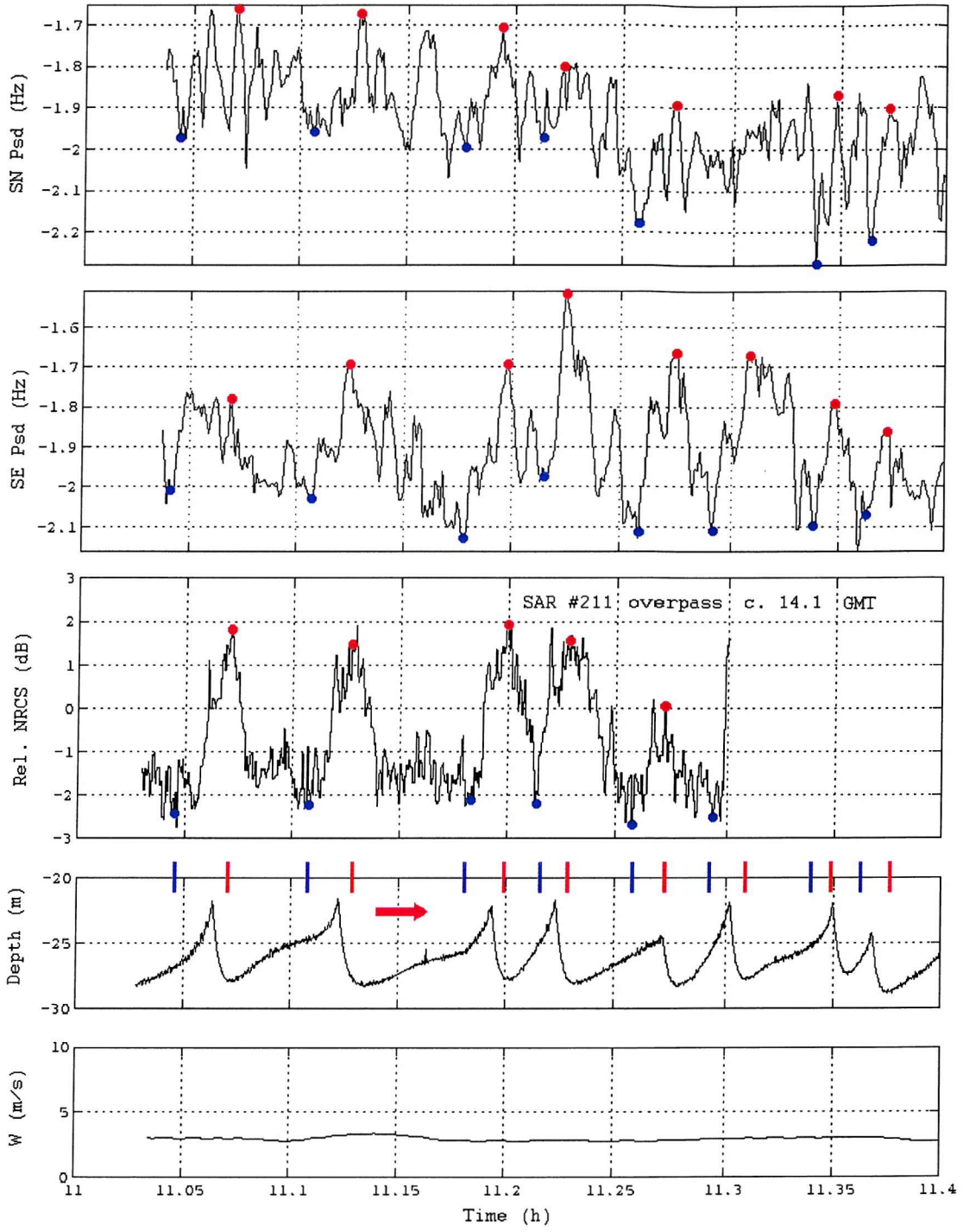

Figure 3. 11. The mean power spectral density of the sea-surface wave slope plotted against time, measured by the TLS, 1) for wave slope components in a Northerly direction and 2) in a easterly direction. 3) The radar backscatter coefficient profile. 4) The depth profile over the same period of time and 5) the wind speed during this period.

3.4. Lessons Learnt from work with the TLS Project

Following the deployments of the TLS in 1996, the main problems with this system were identified. The improvements suggested here are concerned with the reliability and maintenance of the laser slopemeter instrument and with the processing and analysis of the slopemeter data. The main points of concern were:

1. The data collected could not be analysed immediately. A real-time display of the data collected would allow much better use of the research vessels time.

2. The catamaran was difficult to deploy in almost all conditions and required continuous attention while at sea. It also tended to pitch heavily in moderate sea conditions, so that the tripod came out of the water completely. This would produce a zero slope reading that could not be removed from the data. The sea surface shape would also have been distorted as the laser collimator approached the surface.

3. The HeCd laser was not well suited for operation at sea on a pitching vessel because it was large and delicate. It also required a 30-minute warm-up period when first powered up. This could be inconvenient if there was a glitch in the power generator that momentarily switched the laser off.

4. The number of components in the overall system made it difficult to deploy and move about. It is therefore desirable to reduce the number of separate components in the system.

5. It is not possible to recover a true wave spectrum from the Doppler shifted spectrum that the TLS instrument recorded. Willoughby [1998] has performed a detailed analysis of the actual spectrum recovered. The results of this investigation indicated that the sea surface height could be used to gain an insight to the true wave spectrum. However, the TLS could not measure a sufficiently accurate wave height for this purpose.

The experience gained from deploying the TLS in the field has been invaluable in evaluating this system. From these trials, the key factors that make a system easy to deploy have been identified. This has allowed improvements to be suggested, both to the instrument and to the method of deploying it. In order to implement these suggested improvements, a new instrument has been developed and the remainder of this thesis will describe its design.

Chapter 4
The Design of a Scanning Laser Slopemeter

4.1. Introduction

It was shown in Chapter 3 that, during the field trials off the coast of Holland in April 1996, the Towed Laser Slopemeter detected modulations in the small-scale surface structure that correlated with the seabed profile. The TLS was towed through the water to measure a natural wave-field and it was initially expected that the true wave spectrum would be recovered from this data. For this reason, Willoughby [1998] has investigated how towing a laser slopemeter over the sea surface affects the recorded wave spectrum. He found that as a consequence of the Doppler shifting of the measured wave components, it is not possible to recover a wavenumber or frequency spectrum. In order to recover a frequency spectrum, a single-point measurement must be made that is completely stationary relative to the water through which the waves are travelling. This is a very difficult measurement to make, especially for small waves, because of the orbital motion of the water caused by the presence of larger waves [Kinsman 1965 P133, Atakturk et. al. 1987]. To measure a wavenumber spectrum, a stationary surface profile must be recorded. This chapter suggests the use of a scanning laser slopemeter, to reduce considerably the effects of Doppler shifting on the wave measurements made. The scan of the sea surface must be fast enough to ensure that the waves observed do not move during the observation. The wavenumber spectrum that may be obtained from the sea surface with the scanning laser slopemeter is described. The effect of Doppler shifted observations of waves will be considered and a suitable scan speed suggested. Finally, an appropriate scanning system that could be deployed at sea will be described.

4.2. Generating a Spectrum

A wavenumber spectrum generated from a surface profile will allow this surface to be characterised in terms of its sinusoidal wave components. This spectrum can be used to describe the sea surface in terms of the wavenumbers of these sinusoidal components. It is apparent that

the sea surface is modulated by ocean phenomena and a study of the changes in strength of these spectral components will permit these effects to be quantified. By considering a two-dimensional wave spectrum then directional properties of the surface can also be studied. For simplicity we will just consider a one-dimensional wave in this section.

The sea surface may be assumed to be a combination of sinusoidal waves of different amplitude ($A(k_x)$). Each of these sinusoidal waves will have a corresponding wavenumber (k_x) and frequency ($\omega(k_x)$). The phase of each of these waves (ϕ_{k_x}) is assumed to be random relative to the other waves that are present. Mathematically, this superposition may be written as a summation of these waves to give the overall wave height η, which varies with time (t) and space (x):

$$\eta(x,t) = \sum_{k_x} A(k_x)\cos\left(k_x x + \omega(x)t + \phi_{k_x}\right) \qquad (4.1)$$

However, a laser slopemeter measures the slope of the sea surface ($s(r,t)$), which is the differential of the wave height with respect to distance along the wave (r) as described in equation 4.2;

$$s(x,t) = \frac{\partial \eta(x,t)}{\partial r} = \sum_{k_x} k_x A(\underline{k})\cos\left(k_x x + \omega(k_x)t + \phi_{k_x}\right) \qquad (4.2)$$

It is unlikely that the ocean surface can be defined in its entirety by a discrete number of wave components. However, the slope ($s(x,t)$) of the sea surface can only be sampled at discrete positions, a continuum of wavelengths can not be measured. According to sampling theory the shortest wavelength that may be recorded must be sampled at least twice along its length. Those waves that are under sampled will be added to the measured spectral range thus causing aliasing. To avoid aliasing, the range of wavelengths that the slopemeter responds to must be limited so that only those that are sampling correctly are recorded. This problem will be considered further in section 4.2.3. With these considerations in mind, a wavenumber spectrum can be generated by performing a Discrete Fourier Transform with respect to position on the surface (x) for an instants in time (t = constant). This Fourier Transform can be written as;

$$S(x) = \sum_{n} s(x)e^{-ink_x x} \qquad (4.3)$$

Although this equation represents a wavenumber spectrum of wave slopes and not wave heights, there is a simple relation between the two, which can be seen from equations 4.1 and 4.2. Each wave slope component is the wave height multiplied by its wavenumber $s(k_x) = k_x \eta(k_x)$ and

therefore each wave slope component in the spectrum is the wave height component ($N(k_x)$) multiplied by the wave number $S(k_x) = k_x N(k_x)$.

4.2.1 The Doppler Shift Effect

As the speed at which the TLS was operated was similar to that at which the waves under observation propagated, a significant Doppler shift was introduced to the measurements made. This lead to a difference between the true and observed wavelength calculated using the boat speed. By considering the nature of this apparent wavenumber that has been generated the error with respect to the true wavenumber can be established.

If the instrument is travelling in the y direction, as shown in Figure 4. 1, the frequency measured (ω_{yo}) depends on the boat speed (v_b) and the velocity component of the wave in the y direction (c_y), that is,

$$\omega_{yo} = k_y(c_y - v_b) \tag{4.4}$$

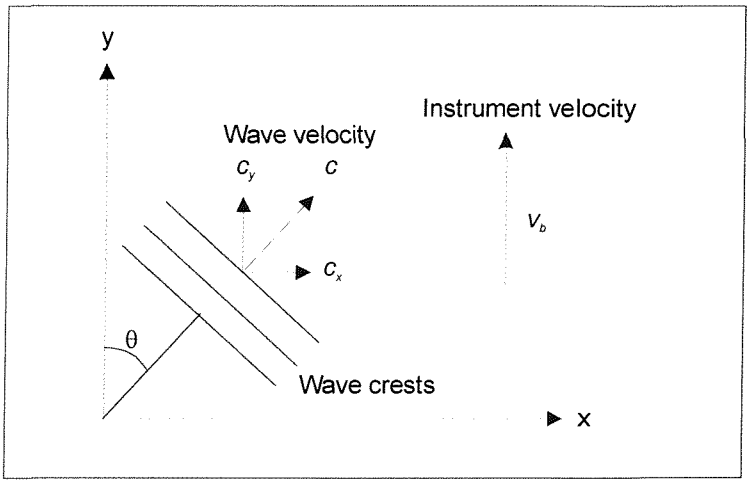

Figure 4. 1. Wave crests travelling with a speed c at an angle of θ to the direction that the instrument is travelling.

If the boat is stationary relative to the water the true frequency of the wave will be measured. Similarly, if the wave was stationary, a true wavenumber could be measured with the boat speed known. However, this is not the case and both of these terms are significant. Consequently, if the wave speed is ignored, the velocity component of each wave in the direction that the

instrument is travelling is Doppler shifted. Willoughby [1998] has shown that the frequency measured by the TLS can not be related purely to the wavenumber or to its frequency.

4.2.2 The Removal of the Doppler Shifting Effect

This Doppler effect can be minimised by scanning the laser beam rapidly over the sea surface. If the scan speed is sufficiently high, both the boat velocity and the speed of the waves will be negligible compared with the scan speed. Wave slopes can be measured at intervals throughout this scan while the sea surface is effectively stationary. To determine the speed at which the laser beam must be scanned to minimise the Doppler shift of the wavenumbers, a similar analysis to that performed by Barter et al. [1990] was used.

In the case of the instrument moving through the water at a speed v_b, as shown in Figure 4. 1, the waves pass the instrument at a speed,

$$v_{yTotal} = v_b - c_y \cos\theta \tag{4. 5}$$

in the y direction. If the beam is now scanned over the sea surface, in the positive y direction, at a speed v_s, the speed at which the beam moves past a wave on the surface is,

$$v_{yTotal} = v_s + v_b - c_y \cos\theta \tag{4. 6}$$

The measured frequency (ω_{yo}) that a wave with a y direction wavenumber component (k_y), will now be given by,

$$\omega_{yo} = k_y\left(v_s + v_b - c_y \cos\theta\right) \tag{4. 7}$$

Assuming the scan velocity is large, then both the wave velocity and the boat velocity can be ignored. The resultant apparent wavenumber that is generated is then given by,

$$k_{ya} = \frac{\omega_{yo}}{v_s} = k_y\left(1 + \frac{v_b - c\cos\theta}{v_s}\right) \tag{4. 8}$$

The bracketed term is known as the compression factor [Willoughby 1998]. For a given phase velocity and boat speed, the compression factor is furthest from unity when the boat and wave are travelling in opposite directions. The waves then pass the instrument at their maximum velocity and consequently the apparent wavenumber measured will be the furthest from the true value. The apparent wavenumber for these conditions is then given by,

$$k_{ya} = \frac{\omega_{yo}}{v_s} = k_y\left(1 \pm \frac{v_b + c}{v_s}\right) \tag{4. 9}$$

In order to plot the relationship between the true wavenumber and the compression factor, the velocity of the wave with wavenumber, k_y, is required. The linear dispersion relationship is

assumed to determine the wave velocities (c) for each wave component [Kinsman, 1965]. Using this relationship the speed of a wave is given by,

$$c = \frac{\omega}{k} = \sqrt{\frac{g}{k} + \frac{\gamma}{\rho}k} \qquad (4.\ 10)$$

where c is the phase velocity of the wave component, ω is the angular frequency of the wave, k is the wavenumber, g is the gravitational acceleration = 9.8 ms^{-2}, γ is the surface tension, which for clean fresh water = 0.074Nm^{-1} [Bowden, 1983] and ρ is the density of the water = 1000kgm^{-3}. The phase speed for waves with wavelengths between 0.3mm and 300mm are show in Figure 4. 2. At very small wavelengths, the restoring force of the waves is dominated by the surface tension and at larger wavelengths the waves are driven predominately by gravity. At $\lambda \sim$ 17mm, these two forces are equal and there is a minimum phase velocity of ~0.23ms^{-1}.

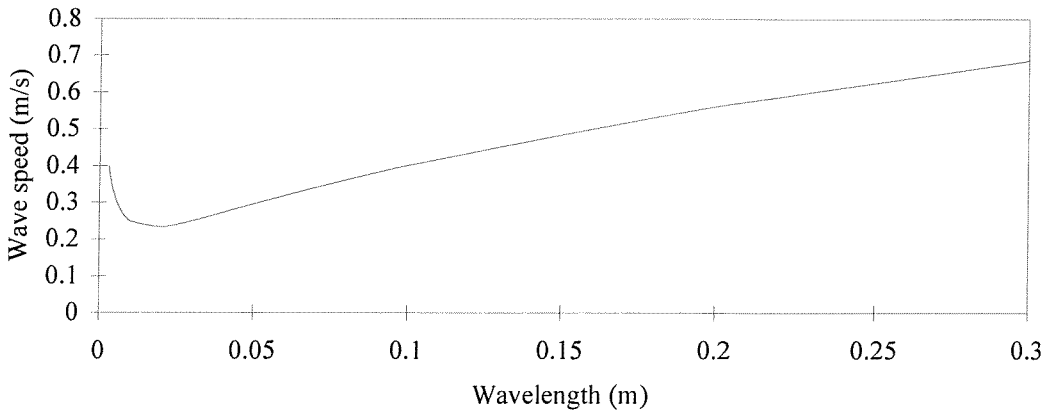

Figure 4. 2. Wavelength against phase velocity for wave in the range 0.3mm to 300mm.

Using these phase velocities and a boat speed of 2kts or ~1ms^{-1}, the compression factor can be plotted against wavelength, as shown in Figure 4. 3. The compression factor has been plotted for five different scan speeds. The value of ~ 100 ms^{-1} was chosen as the minimum scan speed. This will cause less than a 2% error in the recorded wavelengths over a 300mm range. If the scan consists of more than one scan line then the time taken for the beam to complete the entire scan pattern must be no longer than the time required for the laser beam to travel between the two most extreme points at a speed of 100ms^{-1}. Consequently, the actual speed of the beam may be required to be considerably faster than 100ms^{-1}.

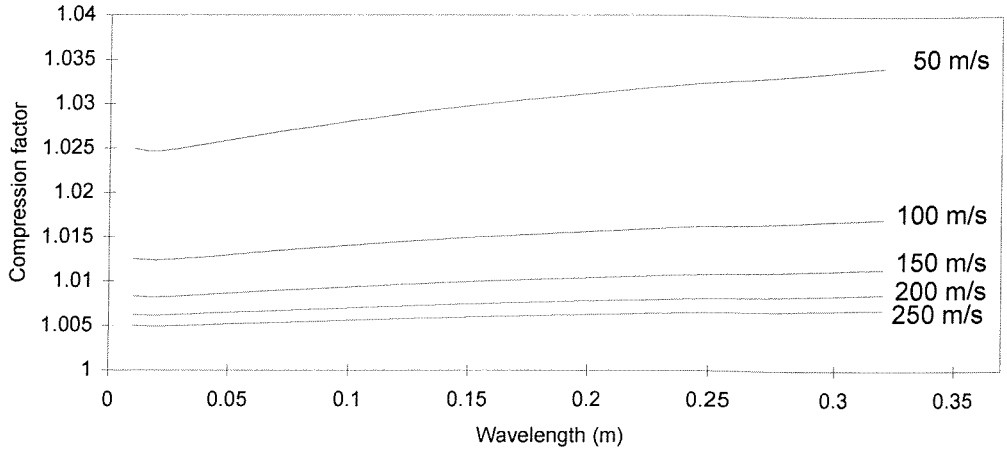

Figure 4. 3. A plot of wave number against compression factor at varying scan speeds.

4.2.3 Choice of Wavelength Range Measured

The minimum wavelength that can be measured is determined by the diameter of the laser beam as explained in section 3.2.1. The beam acts as a low pass filter by not responding to waves that have a comparable length to the beam diameter. This diameter on the sea surface is determined by the design of the laser and focusing optics. A 2 mm laser beam diameter on the sea surface had proven achievable whilst working with the Towed Laser Slopemeter and has consequently been chosen for this instrument. The minimum wavelength that can, therefore, be measured is 7mm, as determined by Cox [1958]. This wavelength must be sampled every 3.5mm to avoid aliasing of the wavenumber spectra by recording under sampled wave components.

The length of the scan determines the maximum wavelength component that may be measured. The choice of scan length must also take into account the number of sample points taken and the dimensions of the laser scanning system required. Ideally, a wavelength range of 7mm to 1m might be measured. However, each scan line would have to be sampled 286 times and the laser scanning system that will subsequently be described would have to have outer dimension of >1m. To reduce the number of samples per line to 64 and to reduce the size of the scanning system a scan length of 224mm was chosen. The scan pattern that was initially chosen, to restrict the data generated to 128 samples per scan, consisted of two orthogonal line scans. This initial scan pattern will allow some directional information to be collected from the surface without the additional data that would be generated by an area scan and without the additional

speed required from the scanner units. For the scan length of 224mm the total scan time is 2.24ms. The two scan lines can be considered as separate scans of the surface and consequently the total time of the scan may be up to 4.48ms long. In the case of an area scan then the total time of the scan must be less than 2.24ms to ensure that the wavenumbers measured throughout the scan are less than 2% Doppler shifted. As a consequence the following criteria where chosen to guide the design of the scanner system:

- The scan pattern would consist of two orthogonal scans lines of the surface, each 224mm in length.
- Each scan line must be sampled 64 times, generating a total of 128 samples per scan.
- The laser beam should move across the surface during the scan with a minimum speed of $100ms^{-1}$.
- Each scan line should be sampled every 3.5mm along its length on the sea surface, which is equivalent to a sample being taken every 35μs (or at a frequency of 28.6kHz), for a scan speed of $100ms^{-1}$.

4.3. Laser Scanner Design Considerations

The steps taken to meet the above criteria while designing the laser scanning system are now described. Four possible designs for this scanner system were considered. The final selection of the laser scanning system design is made taking into account the speed with which it must run, the simplicity of the design and the impact of its design on the aerodynamics of the submersible housing that it will be deployed in.

4.3.1. Choice of Laser Scanner Unit

A number of commercially available scanners were considered for this application. The specifications of these scanners are summarised in Table 4. 1. A galvanometer scanner was chosen for the preliminary development of the laser scanning system. These scanners can follow complex scans by positioning the scanner mirrors using a moving coil. An acousto-optic scanner may also be used to move a laser beam through a complex scan and are considerably faster than the galvanometer scanners. They are, however, an order of magnitude more expensive than the equivalent galvanometer scanner.

Scanner Type (and Model)	Manufacturer (reference specification sheets)	Maximum Specified Frequency	Maximum Optical scan angle (degrees)	Dimensions of scanner (mm)	Relative Cost
Resonant (TRS)	Laser Scanning Products.	2000Hz	30	102 x 45 x 26	medium
Rotating Polygon (M-660-010-LVWOB)	Lincolin Laser Co.	2000 lines per second	90	97 x 97 x 94	low
Galvanometer (6800)	Cambridge Technology Inc.	>600 Hz at 40° optical scan angle	80	46 x 36 x 25	low
Acousto-Optic (N45035-3-6.5DEG-1.06)	NEOS.	>33000 lines per second	10	86 x 32 x 20	High

Table 4. 1. The details of the scanners that were consider for this scanning system.

The angular position of the galvanometer scanner mirror can be moved 1° by changing the input signal to the servo card, driving the scanner unit, by 0.51 Volts [Cambridge Technology Inc.]. However, at high frequencies, the drive electronics limits the amplitude of the scan in order to prevent the scanner over heating. By measuring the scan length on a flat surface at a given frequency the maximum scan angle for that frequency can be measured. This was carried out for frequencies in the range 200Hz to 1400Hz, for both sinusoidal and triangular drive waveforms, these results are plotted in Figure 4. 4.

At low frequencies, the scanner's performance is not limited and so both the triangular and sinusoidal scans achieve the same amplitude. In the mid range of frequencies, there is greater attenuation of the triangular scan amplitude, as the scanner requires more drive current to change the angular velocity of the mirror at the end of each scan. At the higher frequencies the maximum scan angles are similar again because the triangular scan becomes sinusoidal in shape as shown in Figure 4. 5. This is because the scanner requires the finite time of ~ 230μs to decelerate to rest and then accelerate in the opposite direction. Consequently, when the time period of the triangular scan becomes comparable with 230μs, the scan becomes similar in shape to a sinusoid. The time taken to scan a length of 224mm at $100ms^{-1}$, is 2.24ms which corresponds to a scan frequency of 223Hz. This is well below the limit of the scanner at all

scanning angles. Consequently, this scanner unit is ideal for the development of the laser scanning system.

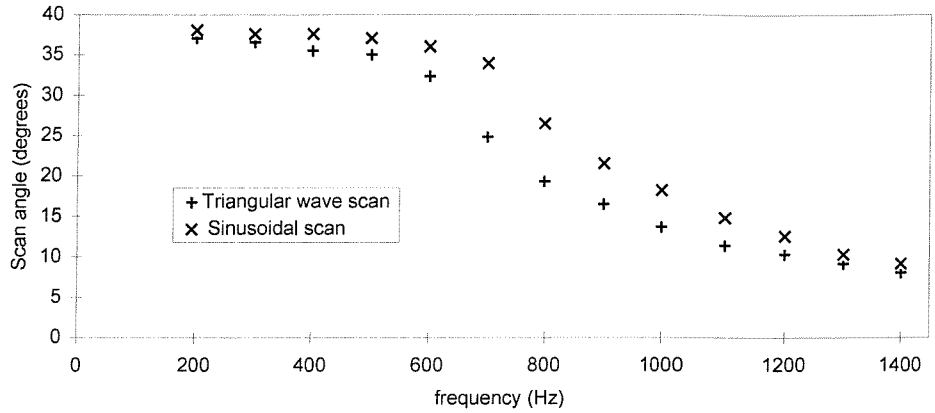

Figure 4. 4. A plot of the maximum scan-angle achievable with a drive voltage of 10.2 V peak to peak for both linear and sinusoidal scans at various frequencies. The measurement errors are ~1.4° and are not shown for clarity.

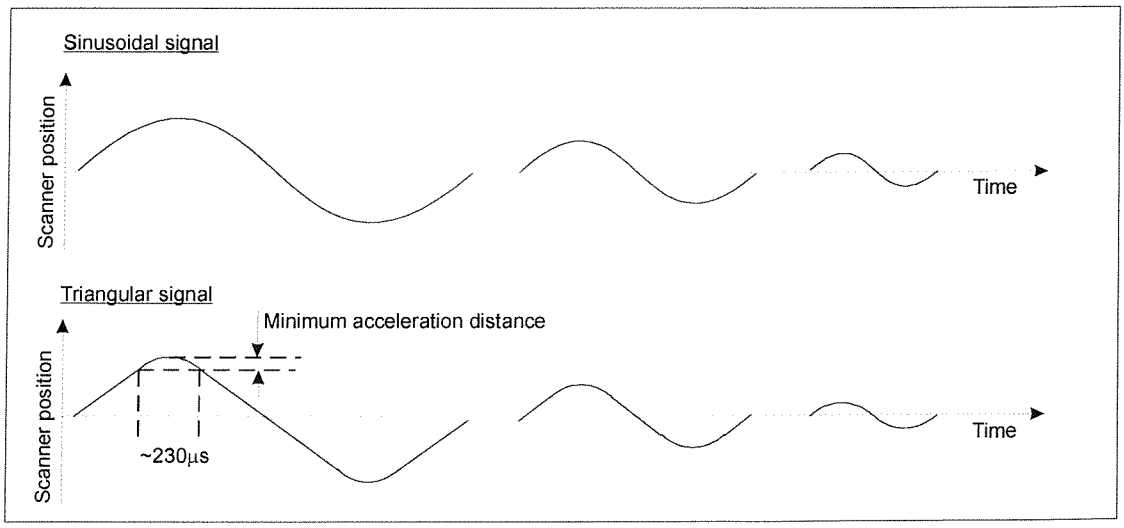

Figure 4. 5. As a triangular scan frequency increases its shape eventually becomes sinusoidal due to the minimum time required to change the direction of the scanner mirror.

4.3.2. The Choice of Scan Systems

Two techniques for scanning the sea surface were considered, an angular scan and a parallel displacement scan. These two ideas are shown clearly in Figure 4. 6. The angular scan enables the laser beam to be scanned over a large area using a small laser scanning system. However, as the distance between the scanner and the surface changes the length of the scanned line will vary. In order to generate a wave spectrum from wave slopes that have been sampled along this line, the position of each sample must be accurately determined.

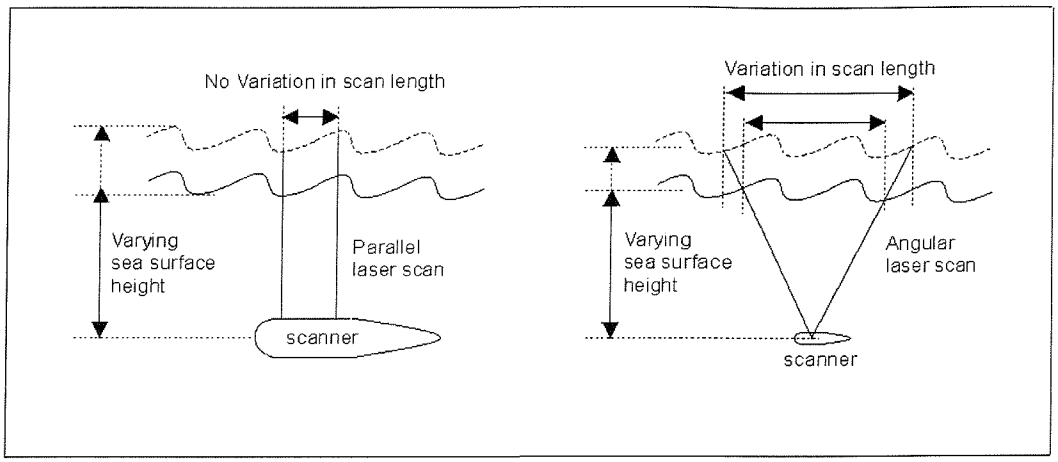

Figure 4. 6. A parallel displacement scan of a laser beam (*left*).
A angular scan of a laser beam (*right*).

An attempt can be made to determine the position of the beam during an angular scan of the sea surface by using the initial and final directions of the laser beam. By considering the geometry of the detector system shown in Figure 4. 7, the initial slope of the laser beam is given by,

$$\frac{x_s}{d} = \tan\phi \tag{4. 11}$$

and the final slope of the beam is given by,

$$\frac{x_d - x_s}{D - d} = \tan\theta \tag{4. 12}$$

where D is known from the detector geometry, x_d and θ are measured using the detector.

Using equations 4.11 and 4.12, the height of the sea surface (d) can be eliminated to give the horizontal position of the laser beam on the surface as,

$$x_s = \frac{x_d - D\tan\theta}{1 - \dfrac{\tan\theta}{\tan\phi}} \tag{4. 13}$$

The problem with this method is that when the initial (ϕ) and final (θ) beam slopes are the same, the position of the laser spot cannot be determined. To calculate the resolution in measuring the position of the beam on surface (δx_s), equation (4.13) is differentiated, to give,

$$\delta x_s = \frac{\frac{x_d}{\tan\phi} - D}{\left(\frac{\tan\theta}{\tan\phi} - 1\right)^2} \sec^2\theta \quad \delta\theta \qquad (4.14)$$

where $\delta\theta$ is the angular resolution of the detector. This was taken as ~0.33° which corresponds to a resolution of 1°. The resolution in measuring the position of the beam on surface (δx_s) is plotted for varying beam slopes (θ) for three different initial scanner angles (ϕ) in Figure 4. 8. The distance between the scanner unit and the detector (D) was set at 1000mm, the distance used by the TLS. For this comparison an arbitrary distance of 200mm from the scanner system to the sea surface was selected. As this distance becomes larger, the sea surface approaches the detector and the resolution will increase. It is clear from Figure 4. 8 that the resolution in determining the position of the laser beam on the surface becomes increasingly poor as the final beam angle approaches the initial beam angle. When the initial beam is vertical its position on the surface is always known. As the initial beam angle moves away from the vertical the position of the beam on the surface becomes more dependent on the water height and so the resolution decreases. Consequently, it may not be possible to determine the position of the beam everywhere in the scan.

The scan length on the sea surface, which varies with surface height, will cause a second complication. The wavelength range and the minimum wavelength resolution, is determined by the distance between wave slopes samples, and will therefore vary. This is not ideal and will make processing this data complex.

It is clear that an angular scan is not ideal and therefore a parallel displacement scan was considered. This technique involves scanning the laser beam parallel to the optical axis of the detector. In this way both the lengths of the scan and the horizontal distance between the sample points are kept constant, regardless of the height of the sea surface. However, all the scanners mentioned in Table 4. 1 produce an angular scan which must be converted to a parallel one. This is achieved using optics within the laser scanning system and consequently, the output aperture of the scanner system must have at least the same dimensions as the scan pattern. The mechanical design of such a system is the main obstacle with this type of laser scanning system.

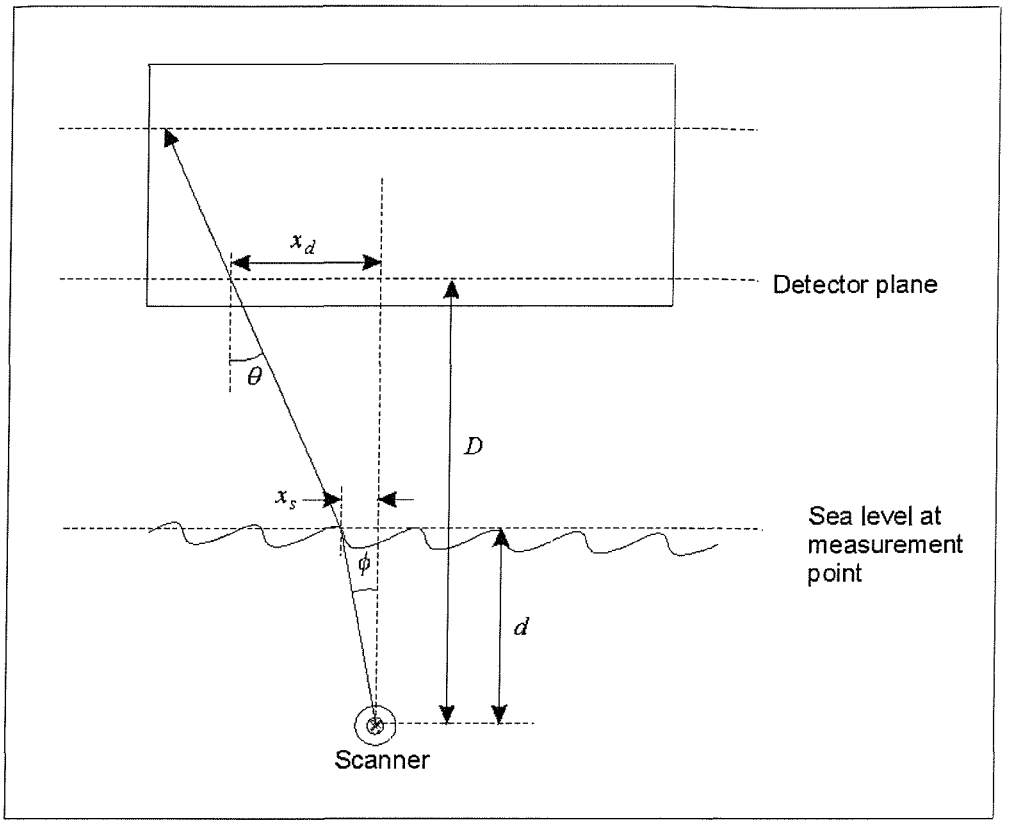

Figure 4. 7. The geometry of the laser beam being refracted at the sea surface while being scanned.

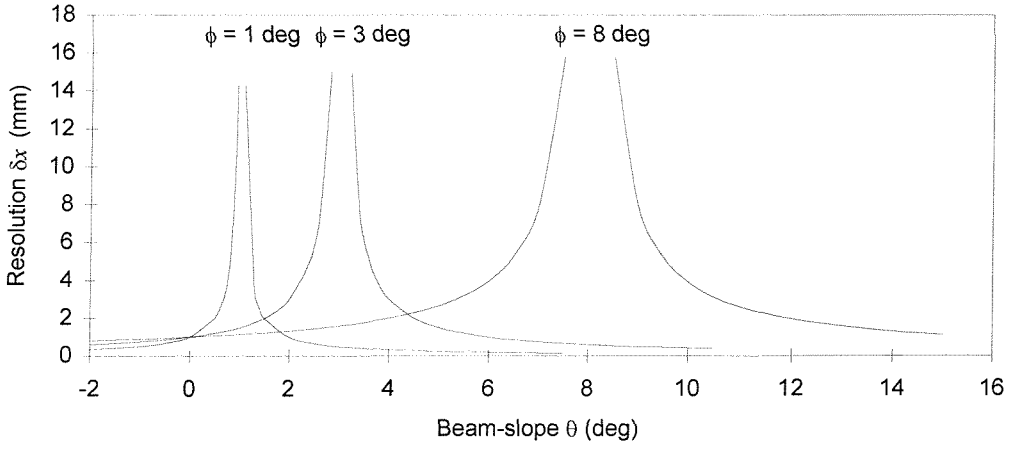

Figure 4. 8. A graph of the beam position resolution on the sea surface with initial beam directions of 1,3 and 8 degrees.

4.4. Laser Scanning Systems - Design Considerations

The laser scanner system design must be robust and relatively simple to use so that it can withstand deployment at sea, in addition to being able to generate a suitable scan pattern at the required speed. With this in mind, the following sections discuss four different designs and suggest the most appropriate design to be deployed at sea.

4.4.1. An Optical Fibre System

Initially, the desire to make the scanner system simple and robust led to development of a laser scanning system that only uses one scanner. Initially a system that used fibres to distribute the light from the laser was considered. The laser beam is scanned across one end of a linear array of optical fibres, the other end of the fibres may then be arranged in the desired scan pattern as shown in Figure 4. 9. This in turn would allow an open grid structure to be used to hold the ends of the fibres in position under the water. This would reduce the amount of drag through the water, however the structure holding the fibres may cause turbulence in the water around the fibre outputs if it is not carefully designed. There are several other design problems regarding the construction of such a system. These difficulties arise in the following areas:

- The laser light has to be launched sequentially into 128 optical fibres. This requires each fibre to be aligned accurately with the laser beam, which is then scanned across them. This is best achieved using a fibre with a large diameter core to provide an easier target.
- The output light from of each fibre must be collimated so that the diameter of the laser beam on the sea surface is ~2mm. This is best achieved using a fibre that has a small diameter core. This will be discussed later in this chapter.
- The collimated laser light from the outputs of the fibres must be aligned so that all the beams are parallel. This ensures that the position of the laser beam on the surface is accurate to better than 1.75mm (half the sample spacing) so that the surface is sampled correctly. If the sea surface were 1m away from the fibre outputs then laser beams would have to be parallel to the axis of the detector to within ±1.75mrads.
- The fibre outputs must be placed 3.5mm apart. This places a space restriction on the collimating optics and alignment systems for each fibre.

Ideally, each fibre would include two lenses, one to focus light into the fibre and one to collimate the light at the output of each fibre. However, when dealing with 128 fibres this

becomes expensive. Alternatively, a single lens could be used to focus the laser light into all the 128 fibres. To assess this option, the beam from a 1mW He-Ne laser was launched into fibres having core diameters of 50μm and 10μm using a standard fused silica lens of focal length 100mm. The best throughput of light for the 50μm core fibre was ~30% whilst for the 10μm core fibre it was ~10% using the same lens. This is not a particularly efficient throughput of light and in both cases very careful alignment was required. In principle, by reducing the focal length of the lens the beam could be focused to a smaller point and therefore, more light could be injected into the fibre, however, this requires even better alignment.

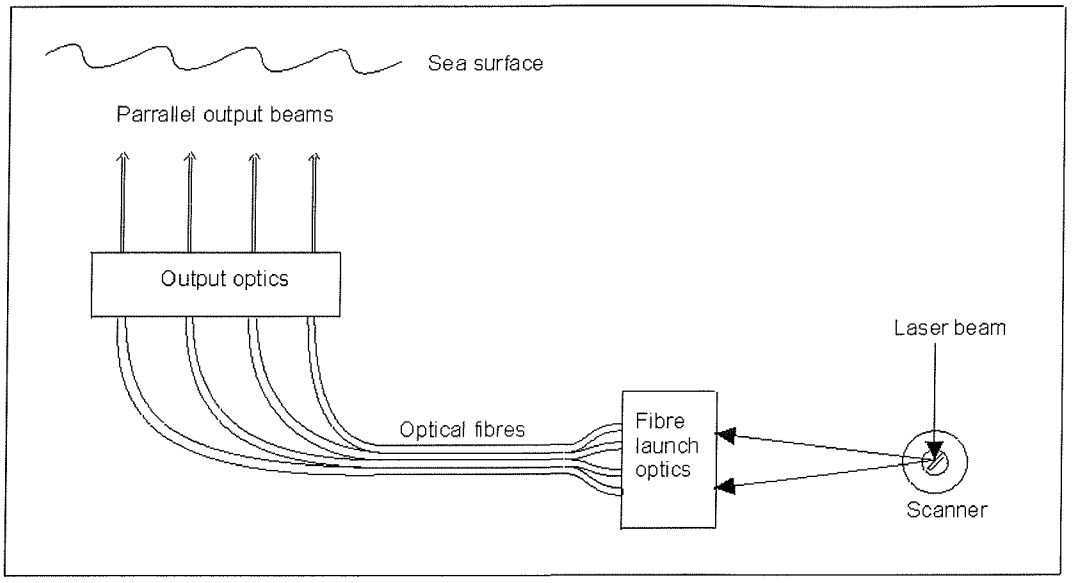

Figure 4. 9. A single scanner can be used to scan light into an array of fibres and at the other end the fibres can be arranged into any scan pattern.

It is not possible to use a similar lens arrangement to collimate the light at the output of the fibres. This is because only light that has emanated from a point source placed at the focal point of a lens will be perfectly collimated parallel to the optical axis of the lens. Light that has emanated from any other point on the focal plane will be collimated but not parallel to the optical axis, as shown in Figure 4. 10. For this reason, a single lens must be used on each fibre output. Unfortunately, commercially available collimating optics for the output of optical fibres are too large to be used in this application. Consequently, a specifically designed optical mount would need to be constructed to hold these lens 3.5mm apart. The alignment of 128 fibres in this way is neither efficient nor robust.

In addition to the alignment of the lenses there is also another problem caused by the limited space available for the collimating lens. If the light exiting the fibre does not emanate from a single point it will not be collimated as previously mentioned. Only a small spherical lens or a gradient index (GRIN) micro lens would be small enough to fit into the available space. For such a lens, the fibre cannot be considered to be a point source. The divergence of light emerging from both these types of lens can be calculated [Appendix A] with the result that neither of these lens can produce a beam of diameter 2mm at a distance of 1m using a 50μm diameter fibre.

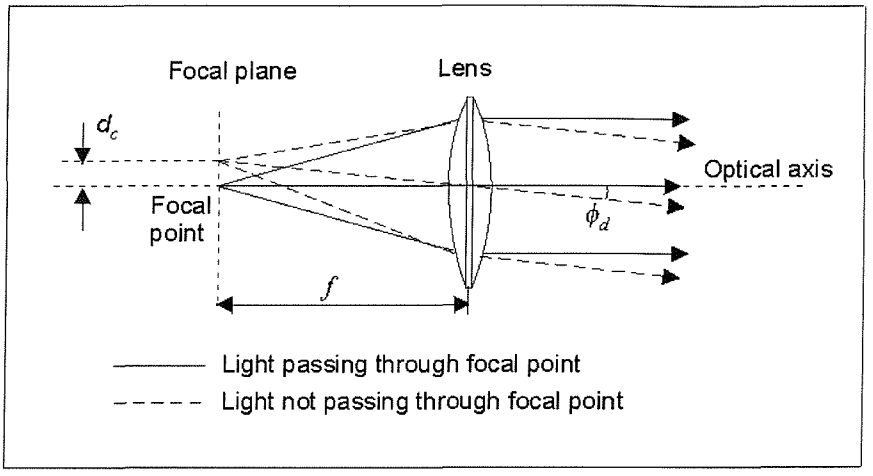

Figure 4. 10. The collimation of light emanating from the focal plane of a lens.

In summary, although a scanned fibre array could provide a flexible method for producing a scan pattern on the sea surface, the throughput of light in such a system is poor. It would also be difficult to develop a system that would allow the fine positioning of the optical components involved.

4.4.2 A Flat Scanning System

The first alternative that was considered was to use an array of small mirrors, to reflect the laser light onto the surface. The mirrors could be arranged so that a single scan across them would produce two lines on the sea surface as required. Each mirror would have to be positioned so that their surface was at 45° to the scanned laser to reflect the light through 90° directly upwards onto the sea surface as shown in Figure 4. 11. This method would have a far better throughput of light, only a few percent of the laser beams initial power is lost at the mirrors. However the mirrors still required fine alignment, which is best avoided.

Alternatively, a single large lens may be used to generate the required parallel displacement scan. By placing the galvanometer scanner at the focal point of the lens, the laser beam may be scanned parallel to the optical axis. The beam leaving the lens could then be reflected onto the sea surface using mirrors in a similar arrangement to that shown in Figure 4. 12.

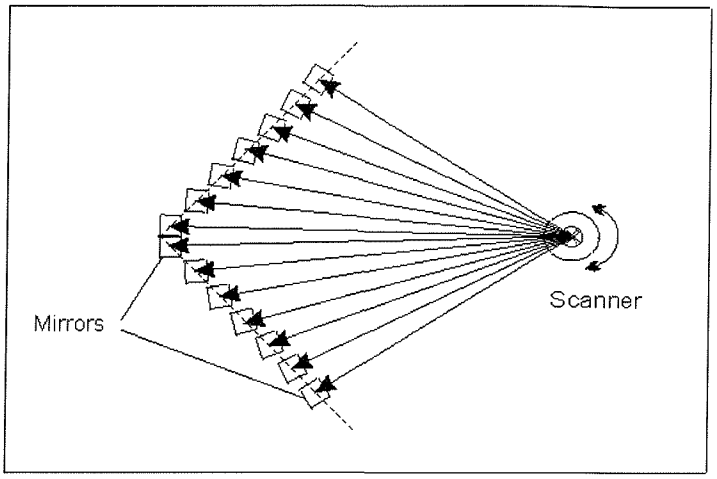

Figure 4. 11. Individual mirrors used to refract the light from a scanner on the sea-surface.

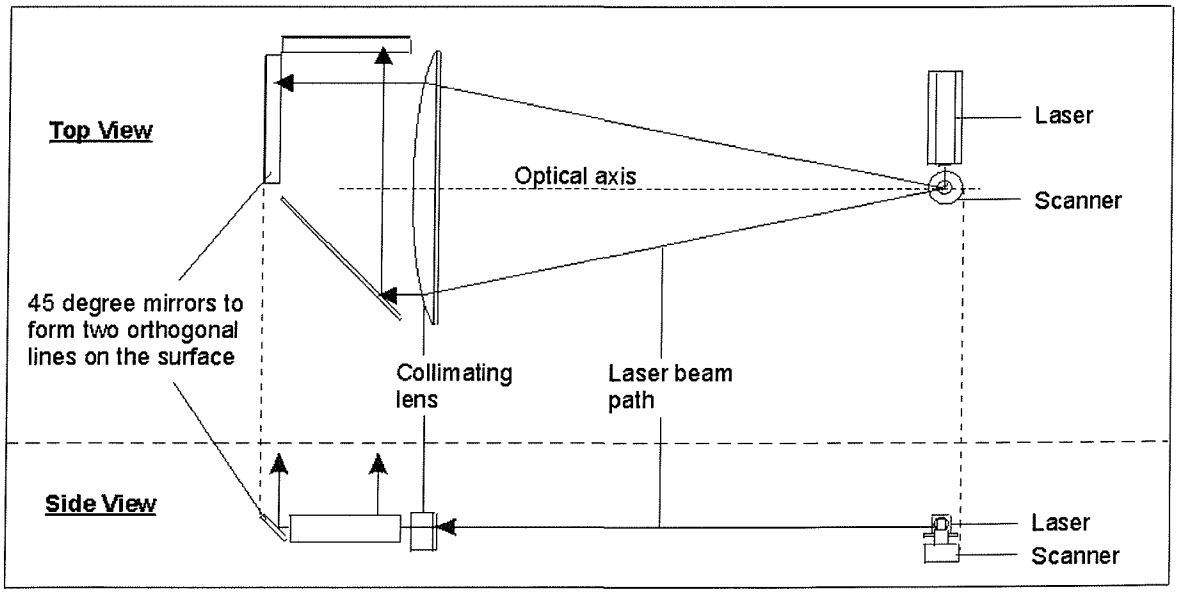

Figure 4. 12. A schematic diagram of the laser scanning components for a single lens scanning system viewed from above (*top*) and from the side (*bottom*).

The optical component layout in this system is relatively simple but it requires a large amount of space. In order to generate a scan length of 224mm the scan lens must be 448mm in diameter. The housing for the scanner unit must be designed so that the drag on it is kept to a minimum as it travels through the water at 1m/s. The best shape for this would resembles a torpedo. For this scanner design the torpedo would have to have a diameter greater 448mm. A laser scanning system that could be housed in a smaller torpedo and offered more flexible scanning patterns was, therefore, considered.

4.4.3 A Spherical Lens System

By placing a two axis galvanometer scanning unit at the focal point of a large spherical lens the laser beam can be scanned across a two-dimensional surface to generate any scan pattern. The scanning unit consists of two galvanometer scanners each moving the laser beam along one of two orthogonal axes. This laser scanning system will fit ideally into a cylindrical housing. The diameter of the lens used only has to be slightly larger than 224mm which is the outer dimensions of the scan pattern suggested. Consequently, the maximum diameter of the housing will be approximately that of the lens. Alternatively, a parabolic mirror that has a similar focal length may be used as shown in Figure 4. 13. Both of these optical systems generate the same results but the lens was chosen because the parabolic mirror option was significantly more expensive.

Several factors determine the dimensions of this laser scanning system. It has already been mentioned that the diameter of such a system is dependent on the diameter of the lens, which must be greater than the scan length of 224mm. The length of the scanner housing, which is less critical in terms of its aerodynamics will depend largely on the focal length chosen for the lens. The longer the focal length the smaller the scan angle required to generate a scan of a particular length. Using a small scan angle allows the scanner to be run at a higher frequency. More importantly the smaller the scan angle the more linear the velocity of the laser beam is, as it moves over the flat surface of the lens. For simplicity, it is easiest to sample at regular intervals in time. However, if the scanner units are run at a constant angular velocity, the velocity of the laser beam over the lens will vary and consequently the spatial intervals between the samples will not be constant. There are two solutions to this problem either the scanner can be run in a way to compensate for this or the scan angle can be kept small so that the non-linearity is insignificant. The simplest solution is to use a small scan angle so that the scanner can be run a constant angular velocity. The nature of this non-linearity was investigated to determine the maximum scan that could be used in this case.

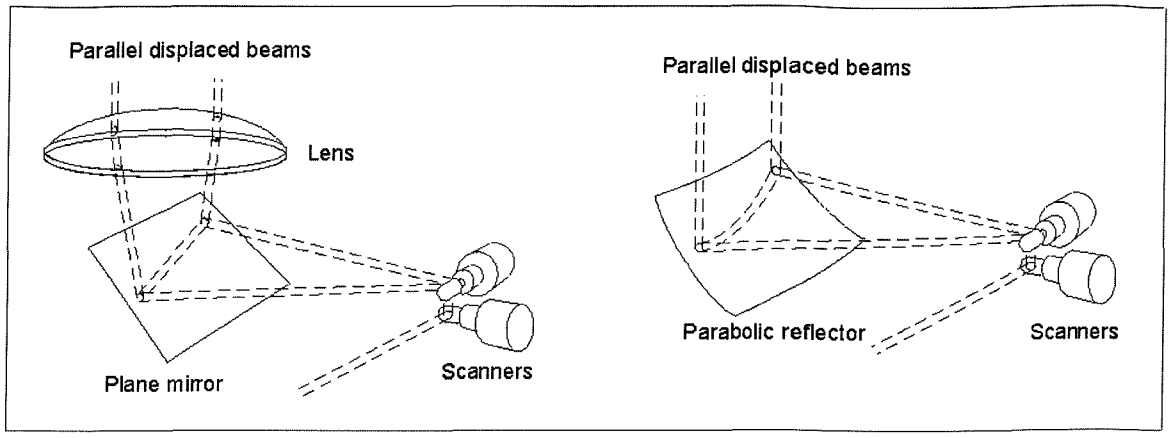

Figure 4. 13. Two methods of generating a 2-dimensional scan using a) a lens and b) a parabolic mirror.

The relationship between the distance that the beam moves (x) on a flat surface, a distance (R) away from the scanner and the scan angle (θ), can be deduced from the geometry shown in Figure 4. 14, and is,

$$x = R\tan\theta \tag{4. 15}$$

Differentiating equation 4.15 the velocity of the beam on the surface is given,

$$v = \frac{dx}{dt} = R\sec^2\theta \quad \frac{d\theta}{dt} \tag{4. 16}$$

To ascertain the non-linearity in the velocity of the laser beam over the surface, the percentage change in velocity was calculated. This was the ratio of the change in velocity over the entire surface to the minimum velocity during the scan. This ratio can be calculated using the minimum velocity that occurs at the centre of the scan. At this point the beam moves the smallest distance over the lens surface for a given angular movement therefore this velocity is given by $v_{min} = R\omega$ and consequently the maximum velocities is given by $v_{max} = R\omega \sec^2\theta_{max}$ (where $\omega = \frac{d\theta}{dt}$). The resultant ratio is then,

$$\%\ \text{Change in velocity} = \frac{v_{\max} - v_{\min}}{v_{\min}} = \sec^2\theta_{\max} - 1 \tag{4. 17}$$

This ratio is plotted for a range of maximum scan angles in Figure 4. 15. From this plot, it can be seen that below 7° the non-linearity in the velocity is less than 1%. The design of the lens and consequently the scanner housing has therefore been chosen appropriately. The detailed design of this scanner housing will be consider further in chapter 7.

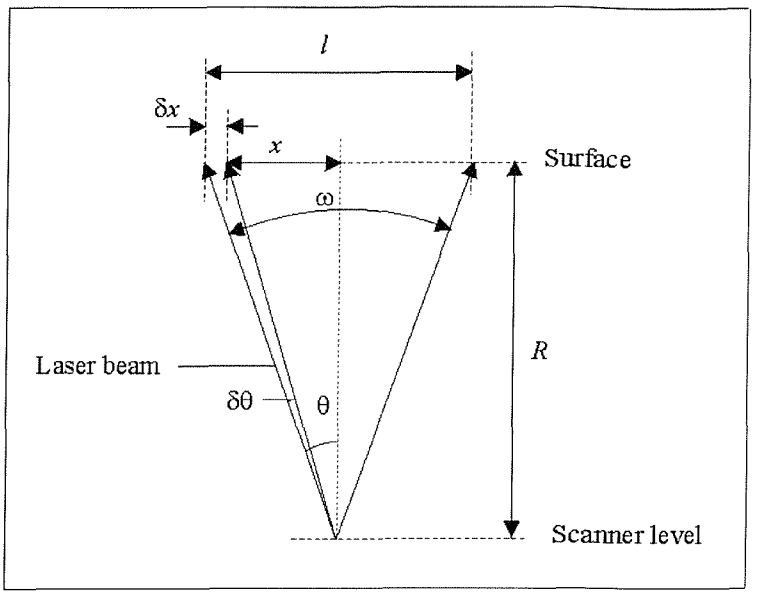

Figure 4. 14. The geometry of a scanned laser beam over a flat surface.

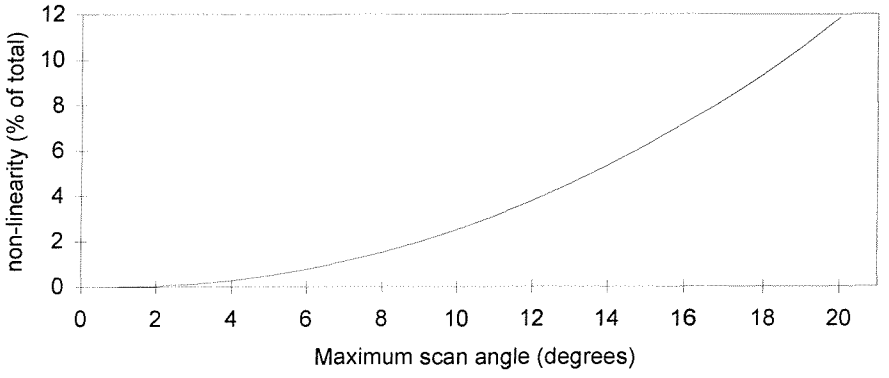

Figure 4. 15. Graph showing the % non-linearity in laser velocity over a flat surface, for varying maximum scan angles.

4.4. Design Implications

A scanning laser system has been described that would allow a wave spectrum to be generated with minimal Doppler shift of the wave components. However, the detector used with the Towed Laser Slopemeter had a wave slope sampling frequency of 250Hz and also generated data that required post processing. This proved to be very time consuming and would not permit a real-time display of the data collected, especially using a higher sampling rate that is required

for a scanning system. It is therefore necessary to design a new detector that could record the wave slopes in a more efficient manner, to allow the scan of the sea surface to be sampled at 28.6kHz and then displayed in real-time. Designing a new detector will also allow the other points discussed in section 3.4 to be addressed so that the instrument is easy to use.

Chapter 5
A New Detector Design Concept

5.1. Introduction

The Towed Laser Slopemeter has provided valuable information about the sea surface roughness. However, it was difficult to deploy, time consuming to retrieve the wave slope information from the raw data and as discussed in chapter 4, the motion of the instrument introduced a Doppler shift into the measurements. Chapter 4 has suggested that a scan of the surface rather than a single point measurement will eliminate this Doppler shift. This requires the sampling rate to be increased from 250Hz to 28.6kHz, so that 64 wave slope measurements could be made along each scan line. Clearly, a re-design of the laser beam detector is required. Ideally, this would allow the data collected to be displayed immediately in real-time. This chapter describes the development of a new laser beam slope detector to record the position of a laser beam on two planes using a digital measurement technique. The concept of this Digital Laser Slopemeter is described. The minimum wave slope range and resolution of the detector is suggested and the dimensions of the detector that are required to achieve this are calculated. A suitable laser will be suggested in the light of the detector concept and a model used to confirm the successful operation of optical components used in the detector.

5.2. Development of the Digital Laser Slopemeter

The Digital Laser slopemeter detector is based on the same idea as the TLS detector. Two detection planes will be used to determine the wave slope without requiring the sea surface height to be known. However, in order to increase the speed with which the wave slope can be measured, the method used to detect the beam position on each of the layers has been changed.

Initially, imaging the bright spot of light generated when the laser beam passes through the TLS's wavelength shifting screens was considered. Either a CCD or a position sensitive detector could be used for this application. However, CCD cameras nominally have a refresh

rate of ~ 50Hz which is not sufficient to for this application. The CCD will also generate a large quantity of data per image that would require processing to generate a beam position. Although position sensitive photodiodes generate a simple voltage signal in a matter of micro seconds, they have a position resolution that is typically 1% of their dynamic range and therefore can not image the detector screen with sufficient precision [Hamamatsu 1995]. Consequently, an alternative approach has been adopted.

Each of the two detector planes comprises of two orthogonal arrays of wavelength shifting fibres as shown in Figure 5. 1. The two arrays will be illuminated as the laser beam passes through each layer. The light trapped within the fibres is detected at the their ends using individual photodiodes. To ensure that the laser beam illuminates both planes, the diameter of the circular fibres is kept small compared to their spacing so that the majority of the beam passes straight through without intercepting a fibre. This beam detection method instantaneously generates the laser beams x and y co-ordinate on the detector layer. The digital slopemeter will, therefore, consist of this detector mounted above the sea surface and the scanner unit that has been described in chapter 4 mounted below, as shown in Figure 5. 2.

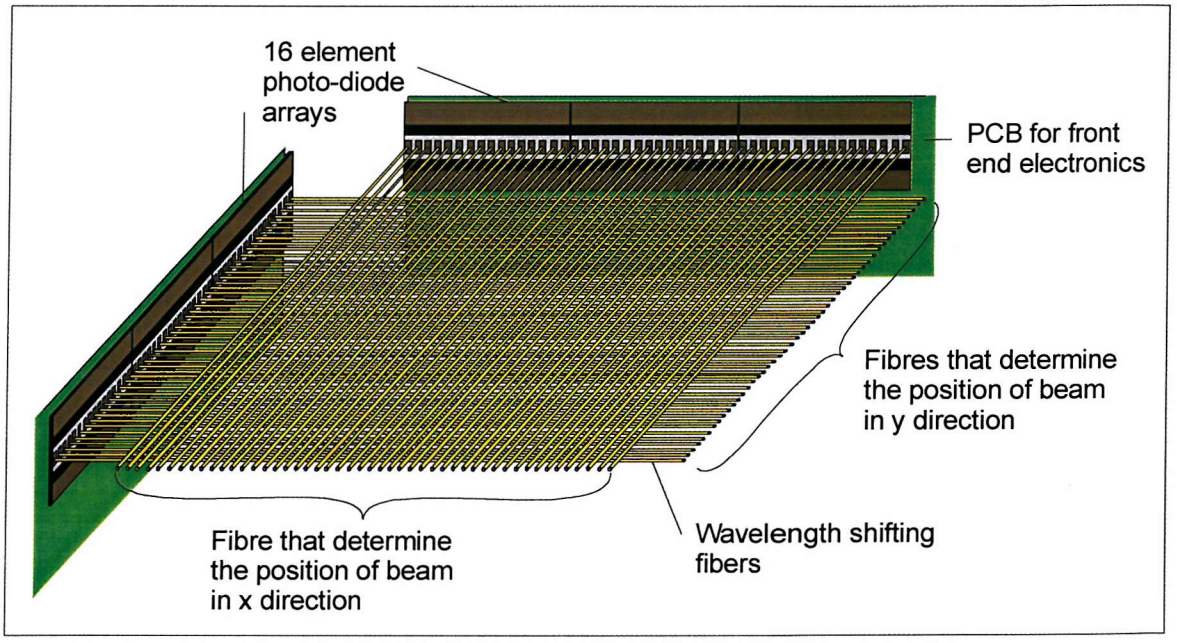

Figure 5. 1. The use of an open grid of fine circular fibres to generated the x and y co-ordinates of the laser beam.

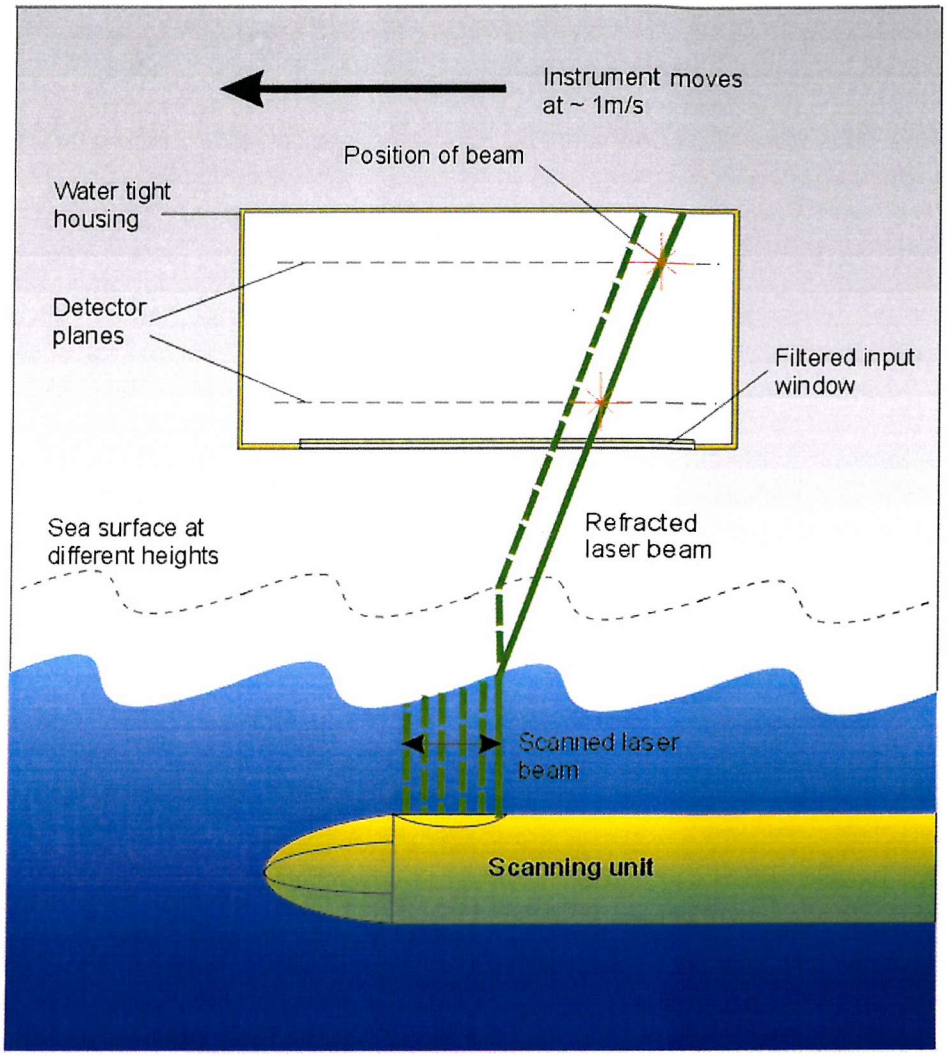

Figure 5. 2. The Digital slopemeter key components.

5.2.1. Detector Geometry

In order to determine the geometry of the detector a wavelength range and resolution must be selected. Although the maximum slope that can be measured is ~48°, after which total internal reflection occurs, such slopes are not frequently observed on the sea. As shown from the data collected in Loch Linnhe by the TLS, which is plotted in Figure 5. 3, there are very few wave slopes greater than ±30° [Taylor, 1996]. This has also been seen during other observations [Shaw et al. 1996, Cox et al. 1954]. The wave slope data collected by the TLS, suggests that the new detector must be capable of measuring wave slopes along the length of the 224mm scan with a range of at least ±30° and with a resolution equal to that of the TLS, of at least 1°. This is equivalent to measuring a beam slope range of ±12° with a resolution of 0.33° (using equation 3.2).

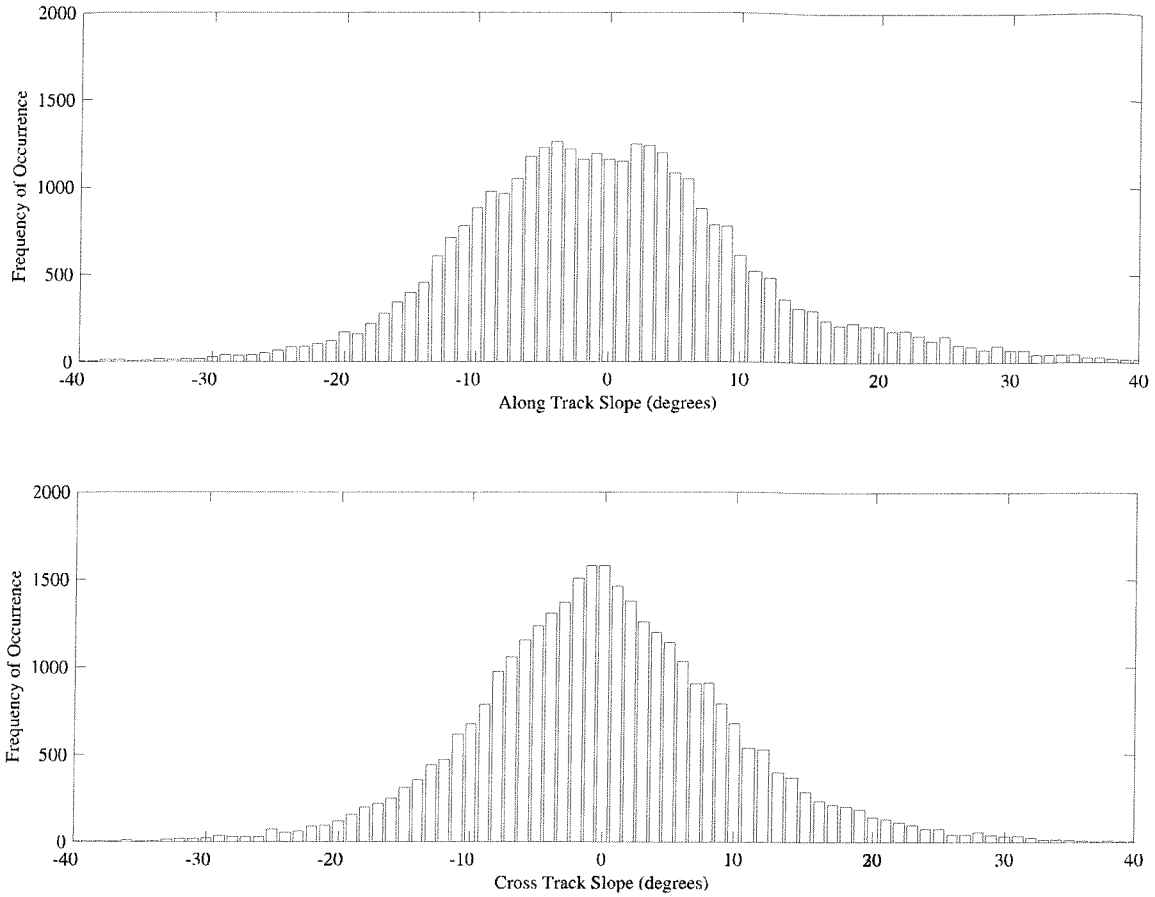

Figure 5. 3. Wave slope histogram of data collected by the TLS during run 3 on the 9th September 1994 in the Loch Linnhe field trials.

Using this range and resolution, the minimum dimensions of the detector can now be determined by considering the following quantities:

- The fibre spacing on each detector plane (δx) and consequently the beam position resolution.
- The distance between the detector planes (D).
- Distance from the bottom detector plane to sea-surface (h).
- The furthest distance between two points on the scan (L).
- The diameter of the top detector plane (d).

These values, shown in Figure 5. 4, will completely describe the geometry of the detector. The electronic and mechanical components can then be designed appropriately for this size of detector.

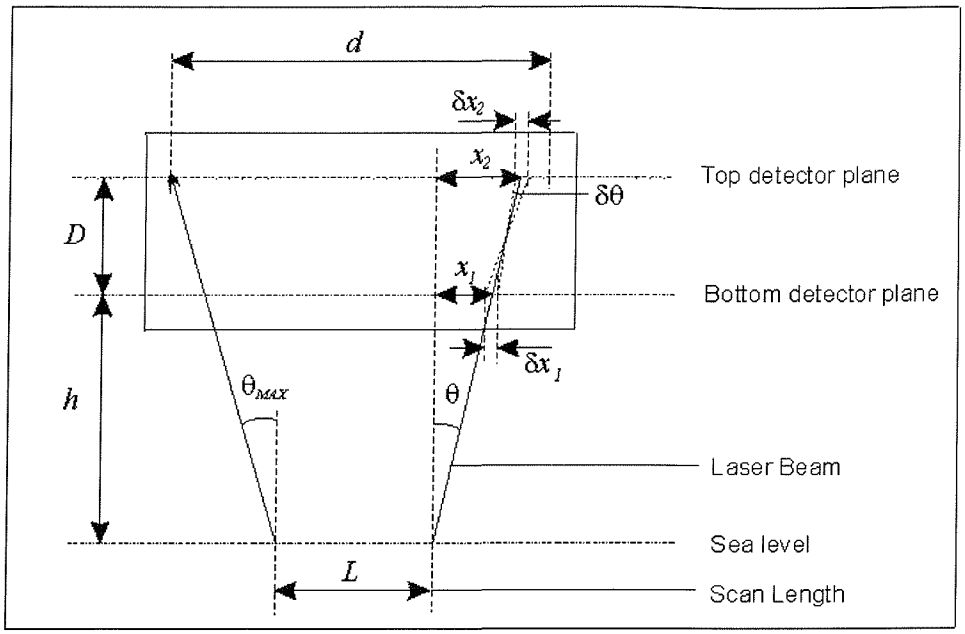

Figure 5. 4. The dimension definitions of the of the laser slopemeter detector.

5.2.1.1. Fibre Spacing

The chosen fibre spacing must allow the majority of the incident laser beam to pass through the grid of fibres, ensuring that subsequent fibre layers are illuminated. Although, it is possible to obtain 250μm diameter fibres, they are not robust enough and are, therefore, impractical for this use. The smallest practical diameter of wavelength shifting fibres is 0.5mm. A suitable photodiode must be chosen to detect the light output from these fibres. A 16 element photodiode array [Hamamatsu, 1996] was chosen. Each photodiode in this array has a detection area of 1.1mm x 2.0mm and is spaced 1.575mm apart. Each array is mounted side by side. The two photodiodes at the ends of adjacent arrays have a spacing of 1.975mm. A fibre spacing of 1.6mm ensures that there is a regular grid of fibre that align with the photodiodes along the entire length of the detector layer.

This spacing also ensures that a 2mm beam will never fall between the fibres, and that sufficient light will still pass between the fibres to fall onto the subsequent layers. It is this spacing and the method chosen to acquire the position of the beam that determines the minimum resolution of the detector.

If the brightest fibre is taken as the position of the beam, then the resolution will be ±1.6mm. However, if all the fibres illuminated are taken into account, then the resolution can be reduced to half this value simply by counting the number of fibres and choosing the central position. The principle behind this method is shown in Figure 5. 5a) and b). Using this technique, for certain beam diameters it is possible that as soon as the edge of the beam leaves one fibre it illuminates another fibre. In this case, the centroid can only be determined to ±1.6mm, as shown in Figure 5. 5 c) and d). In either of the two methods the resolution is never less than ±1.6mm.

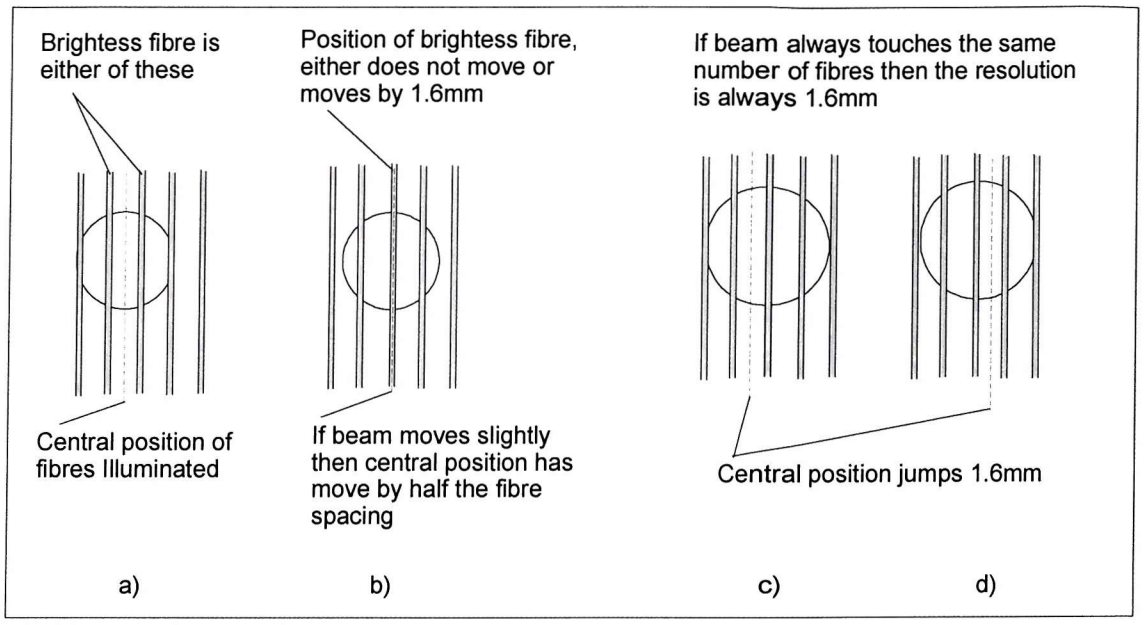

Figure 5. 5. a) and b) show how the resolution is reduced to half the fibre spacing by taking into account all the fibres illuminated, c) and d) show how this is reduced back to the original resolution for certain beam diameters.

5.2.1.2. Detector Plane Separation

Using a value of 1.6mm for the beam position resolution (δx) and the required beam slope resolution ($\delta\theta < \pm 0.33°$), the plane separation (D) can be determined. By considering Figure 5. 4, the positions of the laser beam on the two detector planes can be related to the slope angle by,

$$\frac{x_2 - x_1}{D} = \tan\theta \qquad (5.1)$$

By adding the errors from both planes (δx_1 and δx_2) in quadrature, the error in measuring the beam slope ($\delta\theta$) with respect to x_1, x_2 and D can be determined as,

$$\delta\theta = \sqrt{\left(\frac{D}{D^2 + (x_2 - x_1)^2}\right)^2 \left(\delta x_2^{\,2} + \delta x_1^{\,2}\right)} \qquad (5.2)$$

The uncertainties in the x positions (δx_1 and δx_2) at worse will be ±1.6mm so that $\delta x_2^{\,2} + \delta x_1^{\,2} = 5.12$. The largest value of $\delta\theta$ is when $x_2 - x_1$ is zero, which corresponds to a zero beam slope ($\theta = 0$). In other words the detectors resolution is poorest for low beam slopes. For zero beam slope, equation 5.2 reduces to,

$$\delta\theta = \sqrt{\frac{5.12}{D^2}} \qquad (5.3)$$

This relationship is plotted in Figure 5. 6 and a line corresponding to the angular resolution of ±0.33° is also marked. This graph shows that the minimum distance between the detector planes (D) which ensures that the angular resolution is at least ±0.33°, is 400mm.

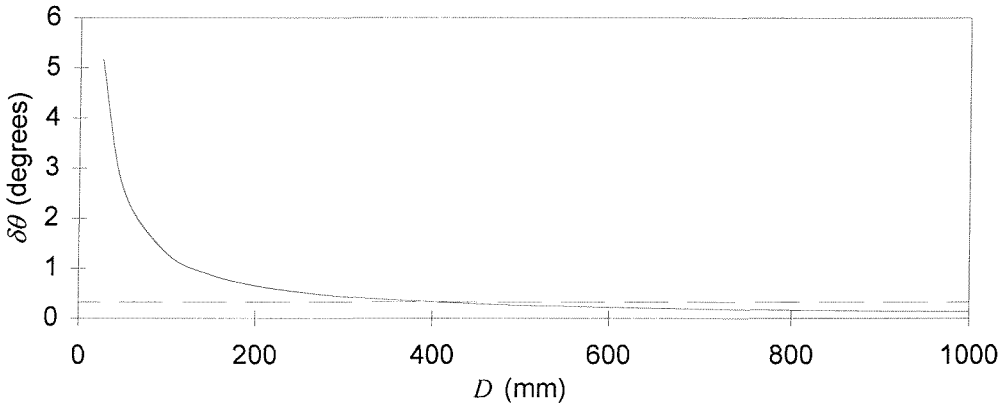

Figure 5. 6. The relationship between the angular resolution ($\delta\theta$) and the distance between the detector planes (D) for beam position resolutions of ±1.6mm. The dashed line marks the angular resolution of ±0.33°.

5.2.1.3. Dimensions of the Top Detector Plane

The dimensions of the top detector plane determine the maximum range of wavelengths that can be measured. The further the sea surface is from this detector plane, the larger it must be to measure a beam slope of ±12°. The relationship between the dimensions of the top detector

plane (d) and beam slope at the extremes of the scan pattern (θ_{max} = 12°) can be calculated from the geometry in Figure 5. 4 as,

$$d = 2(D+h)\tan\theta_{\max} + L \qquad (5.4)$$

where L is the distance between the two most extreme points in the scan, which in this case is 224mm. The minimum distance for plane separation (D) has already been chosen to be 400mm. During the deployments of the TLS, it was observed that the change in sea surface height relative to the vessel in the sea condition that the instrument was deployed, was <1m. This was, therefore, chosen as the maximum distance from the sea surface to the detector (h). Using these values the minimum dimensions of the top detector plane should be at least 819mm.

The readout electronics has been designed in modules that will read out 64 fibres. Each of these PCB modules was 265mm long in order to layout the required readout circuit. Consequently, a convenient distance between the detector planes for the electronics designed in chapter 7 was 550mm. From Figure 5. 6 the beam slope resolution of the detector will, therefore, increase to ±0.24° calculated using equation 5.3. This corresponds to a wave slope resolution of ±0.71°, calculated using,

$$\tan\theta_s = \frac{\sin\theta_b}{\frac{n_w}{n_a} - \cos\theta_b} \qquad (5.5)$$

where θ_s is the sea surface wave slopes, θ_b is the laser beam slopes and n_w = 1.33 and n_a = 1, are the refractive indices of the water and air respectively. This equation is discussed further in section 6.5. Using equation 5.4, the dimensions of the top detector planes must therefore increase to at least 959mm. The number of fibres, spaced 1.6mm apart that are required to cover this length, are 600. The next suitable number of fibres that may be read out by the 64 fibre PCB modules, are 640. This detection area has the dimension 1022.4mm x 1022.4mm and requires 10 PCB readout modules per axis. This will consequently increase the range of beam slopes that can be measured to 14.4°, calculated using equation 5.4. This corresponds to a wave slope of 34.6°, using equation 5.5.

5.2.1.4. Summary of Detector Geometry

A detector concept has been selected that will be capable of recording the wave slopes from a 2-dimensional scan of the sea surface in a simple and efficient manner. The final dimensions of the detector are summarised in Figure 5. 7.

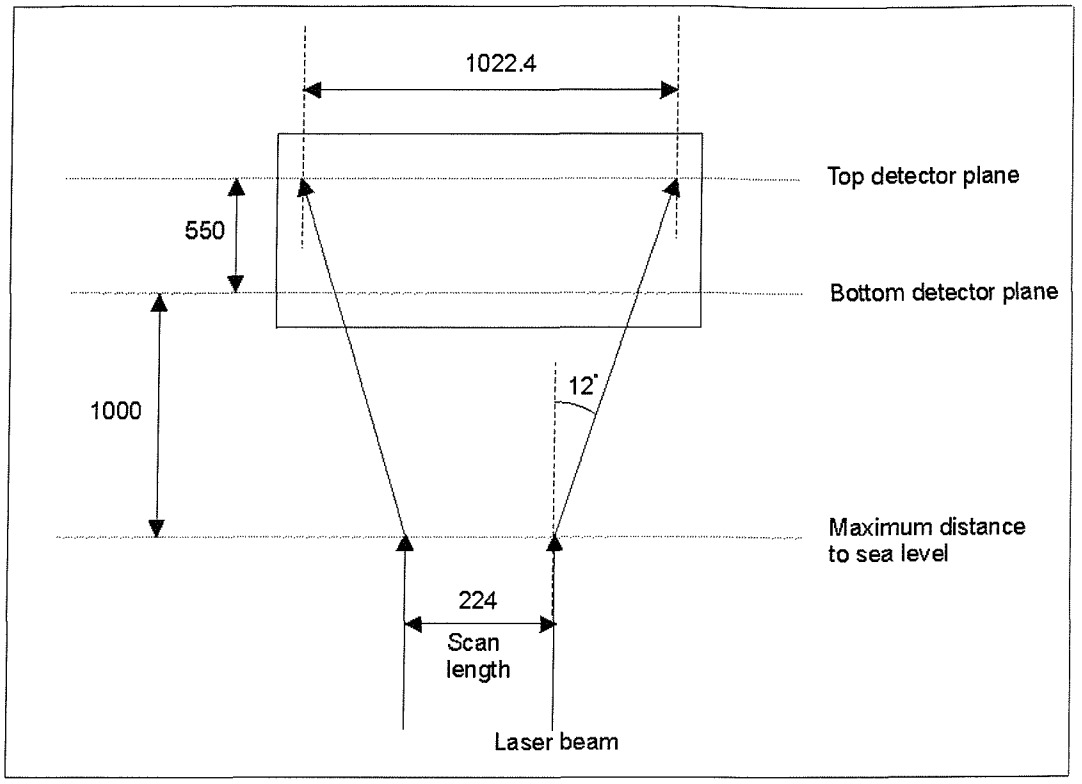

Figure 5. 7. Minimum dimension of the detector.

5.2.2. Laser Light Source

The large HeCd gas laser incorporated in the design of the TLS was difficult to use at sea because of its size and fragile nature. The obvious choice for this application would be a diode laser, which in spite of its compactness can produce relatively high output powers. These laser diodes emit light at wavelengths greater than 635nm [Melles Griot, 1994]. However, the maximum wavelength that can be absorbed by a commercially available wavelength shifting material is around 530nm [BICRON, 1991]. There are, however, many laser dyes that can absorb the light generated by a laser diodes. Whilst these dyes are usually soluble in ethanol for example, they can not be suspended in a plastics material. For this application, a dye dissolved in a liquid could be held within a fine glass capillary tube in order to produce a wave-guide that absorbs red light. The efficiency of such a glass light-guide containing Ethanol is 13.2%. [Appendix B]. The assembly and sealing of such a capillary fibre detector is difficult, it requires the dye solution to be sealed into capillary tube over a meter long, without trapping air bubbles. Furthermore, the red light generated by laser diodes is attenuated by water considerably more than blue and green light, as shown in Figure 5. 8 [Pickard et. al., 1990]. Consequently, an alternative combination of a detection material and a laser were sought.

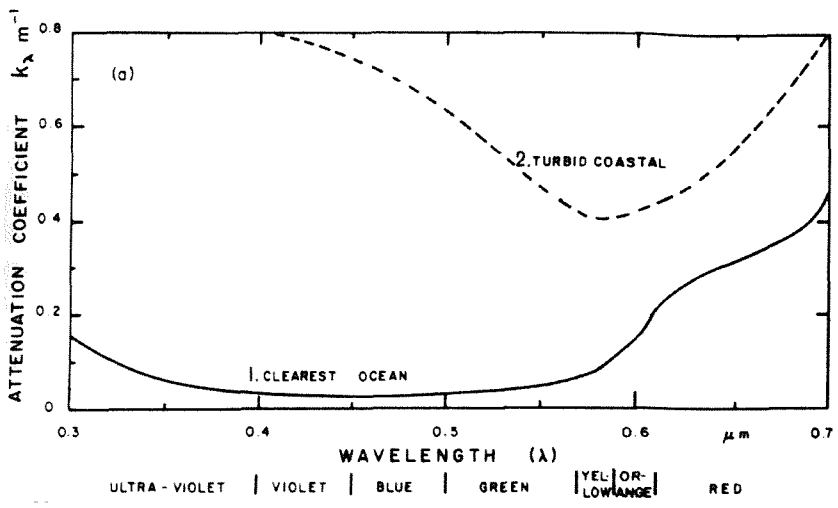

Figure 5. 8. The attenuation coefficient for clear sea water and turbid coastal water as a function of wavelength.

In 1996 a high power frequency doubled, diode pumped, Nd:YVO4 crystal laser became commercially available [Laser 2000, 1996]. This generated green light at a wavelength of 532nm. This wavelength corresponded to the absorption band of a wavelength shifting material produced by BICRON [1991]. The absorption spectrum of this material is shown in Figure 5. 9.

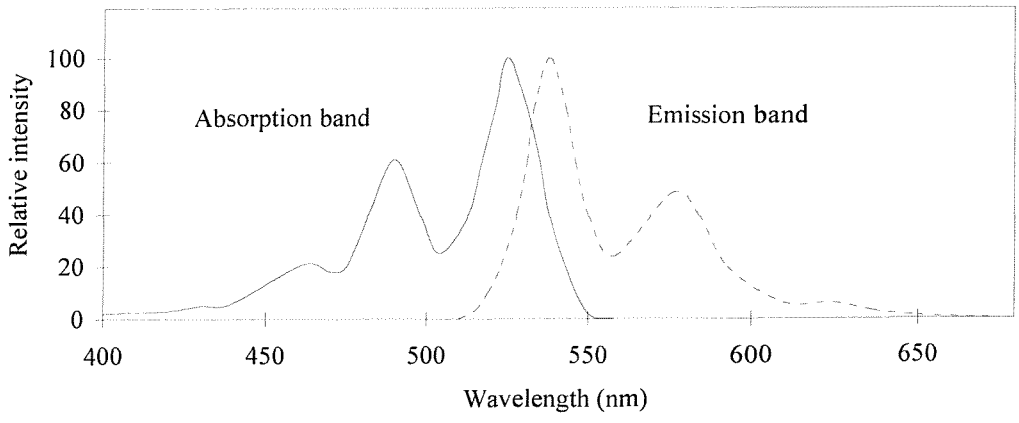

Figure 5. 9. Absorption and emission spectra of the wavelength shifting dye BCF-99-06A.

The combination of this new laser and the wavelength shifting material meant that green light, which is attenuated relatively little in water, could be detected effectively. Although not as small as a diode laser, this laser is much smaller than the HeCd laser originally used with the TLS, as shown in Figure 5. 10. This diode pumped laser only requires 19W of power compared with the 500W required by the HeCd laser. The diode pumped laser also requires a warm up

period of only 10 minute before it produces a stable output, compared to the 30 minutes that the HeCd laser required. The combination of this new laser and the BCF-99-06A wavelength shifting material, therefore, formed the basis for the design of the new instrument.

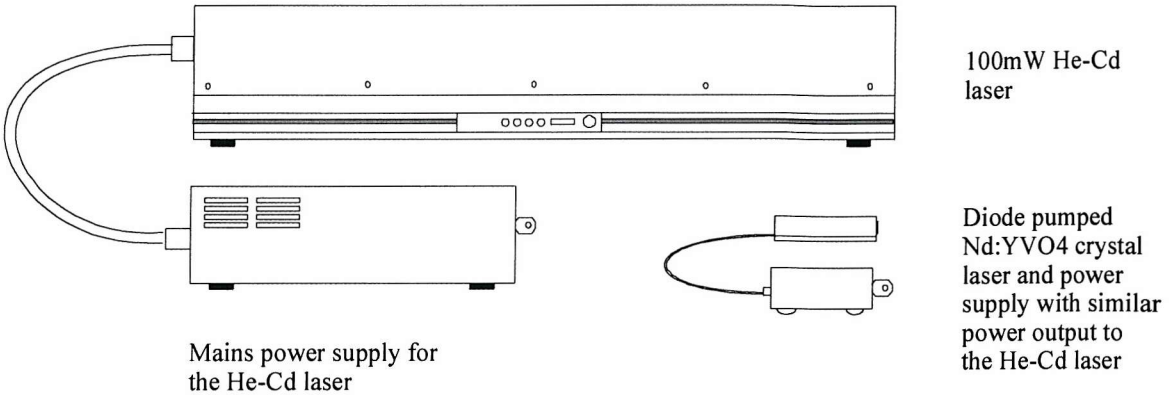

Figure 5. 10. The relative size of the He-Cd laser used with the TLS and the new diode pumped Nd:YVO4 crystal laser.

5.2.3. Detector Concept Evaluation

Using the detector and a fast electronic readout, 128 beam slopes will be recorded throughout a scan of the sea surface. This will allow a wave spectrum to be constructed and a real-time or near real-time display of the data to be provided. To evaluate the operation of the fibre detector, some simple optical simulations were run to evaluate whether the laser beam generated a sufficiently strong signal in the fibres illuminated.

Two simulation where run. The first was to determine whether scattered light would cause a significant signal in any of the fibres in the detector that where not being illuminated by the primary beam. The second simulation gave an indication of the output signal levels that might be expect at the ends of the fibres throughout the detector.

When the laser beam illuminates a fibre approximately 30% of the light that is actually incident of the fibres is absorbed and wavelength shifted. The remaining light is refracted as it passes through the fibre and is spread along a line that is perpendicular to the fibre as shown in Figure 5. 11. This scattered light will be significantly less intense than the primary beam, however, this was verified using a ray-tracing simulation.

The ray-tracing program [Lambda Research Corp, 1995] was used to simulate the path of the laser light through a single fibre. In the simulation a beam with diameter 2mm illuminated a fibre of diameter 0.5mm as shown in Figure 5. 11. The exit plane shown in Figure 5. 11 corresponds to the top detector plane. The simulation showed that for the area of the exit plane that was directly illuminated by the beam the intensity of the light was three orders of magnitude greater than the scattered light. This was later confirmed experimentally, using a photodiode to measure the intensity of the light scattered along the line perpendicular to the fibre.

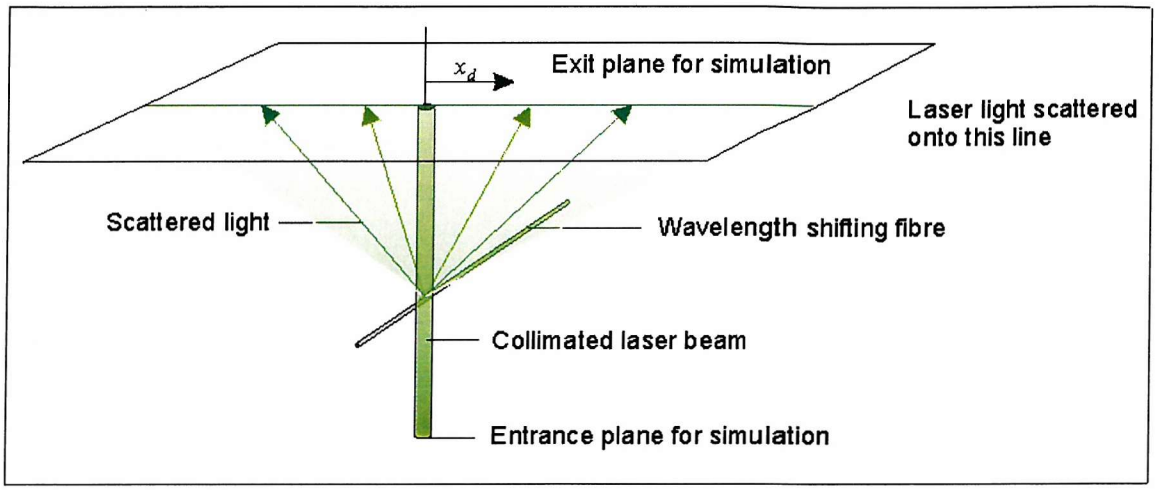

Figure 5. 11. The geometry used to simulate the path of light as it passes through a cylindrical fibre.

To ensure that the fibres in the upper detector layer are never completely shadowed by those in the lower detector layer, the two detector planes are placed at 45° to each other, as shown in Figure 5. 12. However, the final layer of fibres in the detector may still absorb significantly less light. The path of laser beam through the detector was therefore, simulated to determine how much light was absorbed by each fibre.

The simulated detector consisted of two planes each having x and y fibre layers. The fibres were placed 1.6mm apart. The cross section of the laser beam was divided into an array of finite elements. The light from each element was then passed through the detector and if a fibre absorbed the light, it propagated no further. This created a shadow beyond that point. The simulation assumes that a perfectly collimated beam of light is used, whereas in practice the beam will diverge slightly and the shadow on the top layers will never be complete. All the elements in the array, that intersect a particular fibre, are summed together to obtain the fraction of the beam that is incident on that fibre. Once the entire beam's path has been traced, the angle at which the beam is inclined is incremented. The beam angle was varied from 0° to 12° in this process. The fraction of the laser beam energy that was absorbed by each fibre within the

detector was measured for a range of angles. The initial position that the beam emerges from the sea surface was kept constant throughout this process.

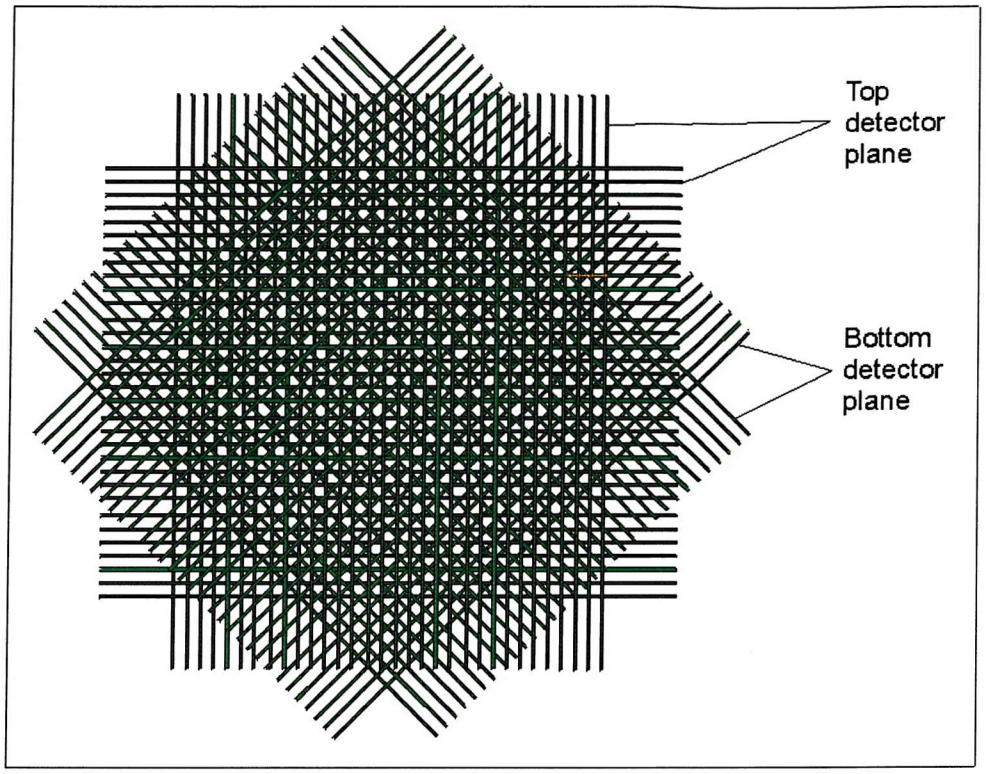

Figure 5. 12. The orientation of the fibres within the detector.

It is possible to calculate the energy that was absorbed by each fibre by multiplying the fraction of the beam absorbed by the initial power of the laser beam. It was assumed that the light intensity was uniform across the diameter of the beam. It will actually vary, however, this will cause the fibre nearest the centre of the beam to absorb more light consequently improving the detectors performance. By considering the way in which the light is trapped and transmitted down the fibre, the energy emitted at its end (P_E) can be calculated using the following equation [Appendix B],

$$P_E = P_I f e^{-\frac{l}{l_A}} \qquad (5.6)$$

where l_A is the attenuation length of the light travelling down the wavelength shifting fibres quoted as 3.5m [BICRON, 1991]. The quantity f is the fraction of the incident light that is trapped in the fibre by total internal reflection after it has been absorbed by the dye and then remitted isotopically as shown in Figure 5. 13. The cone angle below which the light is trapped within the fibre depends on the refractive indices of the core material of the fibre and that of the air. The total trapping efficiency of this fibre is 16.4% [Appendix B]. Therefore, the total fraction of light trapped in the fibre (f), taking into account both the trapping efficiency of the

fibre (16.4%) and the fraction of light initially absorbed (30%) is 4.9% of the initial incident energy.

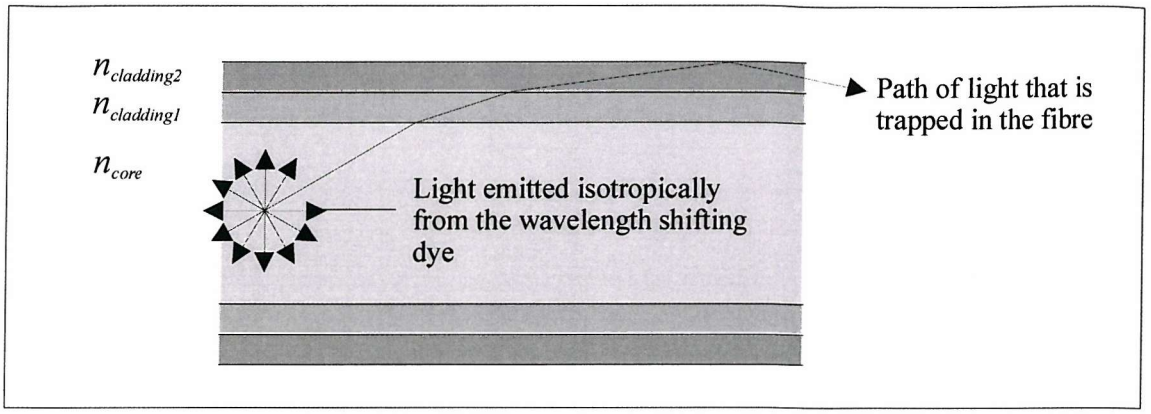

Figure 5. 13. The construction of a wavelength shifting fibre and the path that light will take when it is emitted from the wavelength shifting dye.

The light intensity at the ends of the fibres can now be calculated using equation 5.6. The wavelength of laser light used lies directly between the absorption and emission bands of the dye. Therefore, there is a significant amount of re-absorption of the light trapped within the fibre. Although, the exact level of re-absorption was not known at this time, a reduced attenuation length of 1m was used in the simulation. Once the power output from the fibres had been calculated the light response of the photodiodes of 0.3A/W, could be used to calculate the current [Hamamatsu, 1996].

In the simulation, the laser beam was scanned from 0° to 12° along a single y fibre in the first plane. The initial position of the beam was 600mm from the output end of the fibre and it was then scanned away from this output. For each position of the beam, the current generated by the photodiodes in each fibre in the detector was calculated. The largest photodiode signals generated on the very top and very bottom layers have been plotted, in Figure 5. 14.

The most important result is that at no point are the fibres in the top plane obscured by those below. The position of the beam is, therefore, always known on both planes, allowing the slope of the beam to be monitored continuously. For the conditions summarised in Table 5. 1, the simulation shows that the signal levels will always be greater than ~40μA. Notice that the attenuation of the signal down a fibre on the upper layer is less. This is because the top layer is orientated at 45° with respect to the bottom layer and therefore when the laser is moved a distance l across the bottom layer it moves a distance $l\cos 45°$ across the top layer. It is

interesting to note that the fibres in the lower layer shadowing those in the upper layer cause the higher frequency oscillations. The lower frequency oscillations on the other hand are shadows caused by the fibres in the upper y layer. For this simulation the distance between the detector planes had not been finalised. However, this distance only affects the position of the fibres being illuminated and not the intensity of the light from the fibres outputs and therefore did not adversely effect the results.

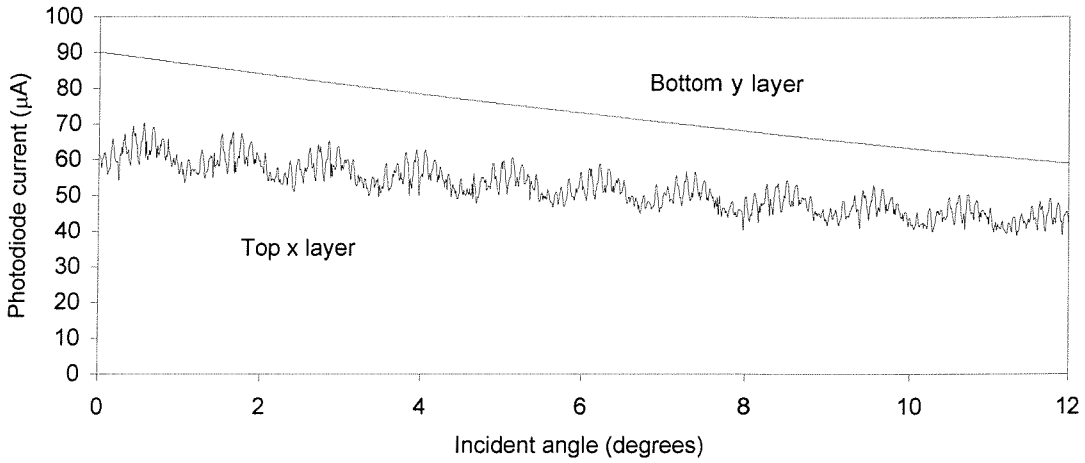

Figure 5. 14. A plot of maximum predicted photodiode current at a given beam angle for the parameters shown in Table 5. 1.

A 150mW laser will be used when this instrument is deployed at sea and its output power will be adjustable to allow for different turbid sea states. The electronic readout that is described in chapter 6 was designed to detect the position of a laser anywhere along the length of the fibre, for a incident beam intensity of 10mW. For this laser beam intensity, the simulation suggested that the largest currents that might be expected on the lowest and highest fibre layers would be 18μA and 12μA respectivily, one fifth of those shown in Figure 5. 14.

The attenuation length of the fibres was measured to determine a more accurate value than initially used in the simulation. The light intensity emitted at the end of a fibre was measured, for the beam at various distances along it. The data that was collected is shown in Figure 5. 15 with two exponential fits also shown. There are two parts to this attenuation curve. The first part has a much larger gradient caused by the immediate re-absorption of light. The logarithm of the output intensity was plotted as a function of distance for this data, which was then fitted using the least squares method. The gradient of this fit gave the attenuation length to be 309 ± 24mm. Similarly, there is an attenuation length of 670 ± 29mm when the laser beam intersects the fibre at a distance greater than 200mm. In this section there is far less re-absorption taking place although evidently it still occurs, as the attenuation length is considerably less than 3.5m.

This measurement has shown that the signal levels at the ends of the fibre will be reduced to approximately 10% of their initial value. The electronics readout system must detect the signal levels when the laser beam is anywhere on the fibre's length. Using the measured attenuation length, the simulation suggests that the lowest currents produced would be 1.2μA and 1.8μA for the top and bottom detector layers respectively.

This simulation has therefore suggested that the detector readout electronics, that will be described in the next chapter, may be capable of measuring output signals that vary from 18μA to 1.2μA. More importantly these simulations have shown that this detector design concept is feasible.

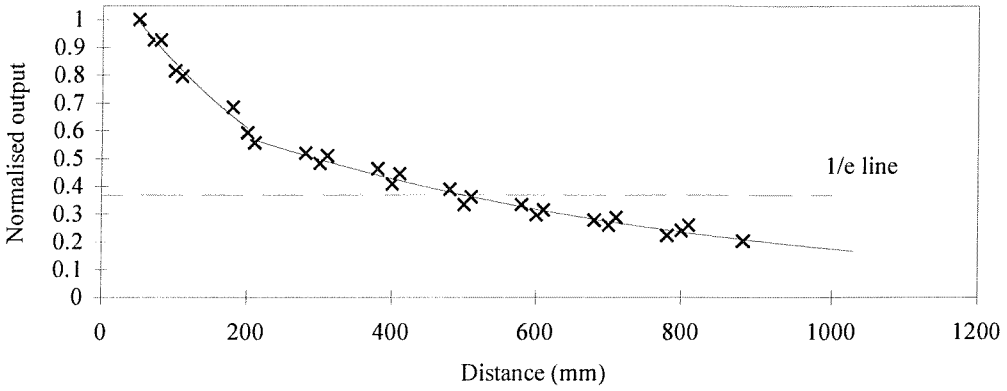

Figure 5. 15. The signal strength attenuation at the photodiode as the laser beam moves down the wavelength shifting fibre. The measurement errors in the distance are ±5mm and in the signal are ±0.02 of the normalised output. These errors are not shown for clarity.

Optical Parameters		**Geometry of Detector**	
Laser power	50mW	Fibre diameter	500μm
Beam diameter on fibre layer	5mm	Distance between fibres	1.6mm
Beam diveragance	0°	Distance between fibre planes	300mm
Fraction of incident light trapped, *f*	4.9%	Orientation of top to bottom plane	45°
Attenuation length of fibres	1000mm	Distance from top plane to sea	1000mm
Photo sensitivity of photodiode	0.3 A/W		
Beam Orientation			
Initial angle of beam	0°	Maximum beam angle	12°
Initial position of beam on bottom *y* fibres	600mm from photodiode	Scan direction of laser beam on bottom *y* fibres	Away from photodiodes
Angular step size between recordings	0.01°		

Table 5. 1. Condition used in the simulation of a multi-fibre laser beam position detector.

Chapter 6

Detector Electronics

6.1. Introduction

To record wave slopes from the multi-fibre detector described in chapter 5, the centroid of the laser beam must be measured on the x and y axis of each of the two detector planes simultaneously. The readout electronics, therefore, has to read the signals from 2560 photodiodes and determine the x and y co-ordinates of the laser beam on both detector planes within 35μs. These x and y co-ordinates must be read for each of the 128 sample positions in each scan of the sea surface. The 4 x 128 words describing the scan are then sent to the PC where the data is stored and the wave slopes are calculated and displayed. The control electronics must synchronise this readout with the scanning of the laser beam by the two-axis galvanometer scanner unit. The steps that are involved in generating the wave slope values that are used in the real-time display are shown in Figure 6. 1.

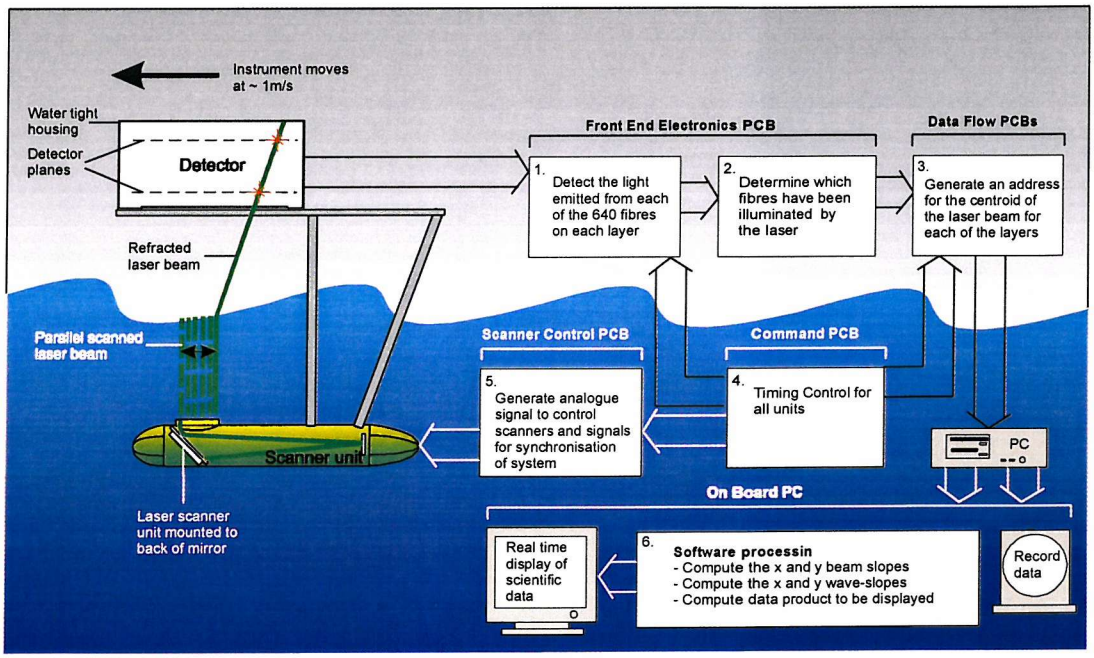

Figure 6. 1. The signal processing used to recover the wave slopes from the photodiode signals.

The PCBs described by sections 1 to 5 of Figure 6. 1, are mounted on the detector platform whilst the PC will be housed aboard the deploying research vessel, along with additional instrumentation such as the Global Positioning System. This chapter will discuss in more detail the electronics design of each of these PCBs and will briefly describe the tasks performed by the PC.

6.2. Front End Electronics Circuit Design

The first stage of the electronics, detects the presence of light at the ends of the wavelength shifting fibres, using the photodiodes arrays described in chapter 5 [Hamamatsu, 1996]. These photodiodes produce a current that is proportional to the intensity of the light falling on them.

Initially, the HX2 chip developed by the RAL Microelectronics Group was considered for reading the current generated by the photodiodes [Thomas et al, 1995]. The HX2 IC is a 16-channel integrating amplifier circuit, which includes a sample and hold circuit. Each channel in the IC will integrate the charge present at its input. The minimum integration time for this device 5μs. Following this integration the signals are held while a multiplexer is used to read out each channel in series. Once a particular channel has been selected by the multiplexer, the analogue output settles to within 1mV of its final value within 200ns. Consequently, for each detector layer, all 640 fibres can be read in a total of ~128μs. Each channel has two storage capacitors allowing the previous 16 measurements to be read during the integration period. This allows 16 simultaneous samples to be made every 5μs. Even with all four detector layers being read in parallel, at least four HX2 ICs must also be read in parallel from each layer, in order to reduce the readout time to <35μs. For each detector layer, this would require serial data to be read from 40 channels in parallel. Consequently for the whole detector, a total of 160 serial data lines must be read in parallel. In order to reduce this large quantity of data before it is transferred to the PC it must be processed in hardware further.

Having detected the light levels within each of the 2560 fibres in the detector, the next stage in the Front End Electronics circuit design was to determine the position of the laser beam on each detector layer. The PC would then only be required to read four co-ordinates per sample. Initially an IC called the 'Winner-Takes-All' (WTA) was considered. This was developed by the Lawrence Berkeley National laboratory [Moses et al, 1996]. It is designed to sample 16 analogue channels simultaneously and then selects the largest of those signals. The IC then returns 16 digital outputs with the winning signal indicated by a digital high. In addition, the address and analogue signal level for that channel are also provided. For a well behaved laser

beam it might be expected that the fibre at the centre of the beam would generate the largest output. Therefore this IC could be used to determine the address of this fibre. The WTA IC can also be used to hold the data, therefore, the HX2 chip can be completely replaced. A useful feature of the WTA is that it can be cascaded so that the winning signal, from up to 16 WTA circuits could be determine by one additional IC [Crossingham 1996]. The advantage with this method is that if the laser light is reflected within the detector, illuminating other fibres, it will be ignored if it is less intense than the primary beam. Unfortunately, a winning signal is only selected when there is a difference in voltage levels of >20mV. Consequently, there would be a point, as the beam passes from one fibre to another, when the winning signal could not be determined.

To determine the extent of this problem a collimated laser beam was scanned over two wavelength-shifting fibres. The light output from each fibre was then detected using photodiodes [Hamamatsu, 1996] which were biased using resistors. A single WTA IC was used to determine the address giving the largest photodiode signal. The position of the output signal was recorded as a 16 bit binary number using a data acquisition board and a PC. A small section of the data collected during the test is shown in Figure 6. 2. The laser beam was scanned over the two fibres at a frequency of 1kHz and a 5kHz sample rate was used. In this section of data an erroneous signal was generated on five occasions, caused by the signal levels being too close.

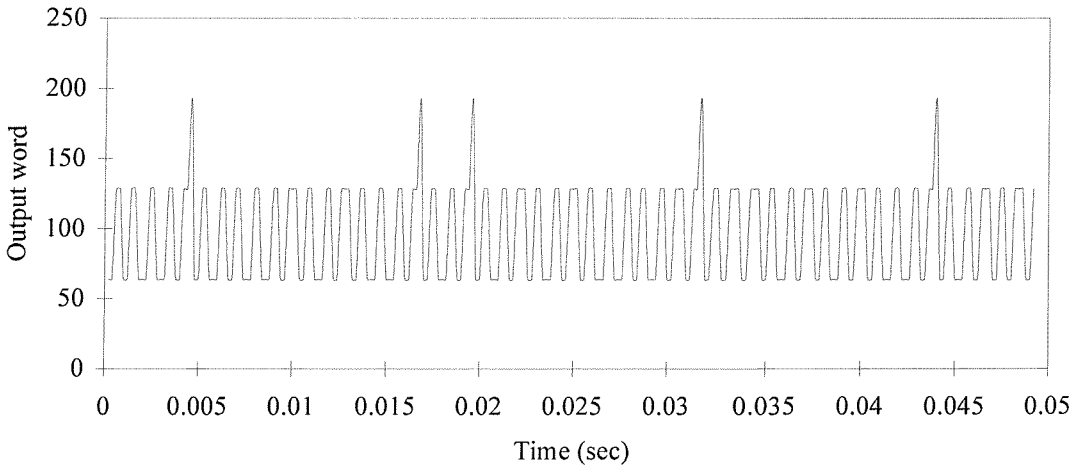

Figure 6. 2. The output recorded from a WTA IC while a laser was scanned over two fibres at a frequency of 1kHz. The sampling frequency was 5kHz.

When the laser beam is being refracted by the sea surface the chances that the difference in signal levels between two fibres could be less than 20mV, can not be ruled out. Therefore this problem must be resolved if this circuit is to be used. To achieve this a logic circuit would have

to be designed to interrogate the outputs of the WTA IC. In considering such a circuit, it became apparent that a simple logic circuit could replace the WTA circuit completely.

A digital signal can be generate by comparing each photodiode signal with a reference level using comparators. When the signal from the photodiode was above this reference level its output would change. By carefully setting the reference level the comparator can be used to determined whether the fibre has been illuminated or not. This generates a series of ones and zeros that representing the positions of the illuminated fibres on the detector layer. From this data, the position of the laser beam can be assigned an appropriate address. This method offers a quick and simple way of reading the position of the laser beam from the fibres and generating a digital signal. However, it requires a separate photodiode amplifier and comparator for each one of the 2560 fibres. This puts a heavy demand on the printed circuit board area required. The first two components, in a single channel of the readout circuit, are shown in Figure 6. 3.

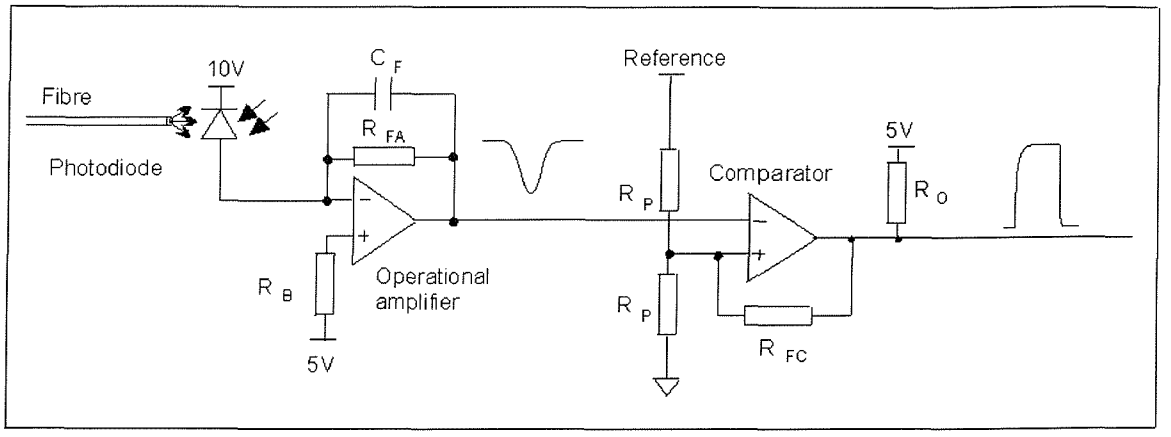

Figure 6. 3. First two components of the Front End Electronics Readout circuit.

The amplifier circuit generates a negative going signal when the fibre is illuminated by the laser beam. Consequently the inverting comparator circuit then produces a positive 5V signal indicating that the laser beam is present. The simplest way to change a current into a voltage would be to pass the current generated by the photodiode through a resistor. However, the reverse bias across the photodiode will vary as the current through the resistor varies. As the voltage across the resistor increases, the voltage across the photodiode decreases. This varying photodiode bias voltage will cause the response time of the photodiode to decrease for larger current signals.

The photodiode bias voltage can be kept constant by using an operational amplifier as shown in Figure 6. 3. By connecting the positive terminal of the operational amplifier to ground, the bias voltage across the photodiode can be considered constant, regardless of the current generated.

Unless a small feedback capacitor (C_F) is used to reduce the high frequency response of the amplifier, the phase-shift between the input and output of the operational amplifier, will cause this circuit to oscillate. The value of this feedback capacitor depends largely on the exact design and layout of the printed circuit board (PCB) but in this case a 2.7pF capacitor was used. A resistor at the non-inverting input of the op-amp ensures that the impedance at both input terminals is similar. This minimises the output offsets voltage that is caused by the small but finite bias current drawn by the input terminals of the amplifier. The value of the feedback and bias resistor (R_{FA} and R_B respectively) must be approximately the same. This is because the bias current will flow through the feed back resistor preferentially as the dark current of the photodiode is small (~ 30pA) and therefore it has a relatively large input impedance compared to the feedback resistor [Hamamatsu 1996].

A voltage hysteresis of 200mV was induced into the comparator circuit using the resistor R_{FC}, to prevent the output from oscillating. The photodiode-biasing circuit was effectively isolated from the comparator by connecting the amplifier output to the high impedance inverting input of the comparator. The amplifier was, therefore, designed to generate a falling signal level when the fibre was illuminated. The characteristic shape of the signals that were generated at the outputs of the amplifier and the comparator when a pulse of light illuminated a wavelength-shifting fibre are shown in Figure 6. 4.

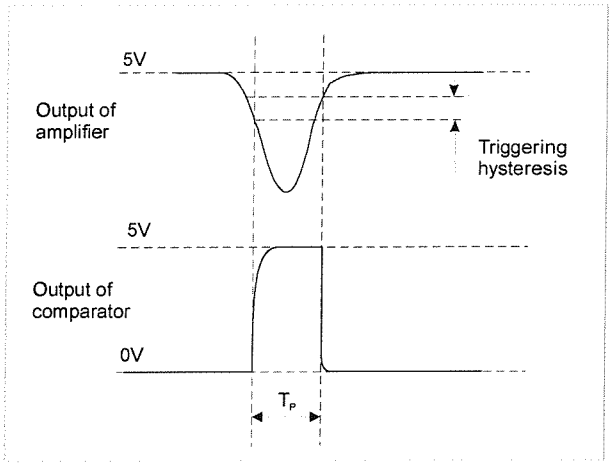

Figure 6. 4. Signals generated by the light detection circuit.

The bias resistors for the amplifiers where chosen so that the voltage levels that were generated varied between 400mV and 4V, depending on which end of the fibre was illuminated. The reference signal was common to a number of comparators but it is undesirable for the hysteresis of each comparator to effect any other. Therefore, the potential divider formed using the two resistors R_P, was required to isolate the non-inverting terminal of each comparator from the

reference level. The resultant signals from the 2560 comparators was then feed into the next stage of the electronics.

6.3. Laser Beam Position Encoding

To determine the position of the laser beam at a particular instant, all the outputs of the comparators from all four layers in the detector were sampled and held using latches. These held the signals steady while the next stage of the processing was carried out. From the array of ones and zeros that were held, an address for the positions of the laser beam on the fibres of each layer was generated. Several different devices where considered that could have been used to determine this address, these included Microprocessors, Programmable Gate Arrays and Programmable Read Only Memories (PROM). The simplest solution at this time was to use PROMs. They were easy to program and the required equipment was already available. The digital signals generated by the comparators were used to address the PROMs. For each combination of signals input into the PROM an output was programmed to give the correct address for the centroid of the group of fibres illuminated.

In order to evaluate the circuit operation and layout, a multi-channel readout system was constructed. This consisted of one 16-element photodiode array, 16 amplifiers, 16 comparators and a single PROM. The Front End Electronics PCB was going to be mounted along the edges of the detector planes to hold the 16-element photodiode arrays in place and aligned with the fibres. Consequently, all 16 channels that were required to readout a single photodiode array could be no wider than 25.4mm, the width of the photodiode itself, so that each photodiode array could be butted up against the next [Hamamatsu 1996]. To meet this requirement the circuit was laid out on a four layer PCB using surface mount components [Appendix C, Figure C.1].

A comprehensive test of this circuit was completed using the arrangement shown in Figure 6. 5. The laser beam was scanned over 8 fibres at various speeds. The digital addresses generated by the PROM were sampled using a data acquisition card within a PC [Amplicon, 1997]. The card was operated at its maximum sampling speed of 260kHz. The highest frequency with which all 8 fibres could be scanned by the laser beam, using the galvanometer scanner, was 2.6kHz. The resulting output is shown in Figure 6. 6.

Throughout these tests, the reference level input to the comparators was set so that it was just above the background noise level at 25mV. In the detector the fibres will be shielded from the background light levels, caused by sun light, by a filter at the input aperture of the detector. This will ensure the background light levels are as low as this in the detector. These tests showed that

this circuit would successfully read the photodiode signals and assign an address to the position of the beam in less than 4μs.

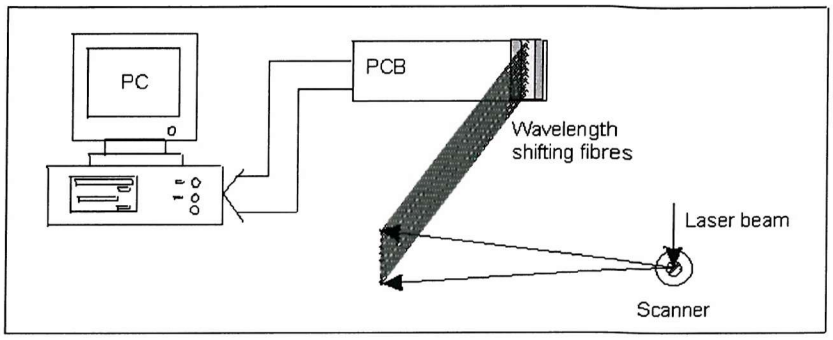

Figure 6. 5. Test arrangement used to verify the operation of the Front End Electronics circuit.

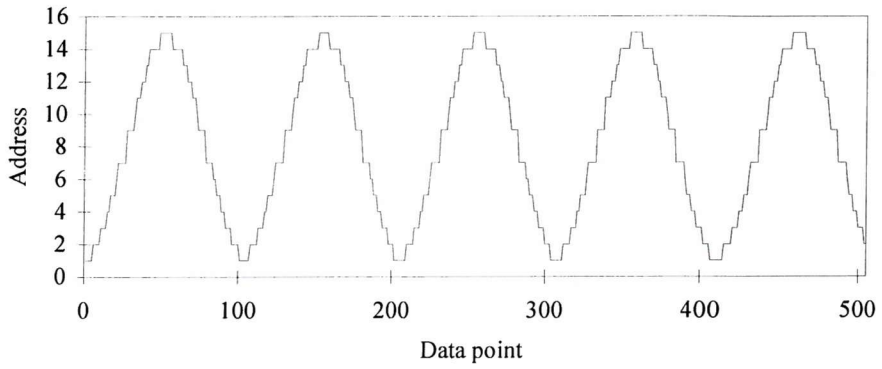

Figure 6. 6. Output from Front End Electronics circuit for the laser scanned over the fibres at 2.6kHz.

This circuit had to then be adapted so that a single address from each of the four layers of the detector was generated. However, as with all the devices that where initially considered, a single PROM can only receive a finite number of signals. Therefore, to address all the fibres in each layer of the detector a number of PROMs are required. Provided a single PROM addresses all the fibres illuminated by the laser beam, the position of the centroid of the beam can always be accurately determined. A problem arises when the illuminated fibres overlap two PROMs as shown in Figure 6. 7. In this case, each PROM sees three illuminated fibres and would provide a position for the centroid of the beam at the centre of the three fibres. Obviously neither PROM gives the correct position of the beam and both of them give an address when only one is required. In order to avoid this ambiguity, a single PROM must address the entire beam. That PROM will then give the correct position of the centroid of the beam.

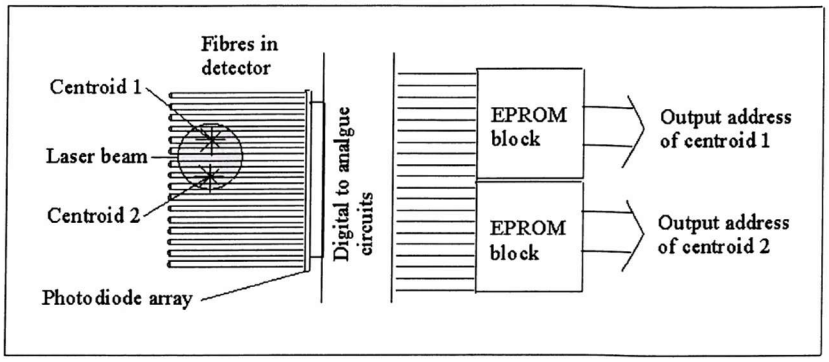

Figure 6. 7. A diagram showing how the laser beam can overlap two PROMs. Both will then give a position for the centroid of the laser beam.

To over come this problem, there must be an overlap in the fibres that are addressed by adjacent PROMs as shown in Figure 6. 8. The number of overlapping fibres must be greater than the maximum number of fibres that are likely to be illuminated at one time. The beam diameter on the detector was measured to be ~5mm in air. To take account of any divergence in the beam caused by the sea, 7 fibres where overlapped allowing a maximum beam diameter of ~12mm to be detected effectively.

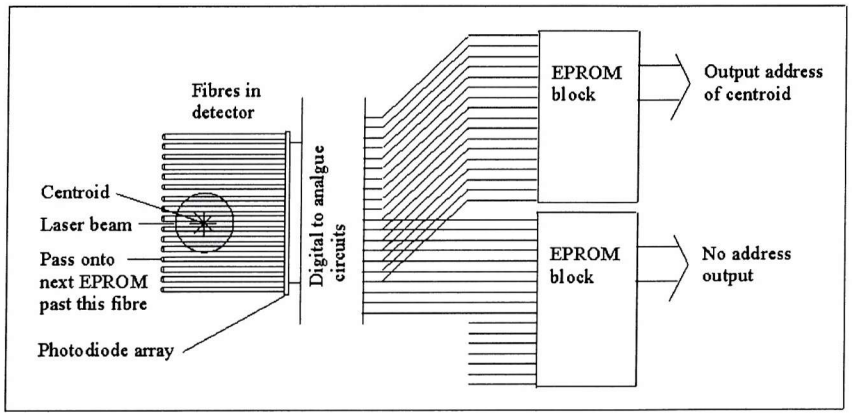

Figure 6. 8. The overlap of photodiode signals into the PROMs to ensure that all illuminated fibres are on only one.

A 16 element photodiode array therefore requires two PROMs, each addressing 8 fibres plus 7 overlapping fibres. Each PROM was programmed to output a 5-bit number identifying where the laser beam is in 1 of 29 possible position either on, or between, the fibres. To allow for changes in laser power and beam divergence, the PROMs were programmed so that any number of adjacent fibres between 1 and 7 can be illuminated to give an address. In all other cases the output was null. So that there would be a smooth transition from one PROM to the next, a particular PROM would give an address until, only the overlapping fibres on that PROM are illuminated. After this point the next PROM will address all of the illuminated fibres and will

only provide an output address when the first fibre, it addresses, stops being illuminated. This indicates that the beam is completely on that PROM.

In addition to a 5-bit address generated by each PROM, a sixth output bit is used as a flag to indicate when the PROM is providing an address. The flag generated by every PROM, on the 10 Front End Electronic PCBs on an axis of the detector, are monitored to ensure that only one PROM at a time is providing an address. Once this has been confirmed then a second latch was enabled that loaded the data from the correct PROM onto an address bus. This bus was common to all 10 Front End Electronic PCBs.

As mentioned previously in section 5.2.1.3, four 16 element photodiode arrays where mounted onto a single PCB. This allowed the photodiodes to be easily aligned with the fibres by accurately mounting the PCB to the detector frames. The relatively small number of photodiode arrays per PCB allowed faulty channels to be easily replaced. Each of these PCBs consists of 64 channels. On each PCB there are eight, 8-bit sampling latches, eight PROMs and eight, 8-bit bus latches, in addition to the amplifiers, comparators and further logic to monitor the flags. A photograph of the finished PCB is shown in Figure 6. 9. Ten of these PCBs were required to read the 640 fibres on each detector layer. The connectors on the top section of the PCB allowed the control signals and data bus to pass through all ten PCBs and at the end of this chain connected to the next stage in the readout electronics.

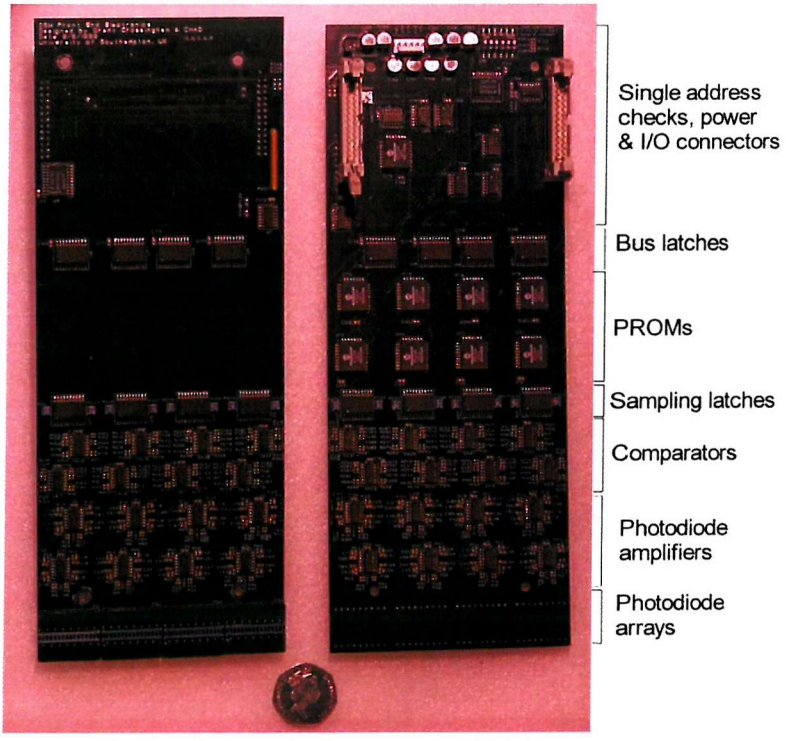

Figure 6. 9. The Front End Electronics PCB design. Front and back views.

6.4. Control and Timing Circuitry

The flow of data from the FEE PCBs to the PC, including all the control signals required to synchronise the Digital Slopemeter is now described. This involves all the systems shown in Figure 6. 10. Also shown in Figure 6. 10 are the interconnection between the various electronics systems in the instrument.

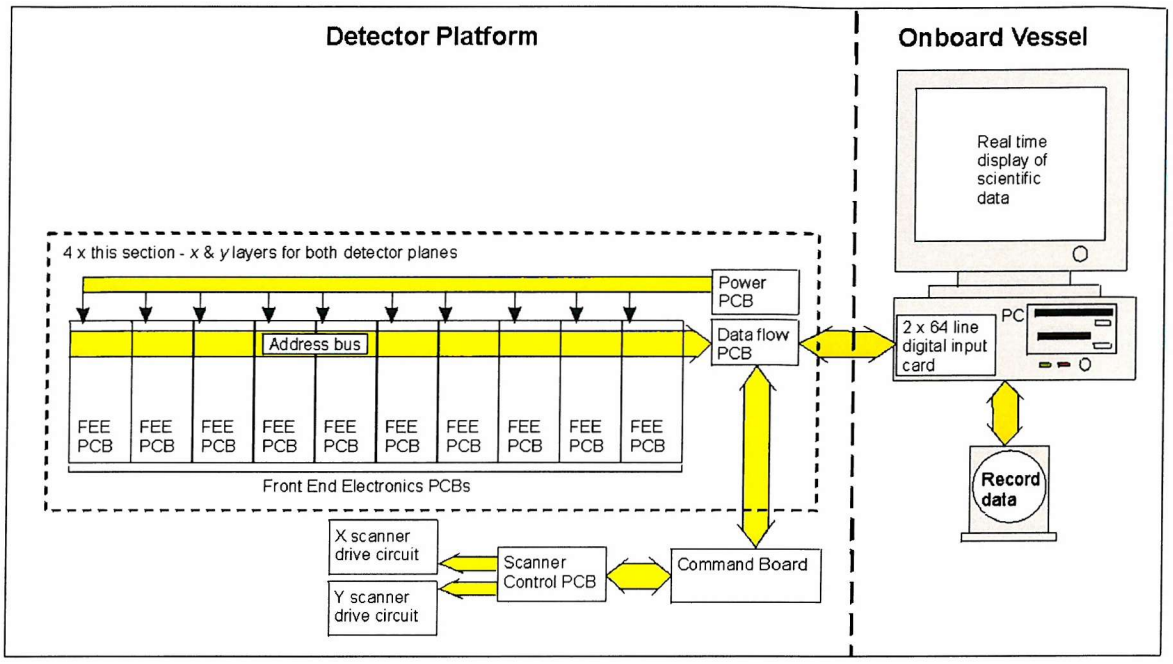

Figure 6. 10. The interconnection of the detectors printed circuit boards.

Each of the four layers of ten Front End Electronics circuits generate an encoded address for the beam co-ordinate. This encoded address is a 13-bit number that uniquely represents the position of the laser beam on that axis. This address consists of the following data bits,

- a 5-bit number describing one of 29 possible positions for the centroid of the beam on a particular PROM,
- a 3-bit number describing which one of the 8 PROMs on each PCB module, was generating the 5-bit address,
- a 5-bit number describing which of the 10 Front End Electronics modules on a single axis had detected the laser beam.

As mentioned earlier, after the output of the comparators has been sampled using the sampling latches, only one PROM on all of the 10 modules provides an address. Once this check has

been completed, the address is loaded onto an address bus that is common to all 10 modules using a second bus latch. This requires two clock signals on the FEE PCBs. One of these signals times the initial sampling of the sea surface and the second delayed trigger loads the address onto the output bus. This address then moves off the FEE PCB to the next stage of the electronics readout, the Data Flow PCB.

This stage in the readout electronics decodes each of the 13-bit numbers to give an 11-bit number between 1 and 1279. This number relates directly to the position of the laser beam on one of the four axes of the detector plane. The conversion of the numbers is achieved using a look up table stored on a 16-bit EPROM on each Data Flow PCB. The decoded number is then stored in a First In First Out buffer (FIFO). There are four Data Flow PCBs each storing 128 laser beam co-ordinates recorded during a complete scan of the sea surface. Once data from a single scan of the sea surface is stored on all the Data Flow PCBs, a Read Data flag is raised that informs the readout PC that a complete set of data is ready to be transferred.

At this point, it is convenient to explain the timing of the instruments electronic systems. The timing of all the electronic circuits in the detector are controlled by a single Command PCB based on a 16MHz programmable timer. The timing of the Detector electronics can be explained using the timing diagram shown in Figure 6. 11. The following points briefly describe each line in the timing diagram:

1. The Master Clock runs continuously at a chosen base frequency.

2. The Scan Clock, which is triggered on a rising edge of the Master Clock, is used to start the scan pattern and determined the frequency at which the scan is repeated.

3. The Scan Clock triggers the start of a series of Scanner Control Pulses that are sent from the Command PCB to the Scanner Control PCB where they are used to count through the addresses of three Erasable Programmable Read Only Memories (EPROMs). Two of these EPROMs are programmed with the required scan pattern for each of the galvanometer scanners.

4. The outputs of these two EPROMs are used to address two Digital to Analogue Converters (DAC) that control the positions of the two scanners (4a and 4b).

5. The third EPROM, on the Scanner Control PCB, is also controlled by the Scanner Control Pulses. This generates a Start-Sampling Flag that indicates when the scanner has reached the correct position to start sampling the wave slopes.

6. The Start-Sampling Flag initiates the Sample Counter that counts through 64 sample pulses. This is used to trigger the sampling latches on the FEE PCBs.

7. The Sample Counter is delayed by several hundred nano seconds and then used to latch the encoded beam positions on the FEE PCBs onto the data bus. This delayed set of pulses is known as the Bus Counter.

8. The Bus Counter was then inverted and delayed by another few hundred nano seconds. This was then used to read the decoded beam positions into the FIFOs on the Data Flow PCBs.

9. At the end of the scan sequence the third EPROM generates an End of Scan Flag that rises a Read Data Flag which is passed to the PC. The FIFOs now contain the beam co-ordinates from a complete scan.

10. The PC looks for the Read Data Flag to be raised before it requests data from the FIFOs.

11. The Read Data Flag stays high while data is being read by the PC.

12. When the last beam position is read the FIFOs generate an Empty Flag that causes the Read Data Flag to be lowered. The PC has then read all the beam co-ordinates from a compete scan.

13. The whole sequence from point 2 to point 12 is then repeated.

There are three main clocks that can be controlled in this sequence:

i) The ***Master Clock*** sets the base frequency at which the whole system runs. This clock uses the 16MHz programmable timer in conjunction with a series of counters, flips flops, and logic, to generate a selectable range of base frequencies.

ii) The ***Scan Clock*** is used to select the frequency with which the scan pattern is repeated. This uses a similar circuit to the Master Clock to step down in frequency from the Master Clock frequency.

iii) The ***Sample Counter*** generates, on request, a selectable number of sample pulses. This uses a simple counter circuit to generate 2^N pulses.

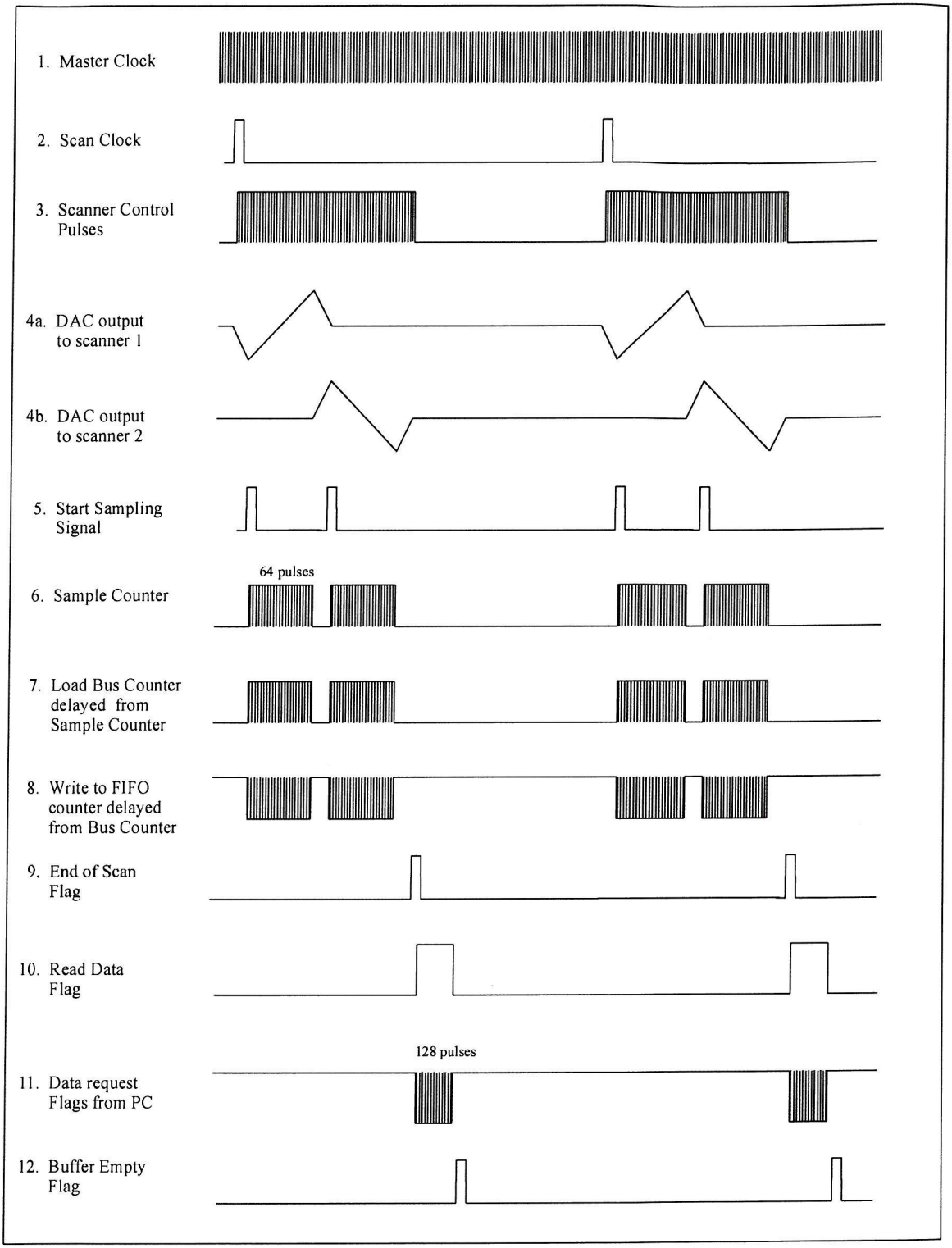

Figure 6. 11. Timing diagram for detector electronics. Each numbered signal is explained in the corresponding bullet point above.

These three clock functions are variable over a range of frequencies so that the timing of the system can be adapted for any desired scan pattern. By using this system of clocks, the sampling rate is locked together with the scanning rate so that the positions at which the wave slopes are sampled along the scan are always the same. For a scan pattern consisting of two orthogonal scans, the master clock frequency was set at approximately 29kHz so that a sample is taken every 35μs.

The PC used to record the data had a clock speed of 350MHz, which was the fastest processor available at the time of purchase. The Data in the FIFO is transferred to the PC on request, one sample at a time, via four separate 11-bit wide twisted pair cables. Each Data Flow PCB uses 11 differential line drivers to transfer the signals down the twisted pairs. At the ends of these cables the signals are received using differential amplifiers and then read using two 32-bit digital data acquisition cards [ADLink Technology Inc. 1998]. The PC reads in each sample as two 22-bit words from which it extracts the four 11-bit beam co-ordinates to it's memory. Once the PC has stored the data it then requests another sample from the FIFOs using the Data Request Flag. In this way the PC can receive a block of data representing a single scan of the surface in its own time so that no data is lost. The PC reads the data much more rapidly than if it was sent, as the detector receives it, once every 35μs. This gives the PC more time to calculate the wave slopes and display the data.

6.5. Real Time Data Display

The raw data received by the PC represent the x and y co-ordinates of the laser beam on the top and bottom detector planes. In addition, to storing the data directly to the PCs hard disk, it calculate the wave slopes throughout the scan of the sea surface. These slopes can then be used to generate a useful history of the sea surface roughness in real-time.

The first stage in this process, is to calculate the slope of the laser beam from the beam co-ordinates measured. If the fibres on the two detector planes were in line then calculating the beam slope would just be a simple case of subtracting the lower beam co-ordinates from the upper ones and dividing by the distance between the detector planes. However, because the upper detector plane is rotated through 45° clockwise, the measured beam co-ordinates have to be transformed into the same co-ordinates system as the lower detector plane. The following transformed co-ordinates are used to achieve this,

$$x_T = y_u \sin(45) + x_u \cos(45) \tag{6.1}$$

$$y_T = y_u \cos(45) - x_u \sin(45) \tag{6.2}$$

where x_u and y_u are the co-ordinates of the laser beam in the upper detector plane and x_T and y_T are the transformed co-ordinates within this plane. Once the positions of the laser beam on both detector planes are in the same co-ordinate system then the beam slope can be calculated using the dimensions shown in Figure 6. 12, in the following way,

$$s_{bx} = \frac{x_T - x_l}{D} \quad \text{and} \quad s_{by} = \frac{y_T - y_l}{D} \tag{6.3}$$

where s_{bx} and s_{by} are the x and y beam slopes respectively, x_l and y_l are the x and y co-ordinates of the laser beam on the lower detector plane and D is the distance between the detector planes. Once the two beam slopes have been calculated, they can be related to the angle between the laser beam and the axis of the detector, in the following way,

$$s_{bx} = \tan\theta_{bx} \quad \text{and} \quad s_{by} = \tan\theta_{by} \tag{6.4}$$

where θ_{bx} and θ_{by} are the beam slope angles in the x and y directions respectively. An equation for the wave slope in terms of the beam slope can be determined from the geometry shown in Figure 6. 12. Using Snell's Law and the relationships $\theta_{wx} = \theta_{sx}$ and $\theta_a = \theta_{bx} + \theta_{sx}$ in the x direction, the following equation for the sea surface slope in terms of the beam slope can be determined,

$$\tan\theta_{sx} = \frac{\sin\theta_{bx}}{\frac{n_w}{n_a} - \cos\theta_{bx}} \tag{6.5}$$

and similarly in the y direction,

$$\tan\theta_{sy} = \frac{\sin\theta_{by}}{\frac{n_w}{n_a} - \cos\theta_{by}} \tag{6.6}$$

where θ_{sx} and θ_{sy} are the sea surface slopes in the x and y directions respectively. The equations 6.1 to 6.6 are performed in software by the PC on each set of beam positions recorded. This enables a wave slope profile to be generated for each scan of the surface, which can then be displayed. However, for real-time analysis purposes it is more useful to display a running history of the sea surface roughness. A wave slope spectrum is a useful measure of the sea surface roughness. A spectrum can be calculated for each scan of the surface using a Fast Fourier Transform [Willoughby 1998]. A time series of these individual spectra can be displayed as a spectrogram with wavenumber along the y-axis, time along the x-axis and colour representing the spectral intensity as shown in the spectrogram in Figure 6. 13, generated by Willoughby [1998].

An alternative measure of the sea surface roughness is the slope probability distribution. This would show the probability of measuring a particular slope value and can be plotted in a similar

fashion to the spectrogram but this time with slope values along the y-axis. It is not clear whether the spectrum or the slope distribution will give the clearest indication of changes in the surface roughness. Therefore, initially the real time display will show both the spectrogram and the wave slope probability distribution for both axes of the scan, across track and along track. Software has been developed by Dr Willoughby to display a running spectrogram and a running wave slope probability distribution. A screen capture of the real-time display with no data is shown in Figure 6. 14. Both the long-term and short-term evolution of the surface roughness will be displayed. The charts on the left hand side of the screen capture show the surface roughness evolution over 10 seconds and those on the right show the evolution over 42 minutes. This real time display will be modified according to the observations made while the instrument is being deployed.

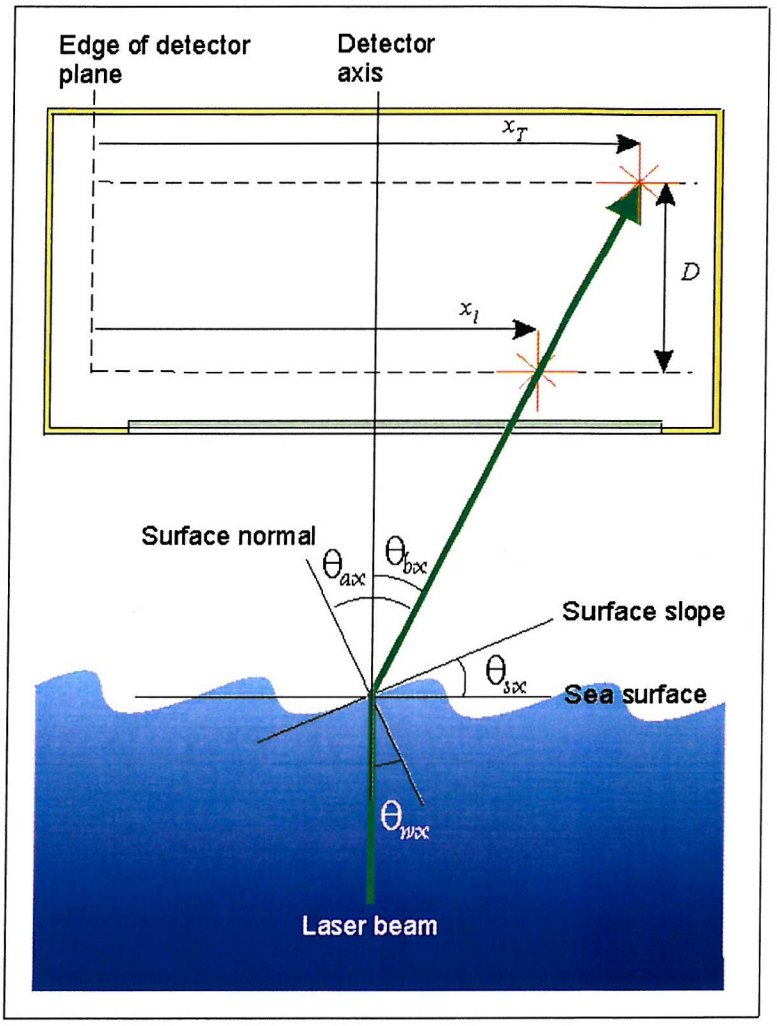

Figure 6. 12. Dimensions used to calculate the wave slope from the beam co-ordinates measured by the detector.

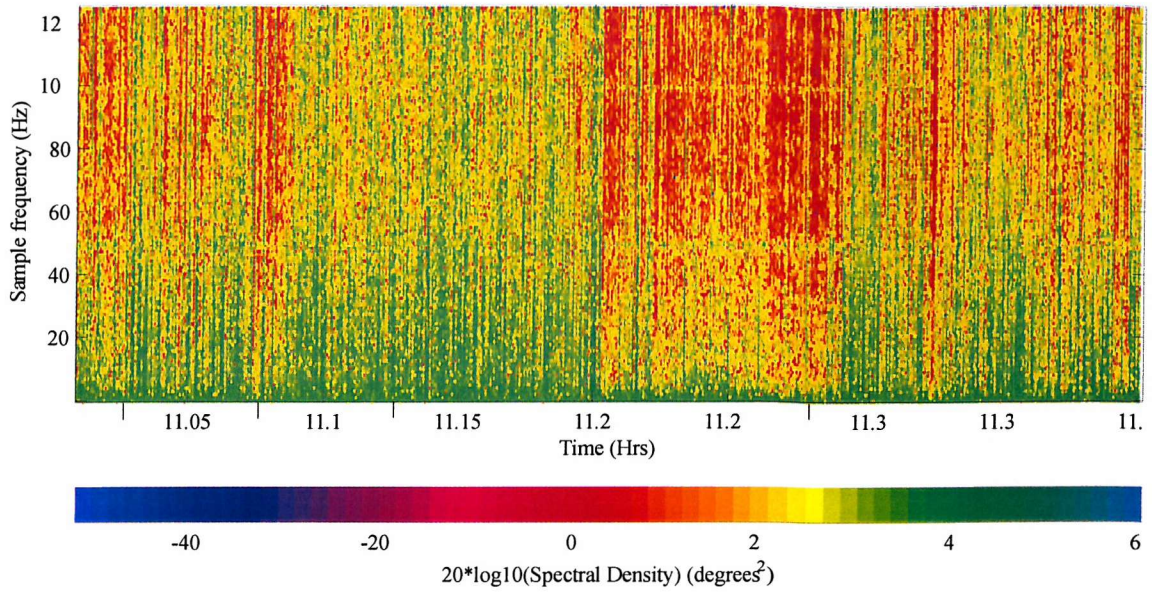

Figure 6. 13. An example spectrogram generated from data collected using the TLS.

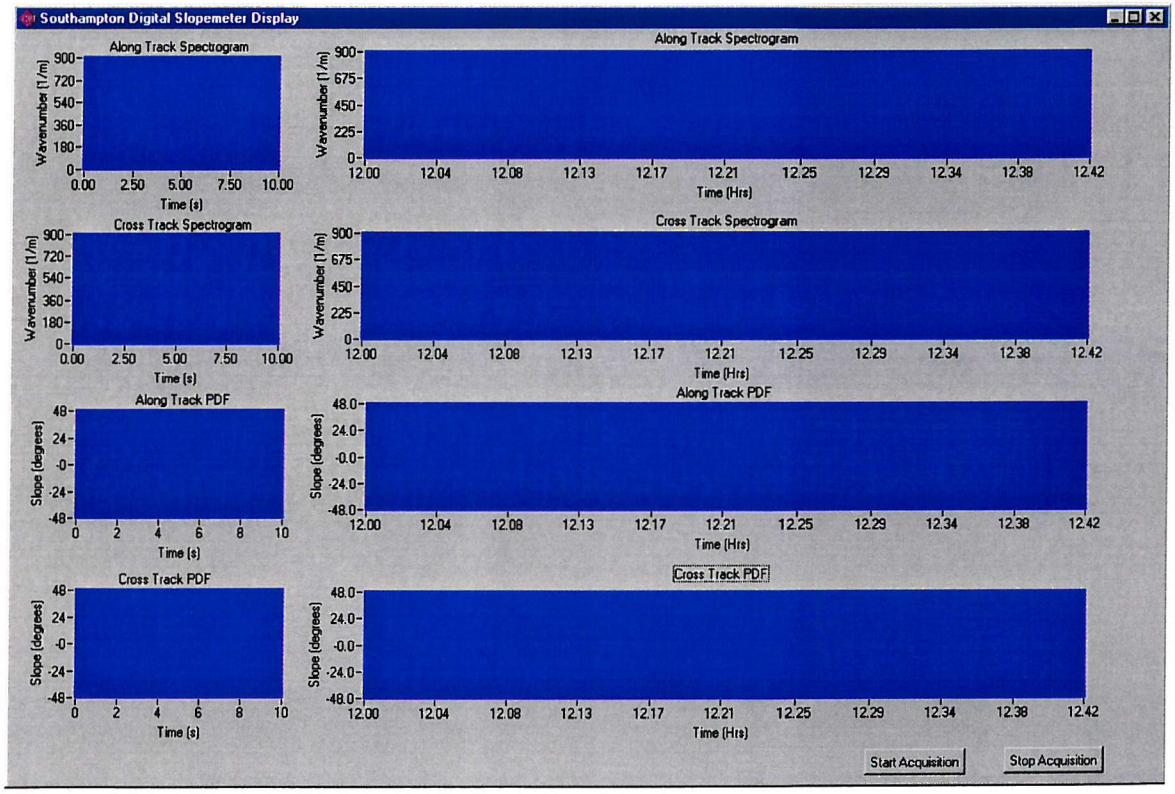

Figure 6. 14. Screen capture of the real time display.

6.6. Operation Positioning of PCBs

All the components of the instrument have to now be brought together in such way that would allow the detector to be deployed at sea effectively. The Data Flow PCBs which are designed to drive signals down cables that are several tens of meters long, to the PC, are mounted next to the Front End Electronic Circuits in the detector. The Command Board and Power PCBs are also mounted close to the Front End Electronic circuit to reduce the length of the signal lines between these circuits and therefore reducing power requirements. In summary all the PCBs to the left of the dashed line in Figure 6. 10, are mounted to the detector frame, which will be mounted within a water tight housing. The PC will be situated inside the research vessel and will therefore not be waterproofed. The Scanner Control Units generate a considerable amount of heat and are therefore mounted in a separate watertight housing. This housing will be mounted next to the detector on the deployment platform. The construction of the detector frames and the submersible laser scanning system will be described in greater detail in chapter 7.

Chapter 7
Instrument Construction and Testing

7.1. Introduction

The previous three chapters have described the underlying principles of the new Digital Slopemeter. This chapter describes the deployment strategy to be employed with this instrument. Also described, is the design and construction of the full-scale instrument that consisted of the submersible scanning system and the laser beam detector. The initial laboratory tests that were performed to confirm the resolution and accuracy of the detector and to assess its capability of measuring a dynamic water surface are presented and discussed.

7.2. Deployment Strategy

The Digital Slopemeter will be mounted to the front of a research vessel as shown in Figure 7. 1. This will provide a deployment platform that is significantly more stable than the catamaran used with the TLS. Ideally the sea surface from which the wave slope profile is measure should be unaffected by the presence of the instrument and research vessel. However, it is unavoidable that a wave that is moving faster than the research vessel may cross the measurement area, after being disturbed in the process of passing the research vessel.

The phase velocities of waves can be predicted by the linear dispersion relationship as discussed in section 4.2.2. The relationship between wavelength and phase velocity for waves with lengths between 0.3mm and 1m are plotted in Figure 7. 2.

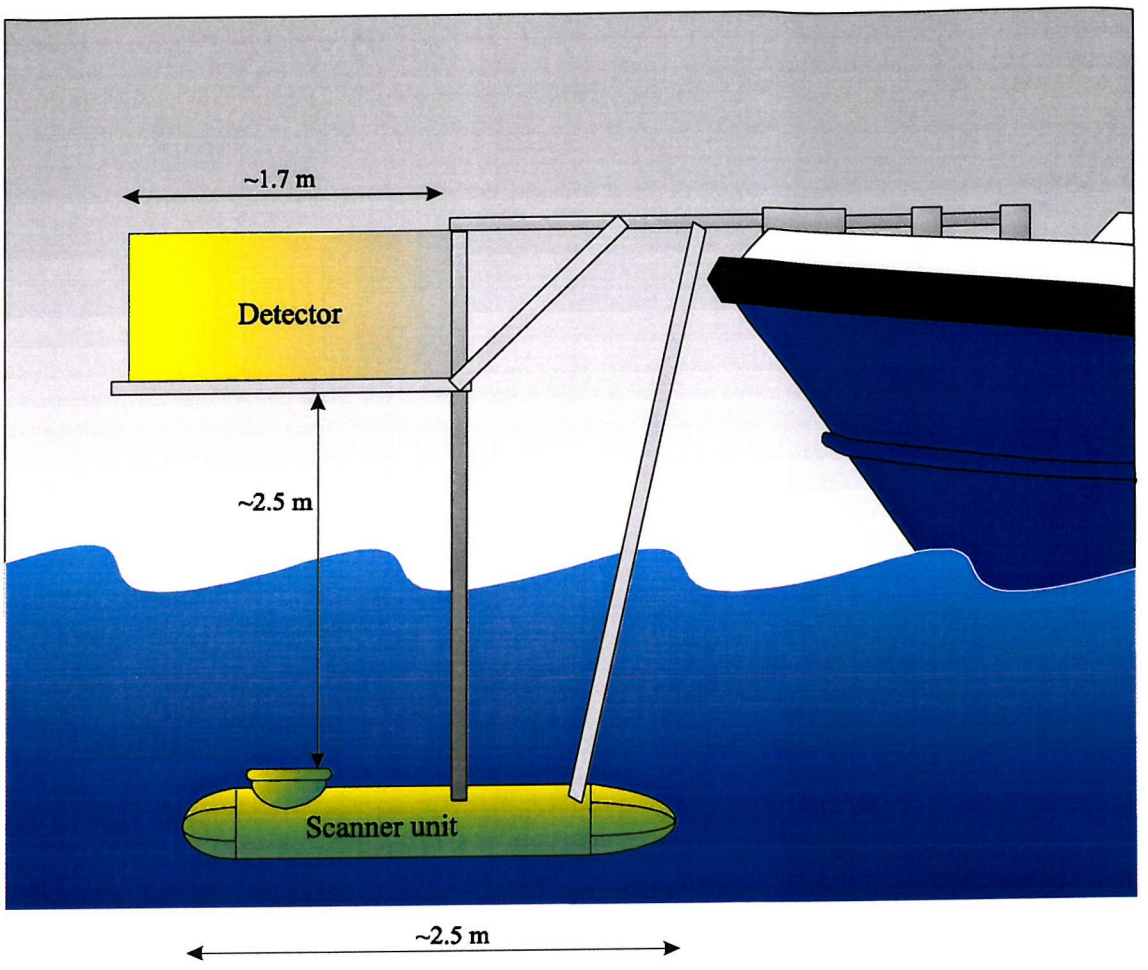

Figure 7. 1. Deployment of the Digital Slopemeter.

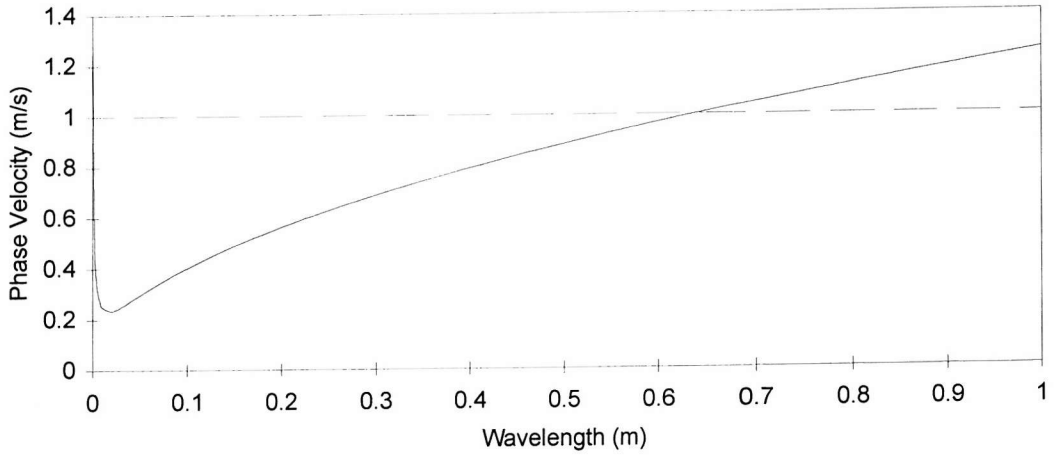

Figure 7. 2. The phase velocity of water waves plotted against wavelength. The dash line represents a phase velocity of $1ms^{-1}$.

The research vessel will be travelling at approximately $1ms^{-1}$ and this will ensure that waves with wavelengths between 650mm and 0.5mm will not propagate forward of the vessel. This covers the range of wavelengths that are being directly measured by the Digital Slopemeter. However the waves being measured could be modulated by the presence of waves outside this range. The shorter waves of less than 0.5mm generated by both instrument structure and the vessel are short lived and are soon damped by the surface tension. However, longer waves generated by the vessel or swell waves overtaking it may interfere with the measurement area. By choosing a suitable direction to travel in, relative to the wave and wind direction this disturbance can be minimised.

The instrument must also be mounted far enough ahead of the bow to ensure that the water displacement caused by the research vessel does not affect the measurement area. During field trials involving the Towed Laser Slopemeter, it was observed that two meters in front of the bow, the sea surface was not noticeably disturbed.

For the instrument to be successfully deployed, the submersible laser scanning system must be connected rigidly to the detector so that the initial direction and position of the laser beam is accurately known. This structure must also attach the instrument to the research vessel. When designing and constructing this instrument all these points must be taken into account. Initially, to allow the instrument to be fully tested in the laboratory a support structure was constructed. This structure allowed the laser be to be scanned over the full extent of the detection areas on both planes.

7.3. Construction of the Detector Planes

Each detector plane consisted of x and y layers each containing 640 fibres. The fibres on each plane were mounted to a square acrylic frame. To ensure that the fibres were held firmly in place and did not touch, each fibre was individually tensioned using a 100 grams of lead weight. Although time consuming, this was necessary because of the difficulties of securely holding more than one fibre at a time. To align the fibres exactly 1.6mm apart, small grooves were cut into the edge of the acrylic frames. The fibres could then be secured with optical glue. This construction ensured that the fibres are surrounded by air which improves their trapping efficiency, as discussed in section 5.2.3 (and in Appendix A). The two layers of the detector where constructed in an identical manner. The construction of a single layer of the detector frame is shown in Figure 7. 3.

Since the detector will be deployed at sea, it will experience a range of temperatures. It is, therefore, important to construct the frames with a material which will expanded and contract in the same way as the fibres. This ensures that the fibres are always kept under the same tension. The core of the fibres are made from polystyrene and the cladding of the fibres are made from acrylic. Fortunately, acrylic is strong and easy to work with and so could be used to construct the detector frames. Once the frames had been constructed their interior was sprayed black to stop reflections of the laser beam within the detector.

Figure 7. 3. A single layer of the detector frame. The fibres are being mounted, using lead to tension them.

With the fibres held accurately in place, the Front End Electronics PCBs can be mounted to the frame so that the photodiodes are aligned with the fibres. In addition to the 40 FEE PCBs, four Data Flow PCBs, four Power PCBs and the Command Board were also mounted to the detector frame. The two square detector planes are then mounted base-to-base so that the two *x*-*y* fibre layers are at the top and bottom of the structure, as shown in Figure 7. 4. In the laboratory this structure was mounted, supported by its centre plate, on a frame, as shown in the photograph in Figure 7. 4. For the detector to be deployed at sea it will be mounted to a base-plate and then a top-hat cover will seal the detector to keep it dry as shown in the diagram in Figure 7. 4. The four 11-bit twisted pair data cables and a power cable will be passed through the base-plate, using waterproof bulkhead connectors.

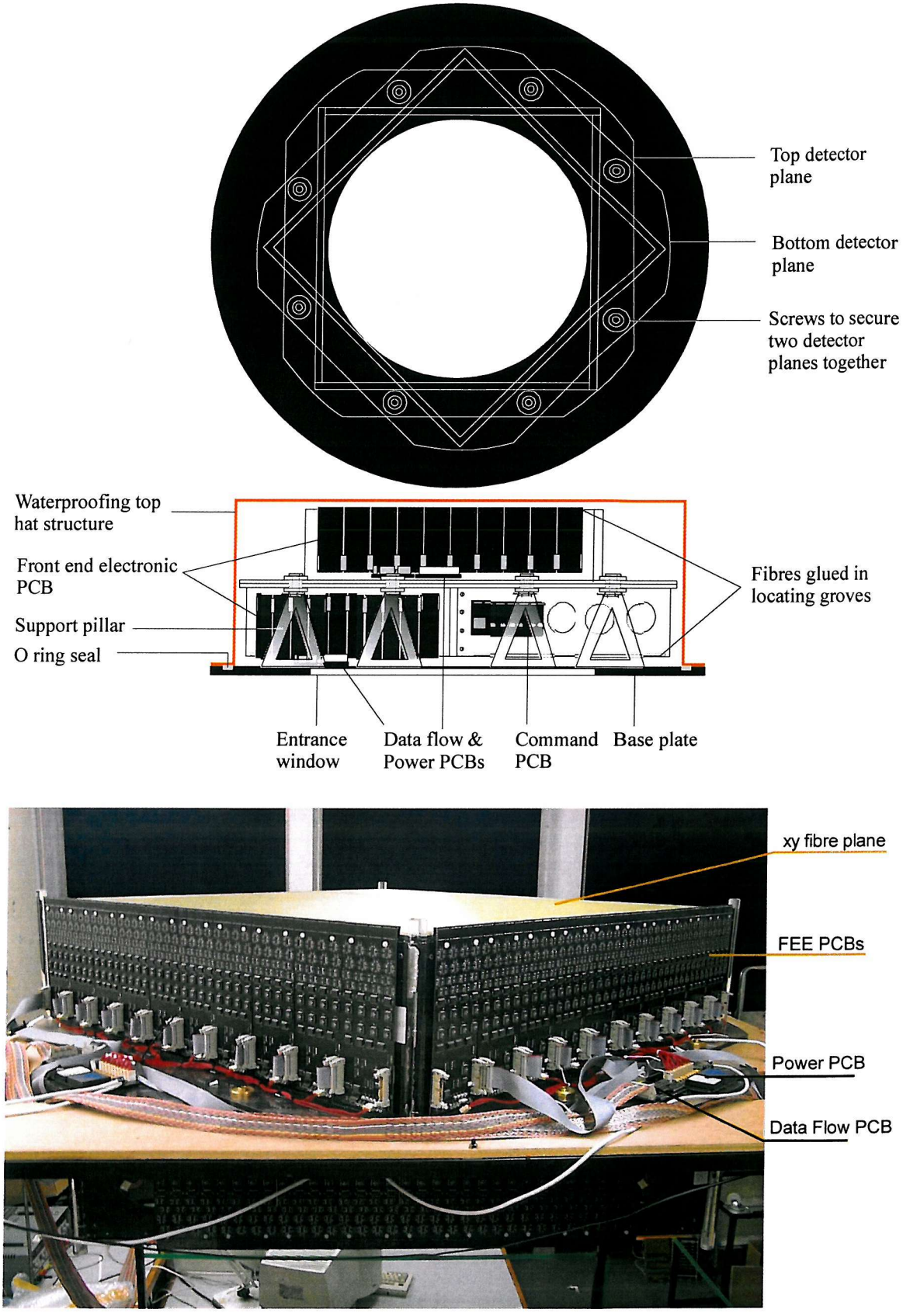

Figure 7. 4. The detector assembled to the base plate showing watertight housing (*top*). Photograph of the detector assembly mounted to the laboratory frame (*bottom*).

7.4. The Laser Scanning Unit

The layout of the optical components within the submersible laser scanner unit is shown in Figure 7. 5. These components where housed within the torpedo shaped structure shown in Figure 7. 6. As discussed in section 4.4.3 the scanner unit consists of a 2-axis galvanometer scanner placed at the focal point of a large lens. The focal length of this lens was chosen to be ~2m so that the scan angle could be kept small. This allowed the scanners to run at relatively high frequencies and ensured that the velocity of the beam over the surface was virtually linear throughout the scan length. Both the lens and the scanner unit are mounted inside a cylindrical housing. The length of this housing was minimised by folding the scanned laser beam back using mirrors, as shown in Figure 7. 5.

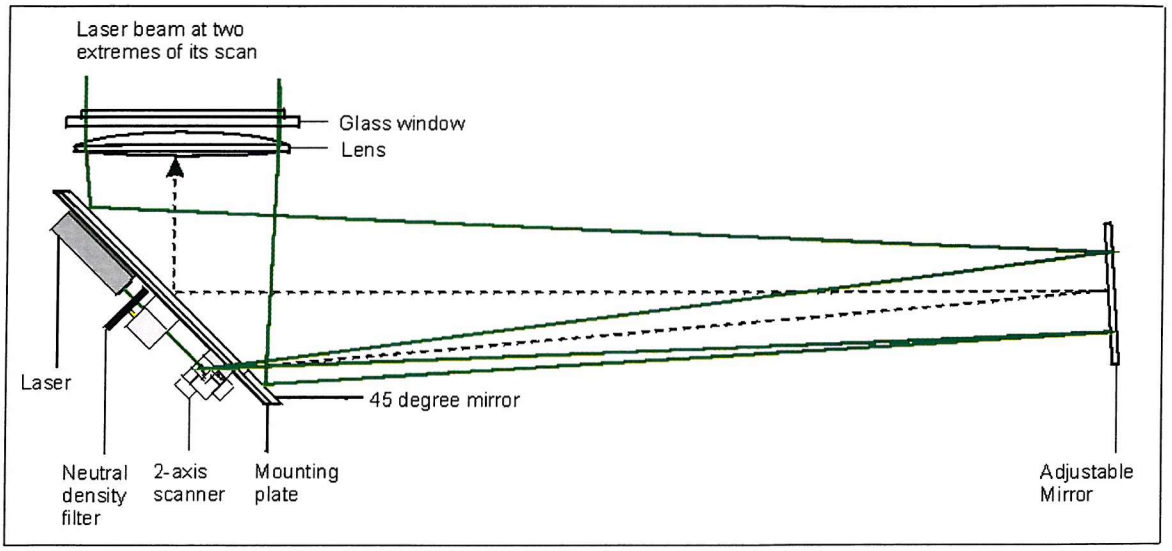

Figure 7. 5. Diagram showing the optical components within a submersible housing. The dotted line shows the optical axis of the unit.

The laser, 2-axis galvanometer scanner and variable neutral density filter, that controlled the laser output power, were mounted behind the 45° mirror. This assembly, together with the laser power supply, was then mounted to the end plate assembly of the submersible housing. The end plate with the 45° mirror mounted is shown in the foreground of Figure 7. 6. This assembly allowed these optical components to be easily aligned and removed from the submersible housing as a unit. Mounted at the other end of this housing is a plane adjustable mirror, shown in the background in Figure 7. 6. This was used to align the scanned laser beam with the 45° mirror and the lens. By adjusting the scanner mirrors and end mirror the central axis of the scan could be placed on the optical axis of the lens (dotted line in Figure 7. 5).

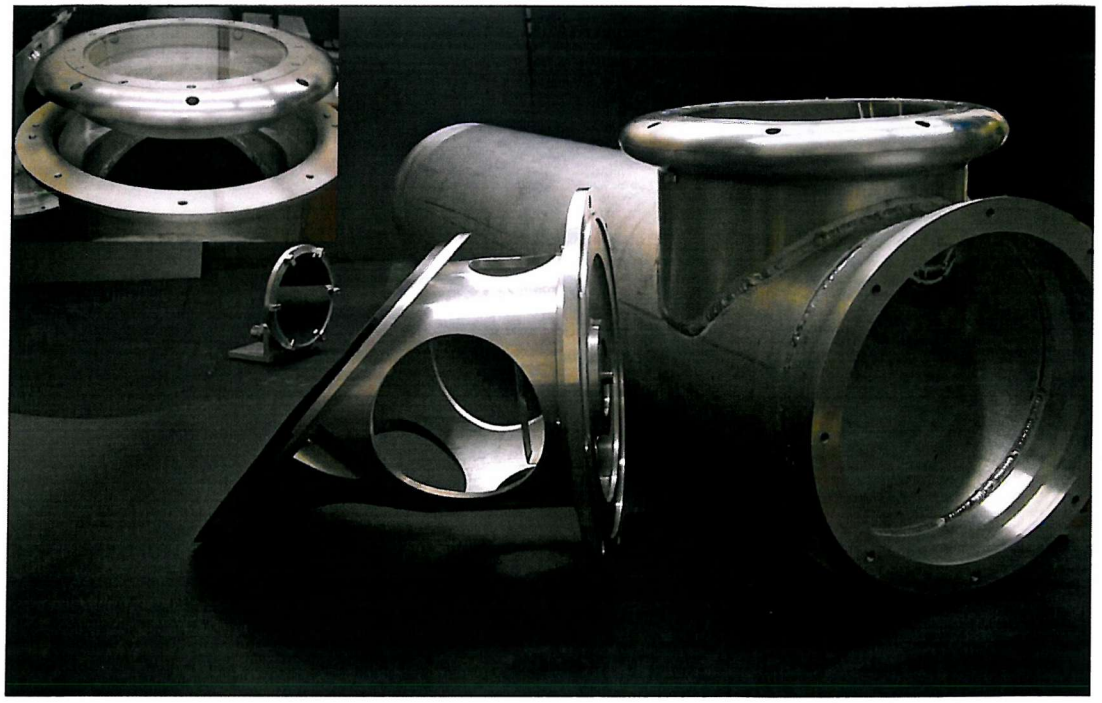

Figure 7. 6. The Laser Scanning Unit submersible housing, showing torpedo structure (*right*), 45° mirror (*foreground left*), plane adjustable mirror (*background*) and glass window and lens assembly (*insert*).

The optics is aligned so that the laser emerges exactly parallel to the axis of the detector. This alignment may be achieved by using the detector to measure the positions of the laser beam on the two detector planes without the sea surface present. When aligned correctly the scan pattern on the top detector plane is identical in size and aligned directly above the scan pattern on the bottom detector plane. When the instrument is deployed at sea the detector and laser scanning system will be mounted to the deployment platform, before the optics are aligned. The submersible housing is then sealed and flushed with nitrogen, to ensure that the optics is kept completely dry.

The deployment platform, shown in Figure 7. 1, consist of a tripod attached to a platform on which the detector is mounted to. This tripod supports the laser scanner system beneath the surface so that it is submerged at a depth of 1.5m. This depth is 5 times the outer dimension of the submersible housing. This was chosen to ensure that the submersible laser scanning system would not disturb the waves that are being measured [Allmendinger E. E. 1990]. The detector is designed to measure waves with a maximum height of 1m, for a mean sea level that is 500mm from the bottom detector plane. Therefore, the total distance between the scanner housing and the bottom of the detector must be 2.5m. The scanner unit must be connected rigidly to the

detector so that the initial direction and position of the laser beam is known accurately. Therefore, the instrument deployment platform must be built so that it can withstand the forces generated by the motion of the research vessel, without it flexing significantly. The design and construction of this platform must be carried out before the Digital Slopemeter is deployed at sea. Before this stage the instrument must be fully tested.

7.5. Detector Performance and Resolution

Once the detector had been constructed its performance had to be characterised. These tests were performed in the laboratory where the instrument was mounted to a support structure as shown in Figure 7. 4. The laser could then be scanned over the entire area of the two detector planes allowing a full investigation into the performance of the detector and Laser Scanning Unit to be performed. These tests are described in the following sections.

7.5.1. Laser Scan Alignment and Beam Position Accuracy.

Initially each detector plane was tested to confirm that all the channels were working. The laser beam was scanned across the detector plane in both the x and y directions and the beam position were recorded. This allowed any faulty channel to be found and corrected before further evaluation of the detector commenced. The correct numbering of the fibres was then checked. The laser beam was placing at precisely known position in the x and y directions on each detector plane and its position was confirmed with the readout electronics. The beam was then scanned over the fibres and their positions were recorded. This measurement was found to be completely repeatable and identical at all scanning speeds.

The submersible laser scanning system was then placed beneath the detector to generate a parallel scan. The detector and the submersible scanning system were arranged so that they were horizontal in both axes and consequently aligned. The scanned laser beam was then adjusted so that it was vertical throughout the scan. This ensured that the beam was parallel to the optical axes of the instrument at all times. The detector was used to measure the position of the laser beam throughout the scan. The difference between the position of the beam on the upper and lower layers in the x and y direction are shown in Figure 7. 7. The error in measuring the position of the laser beam due to the fibre spacing was discussed in section 5.2.1.1. It was explained that it was possible to have an error of either ±1.6mm or ±0.8mm depending on the diameter of the laser beam when it reached the detector layer. It might, therefore, be expected that there would be three possible errors in the slopes measured. If both planes detect the beam

carefully aligned would be ±2.26mm. If both planes detect the beam with the minimum error then the total error would be ±1.13mm and finally for the beam detected on each plane with different errors the total error would be ±1.79mm. These three error lines are plotted about zero in Figure 7.7.

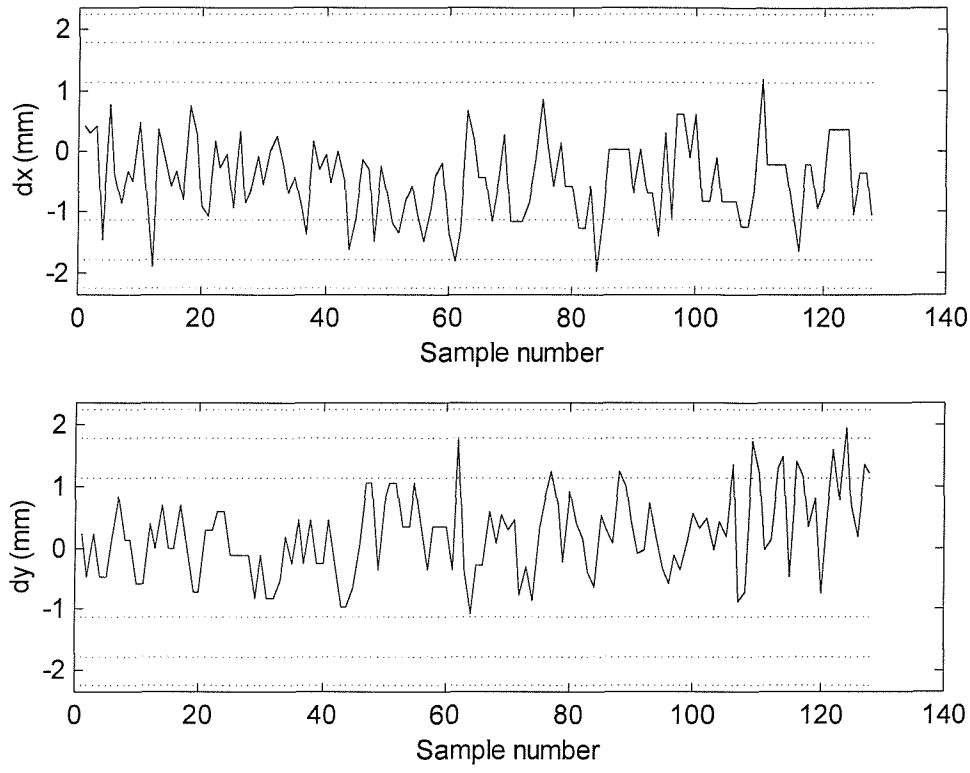

Figure 7. 7. The differences in beam position between the upper and lower layers in the detector for the x and y direction.

There is a small systematic error between the beam positions on the x-axes, caused by laser not being aligned precisely parallel with the optical axis of the detector. Nevertheless, the error in measuring the positions of the beam on the detector is generally less than the minimum error of ±1.13mm and is hardly ever greater than ±1.79mm. This might be expected, as the beam resolution of ±1.6mm only occurs at precise beam diameters, which is unlikely to occur on both detector planes because the beam is diverging slightly. As a direct consequence of this reduced error the beam slope resolution will have improved to 0.19° (using equation 5.1). This beam slope resolution corresponds to a wave slope resolution of ±0.56° (using equation 5.4).

7.5.2. Surface Reconstruction Tests.

A plano-convex lens with uniformly varying surface slope was used as a test surface. The profile of this lens and its surface slope are shown in Figure 7. 8. The laser was scanned across this surface in two orthogonal directions using the Submersible Laser Scanning System and the beam slopes were measured using the detector. The slope profile measured using the digital slopemeter is shown in Figure 7. 9. These measured slopes were compared with the theoretical slopes that are plotted in Figure 7. 10. Also shown in this figure is a 1-dimensional cross section though the lens showing the corresponding surface height profile.

The differences between the theoretical transect of the lens and the measured data is shown in Figure 7. 11. The data agrees with the resolution of ±0.56°, predicted in section 7.5.1, with exception of the last data point on the second plot. This is due to the scanner slowing at the end of its scan as it starts to change direction. This is easily avoided by only sampling over the linear part of the scan but this modification was not implemented for these tests.

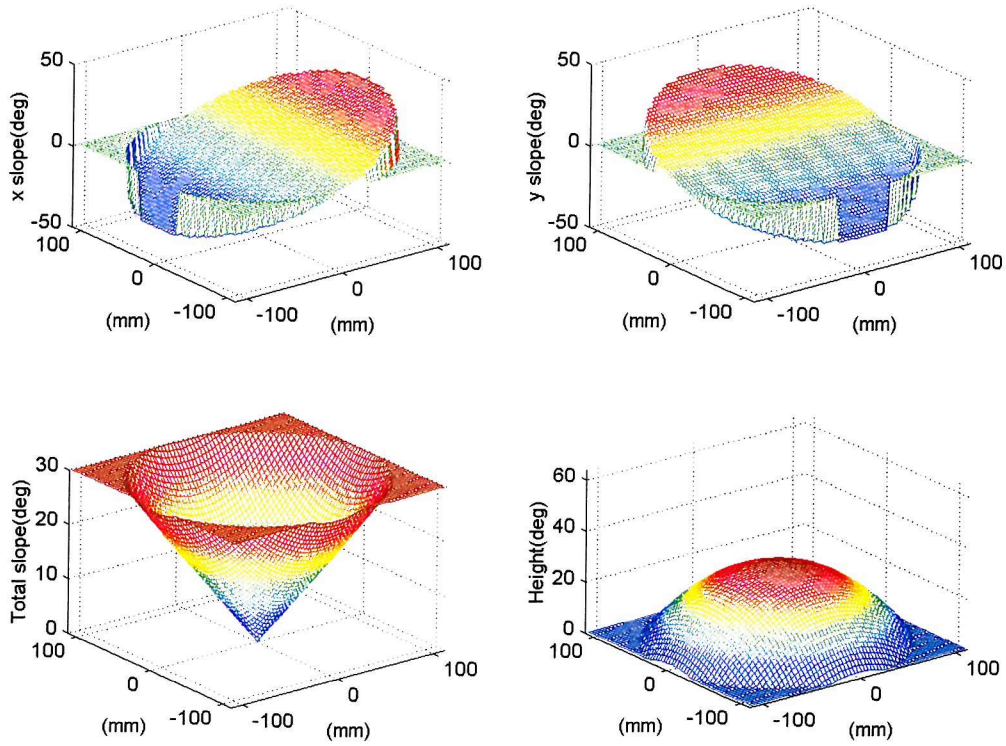

Figure 7. 8. Plots of the *x* slope (top left), *y* slope (top right), and total slope (bottom left) of a lens with the surface profile shown (bottom right).

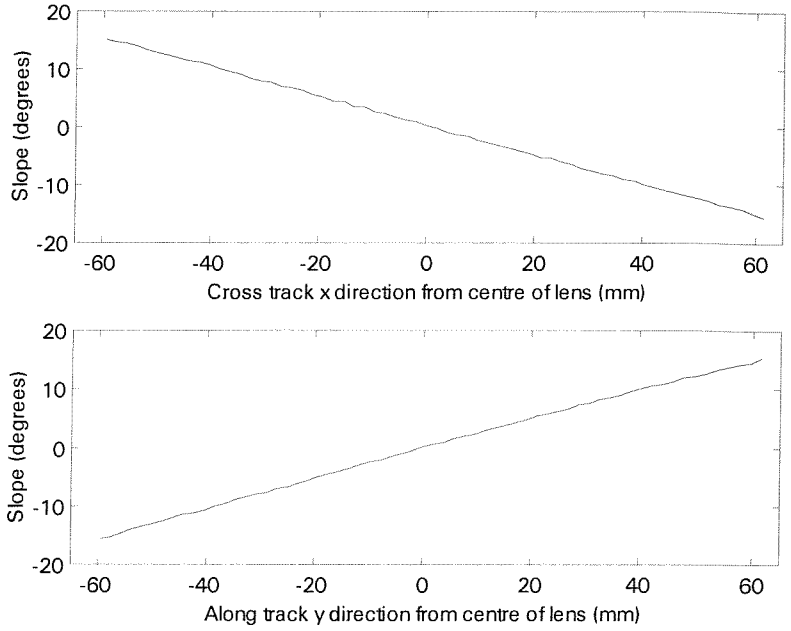

Figure 7. 9. The measured x slopes in the cross track and the measured y slopes in the along track directions.

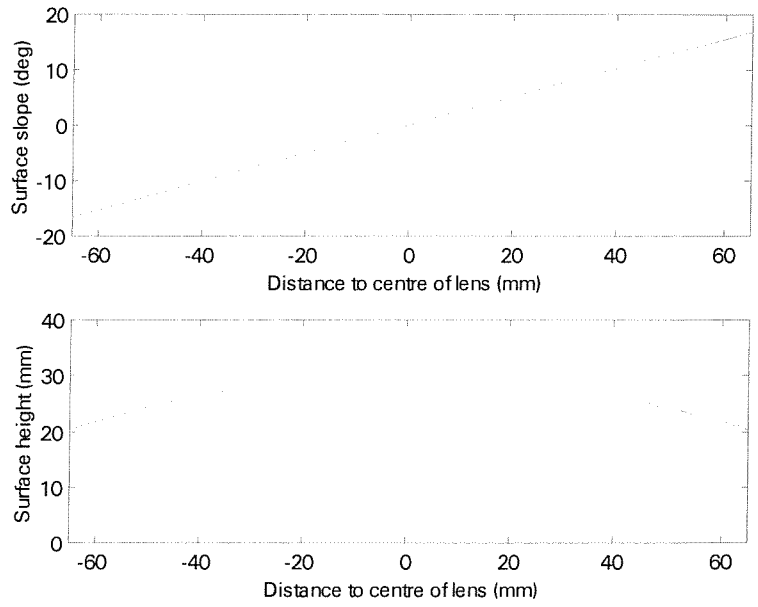

Figure 7. 10. The one-dimensional cross-section through the lens profile shown in Figure 7. 8 and the corresponding surface slope profile.

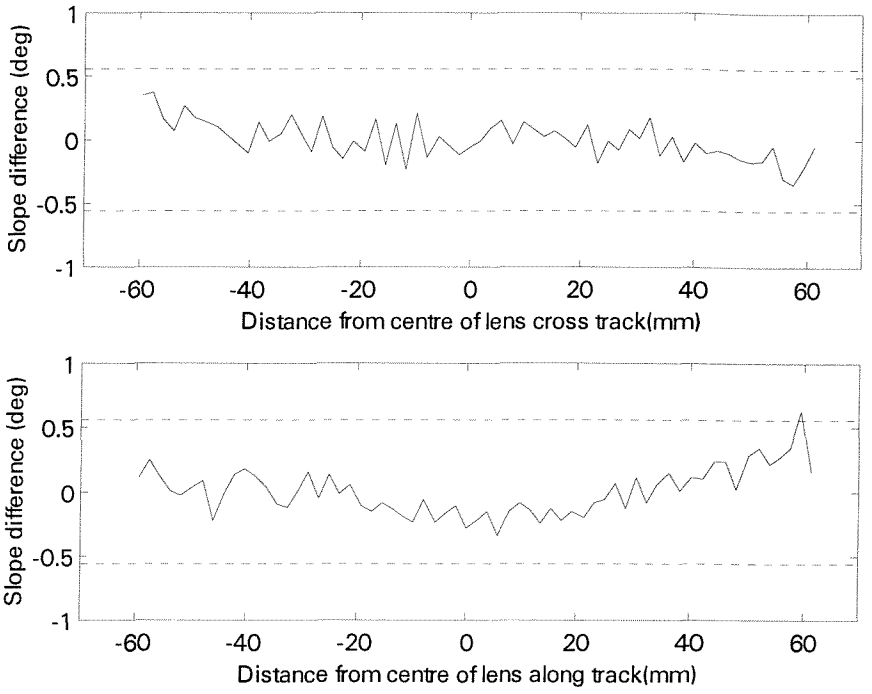

Figure 7. 11. The variation in surface slope profiles between the predicted and measured lens surfaces for the along track and the cross track directions. The dashed lines represents a slope resolution of ±0.56°.

These results are similar no matter where on the detector planes the measurements were made. They were also similar at all the speeds that the detector was run at. At higher speeds the scanning amplitude begins to be limited as discussed in chapter 4. Despite this scanning limit, it was still possible to run the detector with a sampling speed of 1MHz, which is the maximum rate at which the command board could run in its configuration at this time. At this speed it was still possible to record the position of the laser beam on the detector throughout the scan. However, the design of the command board is such that the time between each scan of the surface can not be made long enough to allow for the transfer time, of the data stored in the FIFOs to the PC. Consequently, the PC does not read the beam co-ordinates stored in the FIFO from the end of each scan line at this speed. The time required for the PC to read all 128 samples stored in the FIFO memory on the four Data Flow PCBs is 1.56ms. This time limitation is caused by the length of the cable used to transfer the data to the PC and could be improved using an alternative telemetry link. However, this was not necessary for the scan presently being used.

7.5.3. Water Surface Measurements.

Although, a measurement of the roughness of a water surface cannot provide any information about the accuracy of the instrument, it is important to show that the instrument can measure this dynamic surface. To investigate the behaviour of the laser beam through the water, the laser was scanned through the side of a small wave tank, where it was then reflected onto the water surface. Waves of approximately 1m wavelength were created in the wave tank using an wave generator. These waves had amplitudes of approximately 5cm. The laser beam refracted at the water surface was then detected using Digital slopemeter. This experimental arrangement is shown in Figure 7. 12.

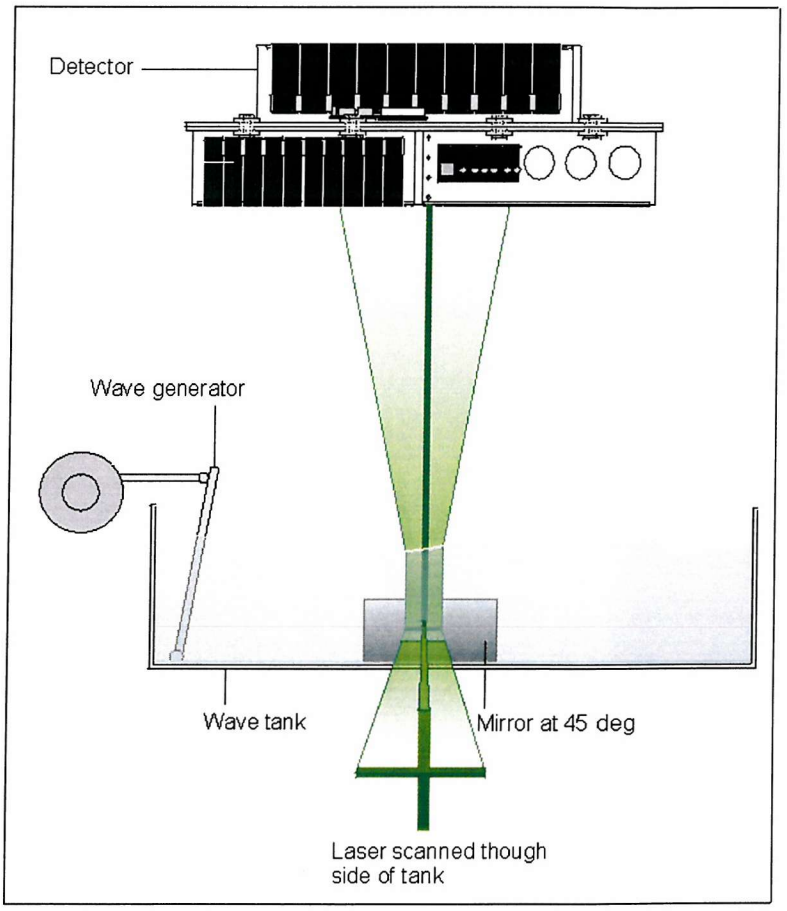

Figure 7. 12. Experimental arrangement used to measure a rough water surface.

An example of the raw beam positions recorded on every layer in the detector while the laser beam was being passed through the water surface are shown in Figure 7. 13. With no water surface present the lines would follow the shape shown in this figure but with out the wobble and the dropouts. The wobbles in these lines were caused by the presence of the rough water surface and clearly some of the features on the surface were causing the beams position to be

lost. It was determined that the long wavelength, low amplitude waves in the tank, caused smaller capillary size waves to be produced at the tank walls. The crests of these waves were aligned parallel with side walls of the tank and propagated perpendicular to them. When these small waves crossed the path of the scanned beam, the detector occasionally lost the position of the laser beam. The number of dropouts observed increasing as the number of these small waves increased which further verified this conclusion.

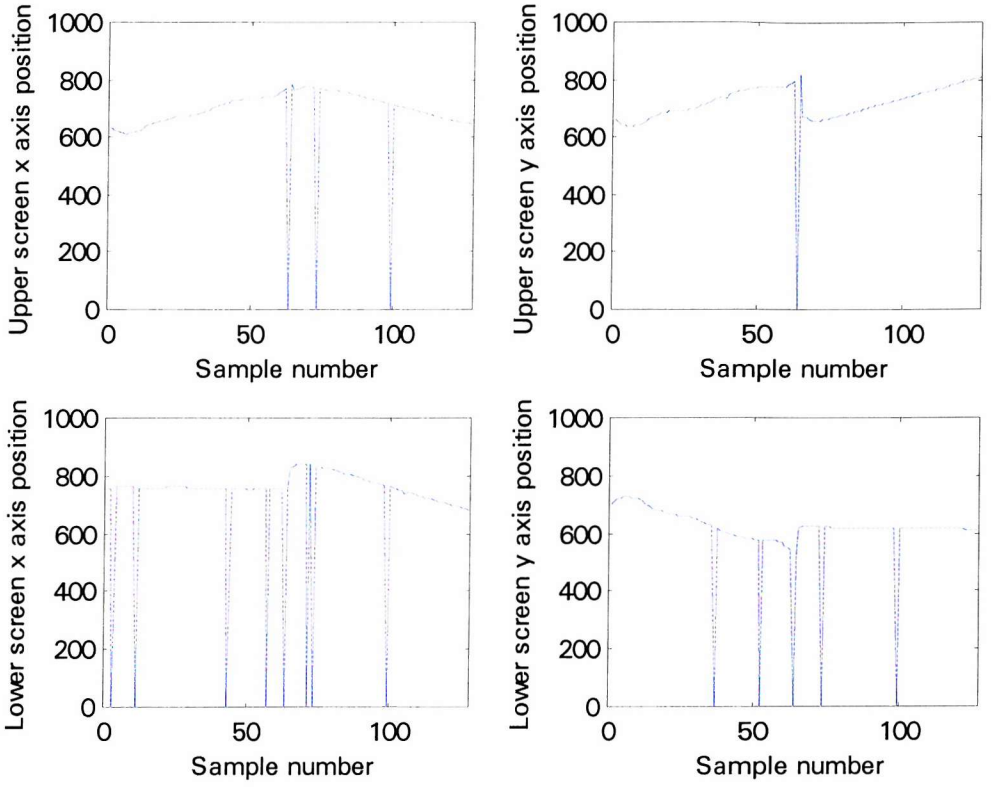

Figure 7. 13. The recorded beam positions from all four axes of the detector, throughout a scan of the water surface in a wave tank.

7.6. Conclusion

It has been shown that the Digital Slopemeter constructed exceeds its initial design specification, for both speed and resolution. With this instrument, it is possible to measure the slope of a surface in less than 1μs. This sampling rate will permit a more complex scan of the surface to be made if necessary. Alternatively, the speed of the scan presently used may be increased. This would allow the speed of the research vessel to be increased providing flexibility in the method of deployment of the Digital Slopemeter, depending on the sea conditions encounter.

However, when measuring a dynamic water surface some features on the surface cannot be detected because they cause the beam position to be lost. It was suspected that the reason for this was the laser beam expanding to more than the 7 fibres (larger than 11.2mm), due to the presence of the small capillary waves on the water surface. To establish how often this is likely to occur, a study of the spreading of the laser by a rough surface was carried out. This study will be discussed further in Chapter 8.

Chapter 8
Detector Modifications and Results

8.1. Introduction

It has been shown that the Digital Slopemeter can measure the surface slope with a resolution of better than ±0.56° over a minimum range of ±34.6°. However, it has also been shown that certain features on a dynamic water surface cause zero slope measurements to be recorded. It was suspected that these zero readings were caused by the laser beam having spread, due to the curvature of the water surface, to more than the 12mm allowed for in the original design. In this chapter, the beam spread caused when a beam of a given diameter passes through the water surface which has been disturbed by sinusoidal waves of different amplitude and wavelength, has been investigated. This permitted a suitable method for recording the beam slope to be suggested. Modifications to the readout electronics to enable the slope of the spread laser beam to be measured have been made. These modifications allowed wind-driven waves in a wave tank to be recorded successfully. The results obtained using the modified readout electronics are presented in this chapter.

8.2. Laser Beam Spreading Effects

As a collimated laser beam of finite diameter passes through a curved water surface, different parts of the beam will be refracted by different amounts depending on the local surface slope. Consequently, the laser beam will no longer be collimated and the beam diameter at the detector planes will therefore vary. At a trough of a wave, the surface is concave so the beam will diverge. At a peak of a wave, the surface is convex and the beam will initial be focused before it diverges. Both cases are shown in Figure 8. 1.

To calculate the spreading of the laser beam, its area was split into discrete rays whose paths where traced as they emerged from a one-dimensional sinusoidal wave surface. The rays that

were refracted most before striking the detector layer a distance h away from the surface were used to calculate the beam spread [Appendix D].

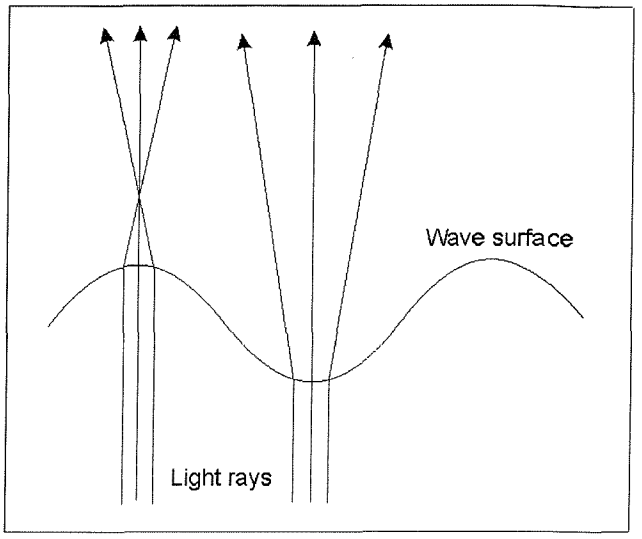

Figure 8. 1. The refraction of light at the tough and crest of a wave.

The beam spread at the detector plane as the beam moves across a sinusoidal wave will vary. Initially, the dependence of this spreading on the beam diameter was investigated to determine whether reducing this diameter would reduce the spreading of the beam significantly. The graph at the top of Figure 8. 2, shows how the beam spread changes across a sinusoidal wave for different beam diameters varying from 0.5mm to 3mm, in 0.5mm increments. This wave hadan amplitude of 32mm and a wavelength of 224mm.

The maximum distance between the top detector plane and the surface from which the instrument is designed to measure waves is 1.5m. At this distance the beam will have reached its maximum spread. Consequently, the beam spreads shown in Figure 8. 2, are calculated at this distance and will be less than this the majority of the time. The wave amplitude and wave slope profiles for this wave are also shown in Figure 8. 2 on the lower graph. Both the graphs in this figure have the same x-axis scale so that the beam spread can be related to a position on the wave. It can be seen that the beam spread increases linearly with beam diameter. Note that at the wave peaks the beam is first focused before it expands (Figure 8. 1) and consequently will spread less than when it is at the trough. It is clearly shown, in Figure 8. 2, that close to the maximum wave slope, the laser beam is focused to less than 1.6mm at the detector layer. This occurs even if the beam diameter is initially greater than this. At these points the beam may fall in between the fibres and would therefore not be detected. The dashed lines in the upper graph

represent the maximum and minimum beam diameters of 1.6mm and 11.2mm respectively, that could be recorded using the original detector.

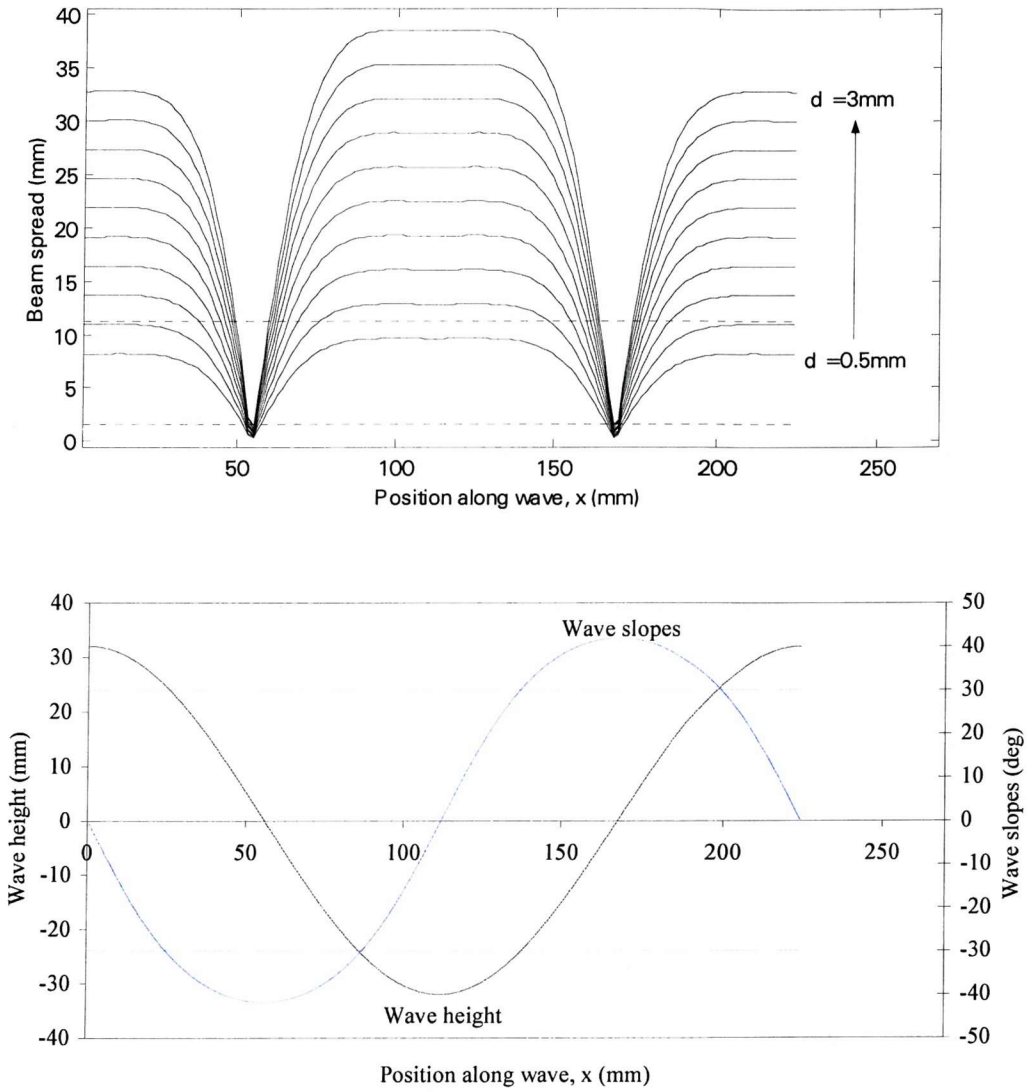

Figure 8. 2. (Top) The increase in beam spread with increasing laser beam diameter for a wave with amplitude of 32mm and wavelength of 224mm. Also plotted are lines representing the maximum and minimum beam diameters, of 1.6mm and 11.2mm respectively, that can be measured with the original detector. (Bottom) The wave amplitude and wave slope profiles that have generated the beam spread on the top graph. The dashed lines represent waves slopes of ±30°.

The laser beam will clearly spread less when the beam diameter is smaller and if the beam diameter is less than 1mm, it would be detected at most positions along this wave. However, in calm seas when the beam will not be significantly spread, it is likely that the beam would be less than 1.6mm the majority of the time. It is important to be able to measure waves on these calm days, consequently, a beam diameter of 2mm was chosen and will be used in the following calculations.

The beam spread will also depend on the wave amplitude. To investigate this dependence, the beam spreading was plotted as a function of wave amplitude as shown in Figure 8. 3. A section through this surface at 10 different amplitudes is also shown in the lower graph in this figure. The maximum beam spread increases with increasing amplitude of the wave, due to the increased curvature of the wave. With the exception of the small region where the beam is focused to below 1.6mm, the detector would be able to measure an amplitude to wavelength ratios of up to $1/6^{th}$, provide the electronic readout is modified to measure a beam spread of up to 50mm. It is unlikely the surface will act as a perfect lens or that the laser would ever be perfectly collimated. Therefore, it is unlikely that the laser beam would be focused to the same extent as shown here. Consequently, the region where the beam diameter is less than 1.6mm is likely to be very small.

It is expected that the wave amplitude is not likely to be greater than $1/7^{th}$ of the wavelength for ocean waves [Kinsman 1965 P6]. This is not necessarily the case for the sinusoidal components that make up the sea surface. However, a sinusoidal wave whose amplitude is $1/7^{th}$ it's wavelength, will generate slopes that are over ±30° as shown in Figure 8. 2. By considering the wave slopes that have been previously measured [Taylor 1996, Shaw et al. 1996 and Cox et al. 1954], very few wave slopes are greater than ±30°, as shown in Figure 8. 4. This suggests that very few large amplitude waves are present. The following discussions will, therefore, be based on waves with amplitudes of $1/7^{th}$ the wavelength.

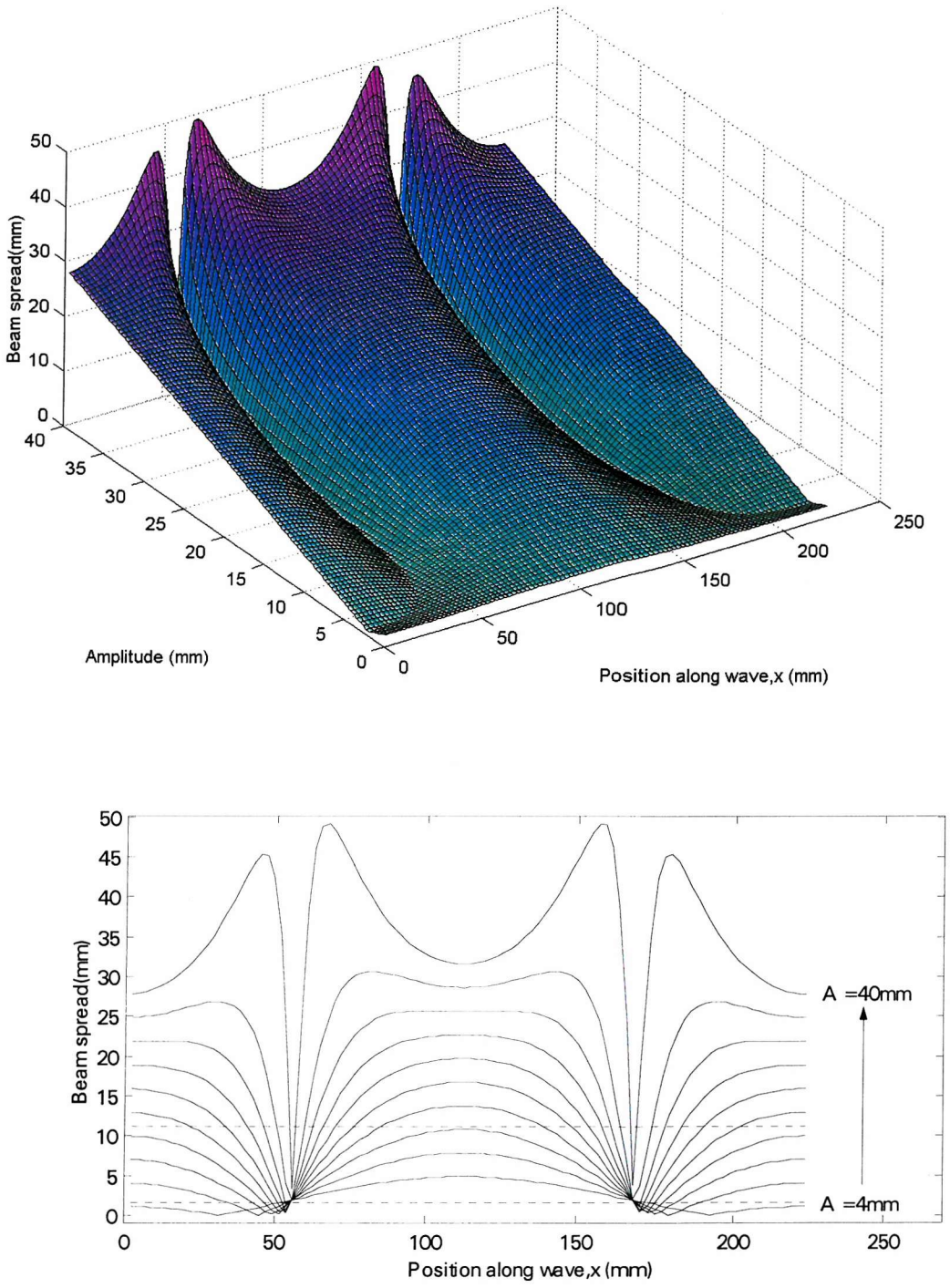

Figure 8. 3. (*Top*) A plot of the beam spread as a function of amplitude and position along a sinusoidal wave. (*Bottom*) Cross-sections through the top graph at constant amplitudes. The dotted lines show the measurement limits of the original electronic readout.

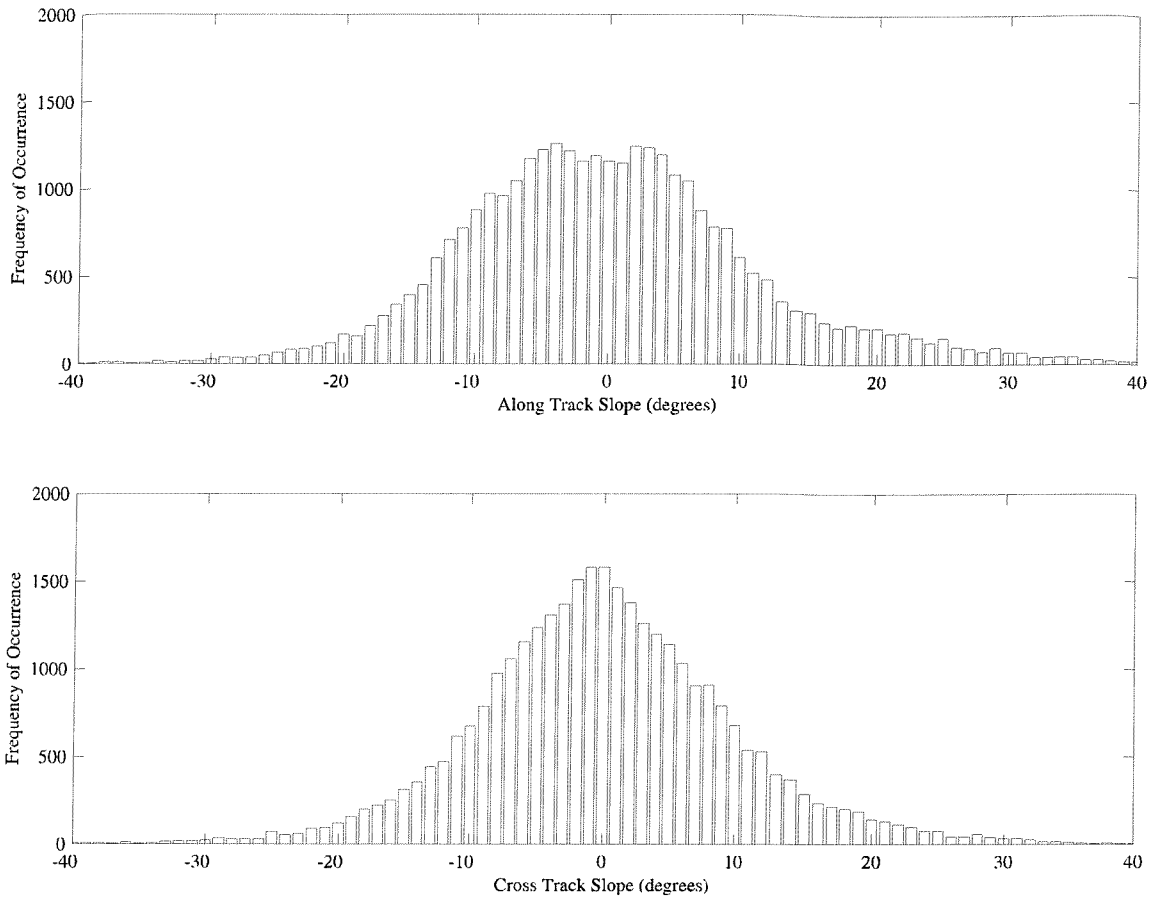

Figure 8. 4. Wave slope histogram of data collected by the TLS during run 3 of the 9th September 1994 in the Loch Linnhe field trials.

Finally, the dependence of the beam spread on the wavelength was considered. The beam spread has been plotted as a function of wavelength in the upper graph in Figure 8. 5, for wavelengths between 224mm to 100mm. A cross-section through this surface at the two extreme wavelengths is also shown in Figure 8. 5. As the wavelength decreases, the beam spread increases again, due to the increased surface curvature. For these wavelengths the beam does not expand over a diameter of 50mm, however as the wavelength decreases below those plotted the beam expands significantly and at a beam diameter of 10mm it expands to greater than 300mm.

In summary, the surface curvature of the sinusoidal waves increases with both wavelength and the amplitude. Consequently, the beam spread will also increase with wavelength and amplitude.

The fraction of any wave with a given wavelength and amplitude that can be measured by the detector in its original configuration may be calculated and plotted as a wavelength amplitude

surface. This surface has been plotted in Figure 8. 6 for a limited range of amplitudes and wavelengths. This amplitude range is limited to 8mm because light incident on the smallest wave that has a 50mm wavelength, will be totally internally reflected if the wave amplitude increases further and consequently, can not be measured. As discussed before it is unlikely that such a wave will occur. The graph in Figure 8. 6 is made up of four regions. At very small amplitudes relative to the wavelength the beam diameter does not vary a great deal from 2mm and therefore 100% of the wave is measured. For amplitudes that are slightly larger than this the laser beam is not detected while it is has been focused to below 1.6mm. As the amplitude to wavelength ratio increases the laser beam spends increasingly more time with a diameter between 1.6mm and 11.2mm. Consequently, the proportion of the time that the beam can be detected increases until eventually it reaches the peak in the plotted surface. After this point the maximum diameter of the beam begins to increases above 11.2mm. The fraction of the wave that can be measured then starts to decrease. The maximum beam diameter then continues to increase with increasing amplitude and decreasing wavelength so the fraction of waves that can be detected continues to fall.

As discussed before, it is unlikely that the beam would be focused to less than 1.6mm to this extent. Therefore, the lower plot in Figure 8. 6 shows the same surface but with the focusing effect ignored. In this plot the beam is only undetectable when its diameter increases above 11.2mm. It is likely that the actual surface would be somewhere between the two plots in Figure 8. 6.

If the sea surface is made up of several wave components then the chance of recording a wave slope from that surface is dependent on the wave component with the highest surface curvature. If small wavelength, large amplitude, waves are present on the surface the likelihood of measuring the slope of any wave on the surface becomes increasingly small. There is a clear cut-off in the lower plot in Figure 8. 6 where the detector stops recording 100% of the waves. Evidently, the waves measured in the wave tank, using the detector with its original readout electronics, were small enough and had large enough amplitudes to cause the detector to stop recording the wave slopes. Consequently, the electronics has been modified so that the detector can record the expanded beam that has been generated by these waves.

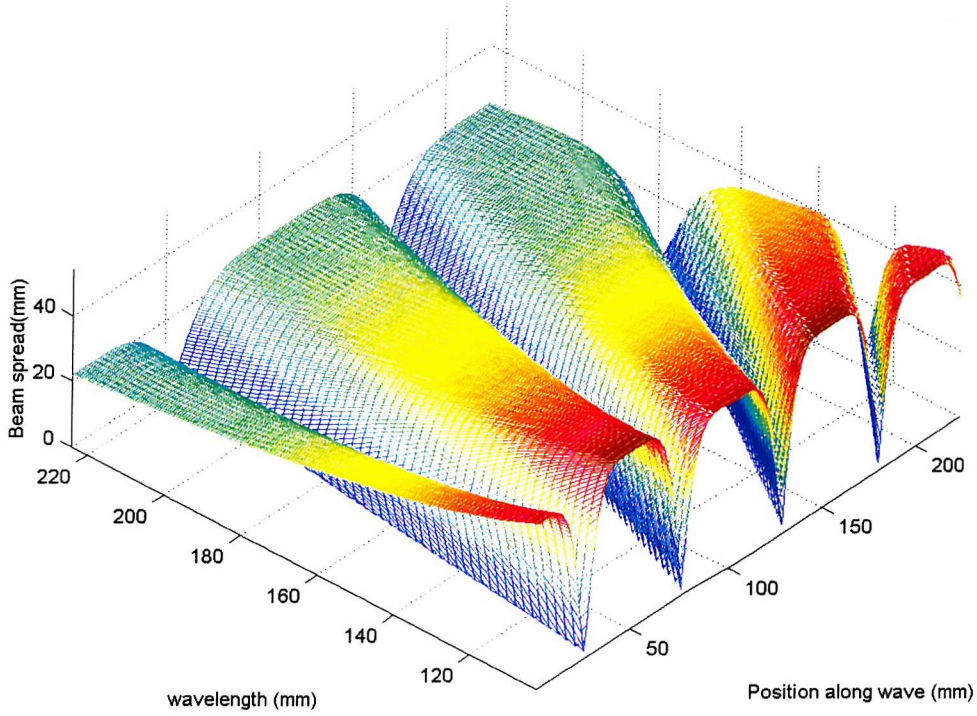

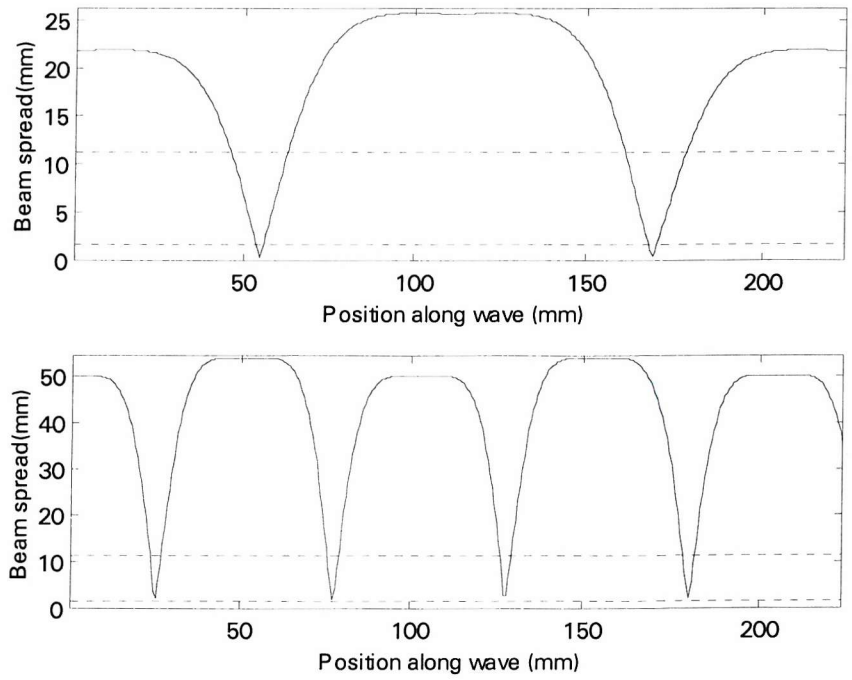

Figure 8. 5. The beam spread generated by different wavelength having an amplitude to wavelength ratio of $1/7^{th}$ (Top). Beam spread curves for 224mm (Middle) and 100mm (bottom) wavelengths.

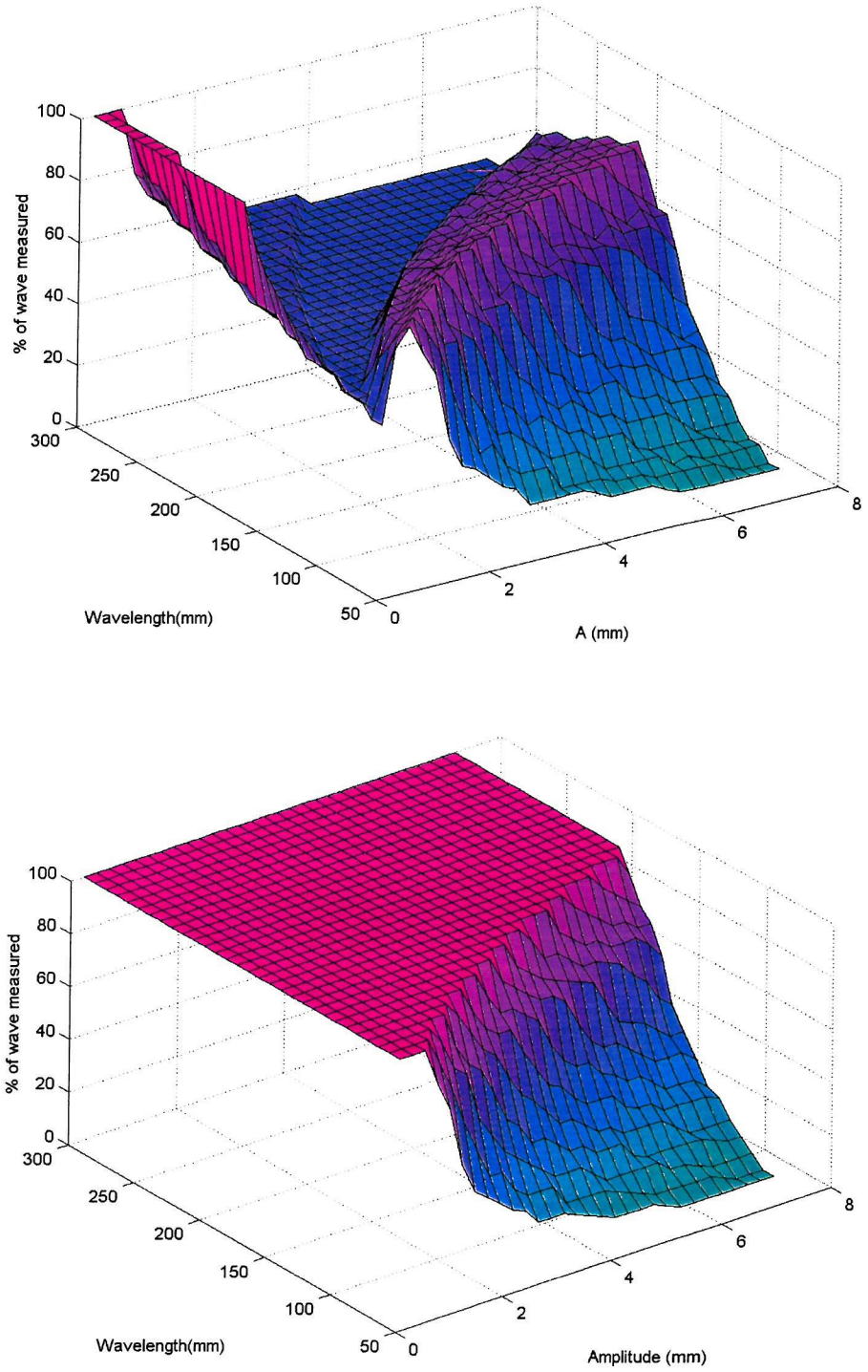

Figure 8. 6. (Top) A graph showing the percentage of waves with varying amplitudes and wavelengths that would be measured with the original detector. (Bottom) A graph showing the percentage of these waves that would be measured if the beam is never focused below a diameter of 1.6mm.

8.3. Initial Electronics Modifications

The original Front End Electronics PCB design determined the position of the laser beam on a detector layer provided less than 7 fibres were illuminated. If more than 7 fibres were illuminated then a zero beam position would be returned. This ensured that there were no ambiguities in determining the position of the laser beam centroid. With the realisation that the laser may expand considerably, the fibre readout system was modified to allow any size beam to be recorded so that the extent of the beam spread could be measured.

Initially, to permit the shape of laser beam on the fibres to be investigated, two Front End Electronics PCBs were modified. This modification allowed the output signals from every fibre to be read into the PC. This involved reading, in series, the 8-bit output from every sampling latch into the First In First Out buffers. The output of each latch was enabled in turn using a 16-pulse strobe signal that was generated on every Sample Count pulse. A single sample of the position of the laser beam from the two Front End Electronics PCBs consisted of sixteen 8-bit numbers representing the 128 fibres being read. For a single axis scan consisting of 64 samples, the PC had to read 1024 8-bit numbers from the FIFOs. The PC collected this data as an array, consisting of 128 fibre positions by 64 scan positions. When using two Front End Electronics PCBs, reading the beam position was 16 times slower than the original detector electronics could have read data from an entire axis. However, the modified readout electronics was still sufficiently fast to sample the beam position every 35μs. However, the time taken to transfer the data stored in the FIFO from a complete scan of the surface, increased from 1.56ms for 128 11-bit numbers to ~ 20ms for the 1024 8-bit numbers. Nevertheless, this allowed the spreading of the beam to be investigated before a more efficient modification was suggested.

8.4. Preliminary Results

The experimental arrangement used to measure wind driven waves created in the wave tank is shown in Figure 8. 7. An example of the raw data collect from the two modified Front End Electronics PCBs is shown in Figure 8. 8. These waves were generated using a air blower pointing at the surface about 30cm from the measurement area. These waves were of relatively low roughness but clearly demonstrate the operation of the instrument. The spread of the laser beam can clearly be seen and in this case does not increase in diameter to more than 7 fibres.

From this spread the centroid of the beam position can be determined for each of the 64 samples. Although both layers of the detector were not in use, it was possible to determine the beam slope by measuring the distance between the detector layer and the surface. This height did not

varying significantly due to the small amplitude of the waves being measured. This allowed the y direction wave slopes of the waves being measured to be estimated using the equations discussed in section 6.5, which are,

$$s_{by} = \frac{y_T - y_l}{D} \tag{8.1}$$

$$s_{by} = \tan\theta_{by} \tag{8.2}$$

$$\tan\theta_{sy} = \frac{\sin\theta_{by}}{\frac{n_w}{n_a} - \cos\theta_{by}} \tag{8.3}$$

In equation 8.1, y_T is taken as the beam position measured by the modified Front End Electronics PCB, y_l as and the known position of the beam on the water surface and D as the distance between the detector plane and the water surface. In this way the beam slope (s_{by}) can be calculated.

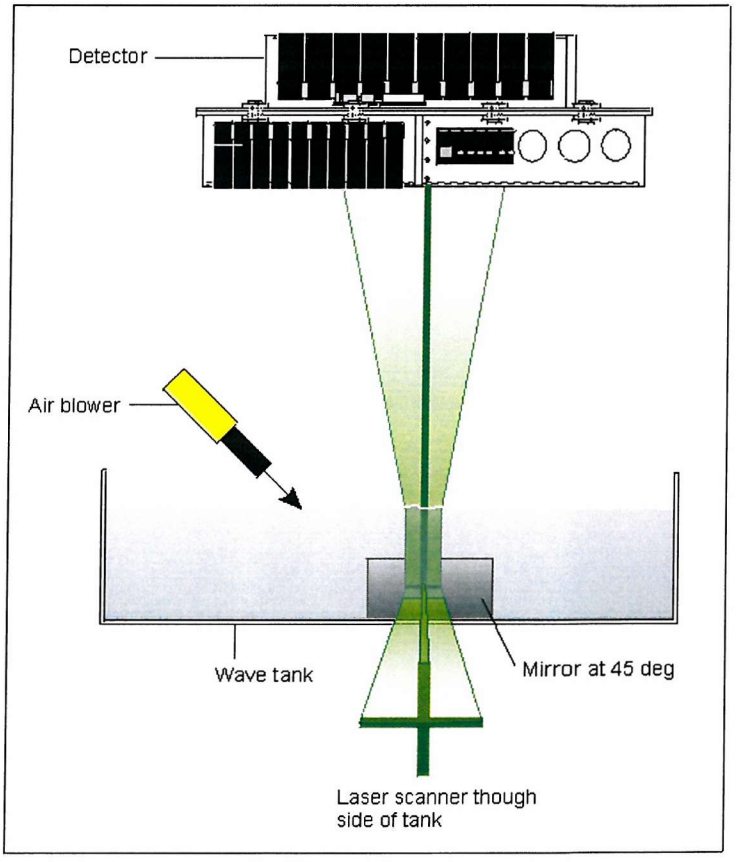

Figure 8. 7. Experimental arrangement used to measure wind driven waves in a wave tank.

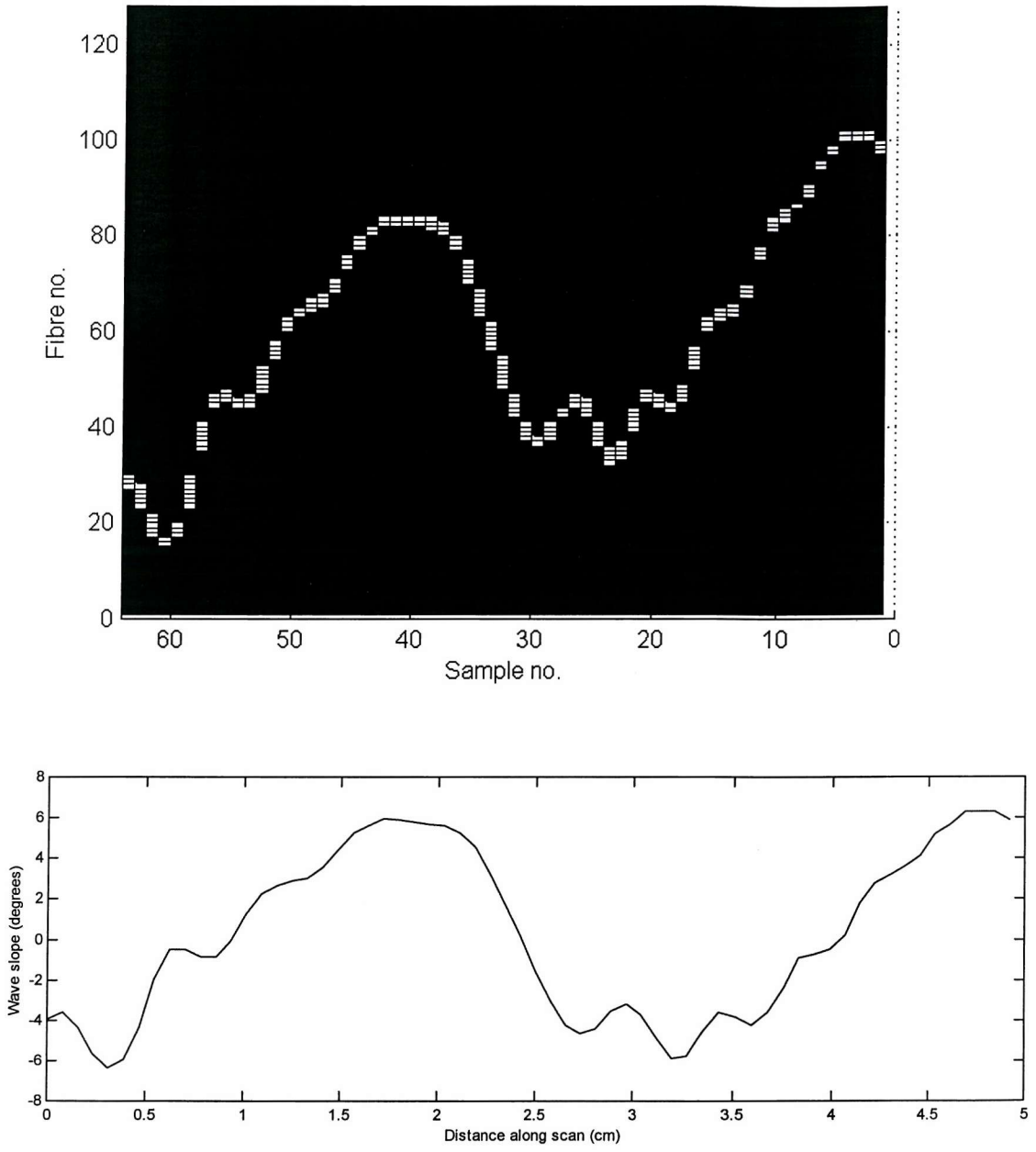

Figure 8. 8. (*Top*) Raw data collect by the modified Digital Slopemeter. (*Bottom*) The calculated wave slopes generated from the raw data, showing wind driven waves with wave slopes up to ±6.5°, over a 5cm scan of the water surface.

The calculated slopes from a 5cm long scan are shown on the bottom graph in Figure 8. 8. The primary waves being measured have a wavelength of 3cm and the secondary waves have a wavelength in the order of a centimetre. A photograph, of these waves along side a centimetre scale is shown in Figure 8. 9. The measured waves were compared with the photograph of the water surface. The wavelengths seen in the photograph may be estimated to be 3cm and 1cm

which correlate with those measured by the digital slopemeter. This correlation shows that the instrument is measuring waves down to 1cm wavelengths. The waves measured here only had relatively low amplitudes and did not spread the beam enough to prevent the original detector from measuring them. However, the data displayed on the top graph in Figure 8. 10, was collected from a rougher surface with wave slopes that are almost twice those seen in Figure 8. 8. This shows the beam spreading to 14 fibres, which would be sufficient to prevent the original readout electronics from recording a valid signal. The signal is also sometimes lost within a beam diameter. These may be caused by the intensity of the laser beam falling to below the threshold level of the detector as the beam expands and would also prevent the original detector configuration from making a measurement.

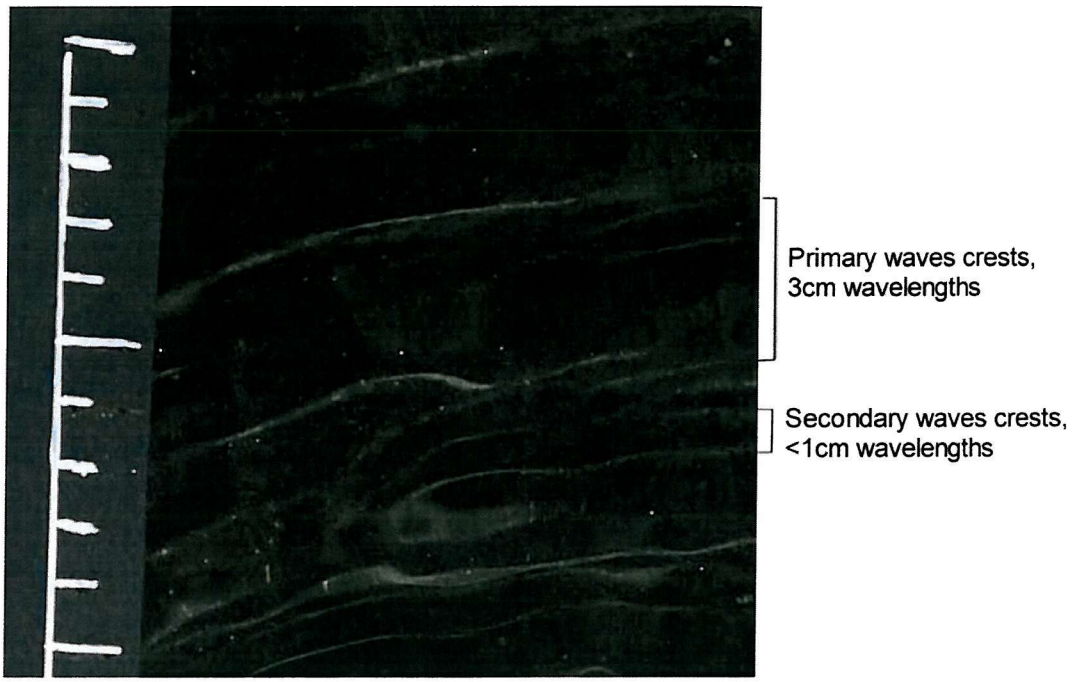

Figure 8. 9. Photograph of wind waves generated in a wave tank in the laboratory. A 1cm scale is shown on left of photograph.

The bottom graph in Figure 8. 10 shows the raw data collected from the roughest surface that could be generated in the wave tank. The maximum slopes of these waves could not be measured using only two modified FEE PCBs. However, the beam spread can be observed to cover up to 35 fibres, which is a beam diameter of 56mm. It is clear, that the modified readout electronics will behave well in these rough conditions. The roughest waves generated in the wave tank were close to breaking and it is unlikely the instrument would be deployed in these conditions when the sea state may be considerable. Nevertheless further investigation into the beam spread at sea will be carried out when the instrument is deployed. This will verify whether

the measurements being made are a reliable record of the wave slopes. It will also determine whether the extra information, about the maximum difference between wave slopes across the beam diameter, gained by measuring the beam spread, is useful.

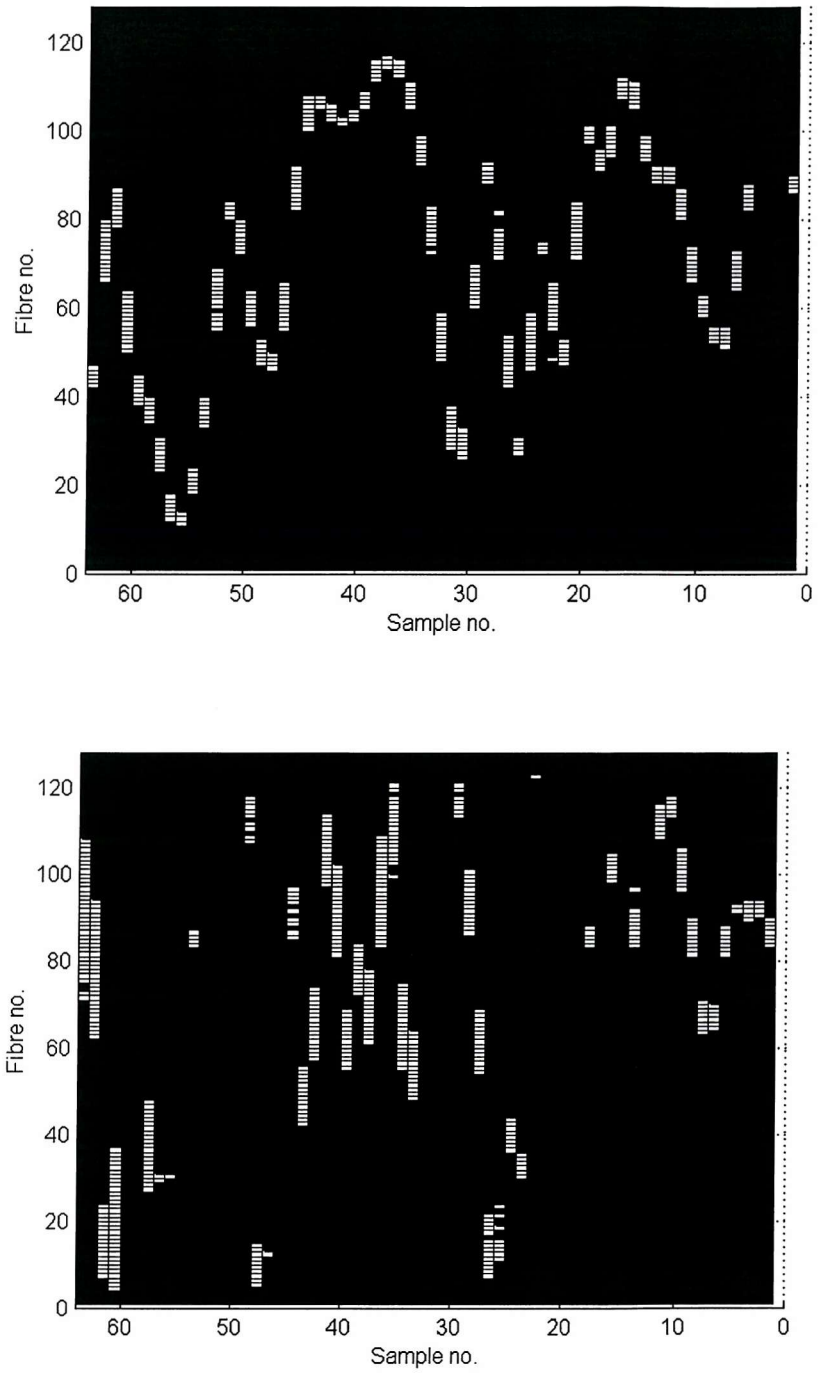

Figure 8. 10. (*Top*) Raw data recorded from a rougher water surface with wave slopes up to ±12°. (*Bottom*) Raw data collected from the roughest surface that could be generated in the wave tank.

8.5. Conclusions

From these results, it is clear that, although the 2mm beam can spread to greater than 5cm as a consequence of the curvature of the water surface, it is still possible to determine the accurate position of the beam by recording its centroid. This is provided the electronics is modified to record the increased diameter of the laser beam. The modifications that were described in this chapter could be used to readout the fibres for the whole detector. However, this would significantly reduce the rate at which the scan pattern could be repeated and would generate a great deal of data for the PC to process. Consequently a more efficient method of recording the beam position will be considered in chapter 9.

Chapter 9
Future Work and Conclusions

9.1. Future Work

It is clear from the previous chapters that the Digital Slopemeter will provide accurate wave slope measurements that will permit a real-time display of the data. This will greatly improve the efficiency with which the instrument can be deployed. In this chapter, modifications to the readout electronic that will enable the laser beam to be detected, even when its shape has been modified by the curvature of the water surface, are suggested. The instrumentation that would be required make accurate and meaningful measurements of the surface roughness will be described. Additional instrumentation that would provide supporting measurements of the environment in which these waves have been generated will also be suggested. Finally, some possible modifications to improve the instrument after the initial trails have been completed, will be proposed.

9.1.1. Detector Modifications

There are several possible modifications to the electronic readout circuits that would allow the beam position to be measured if its diameter at the detector planes increases to greater than the 11.2mm that the original detector was designed to measure. The initial modifications that were made to just two of the Front End Electronics PCBs described in chapter 8, allowed all the fibre outputs to be measured. Using this technique it would be possible to examine every one of the 2560 fibres in the detector. In fact the fibre data from each of the four axes of the detector could be read in 5μs. This is provided the data is read in a similar way to the original detector design, using the maximum Command Board clock rate of 16MHz for the strobe signal. However once this data had been stored in the FIFOs the time taken to transfer the fibre data to the PC would significantly increase compared to the transfer time required with the original detector configuration. It would take ~125ms to transfer the data stored in the FIFO to the PC as opposed to 1.56ms. Once the PC has received this large amount data it must then deal with it to generate the centroid of the beam on the four axes. This will reduce the time available for the PC to carry

out the real-time processing tasks. Therefore, a solution that requires less data to be sent to the PC is preferable. Ideally, the data generated by the modified system should be processed in hardware. This would reduce the quantity of data transferred to the PC.

Two ideas have been considered, both of which still examine the individual fibres in the detector. In the first method (Figure 9. 1 a)), the fibres are examine sequentially from one side of an axis of the detector. When the first non-zero output is detected a predefined block of data is read consisting of 8 latch outputs. Using this technique, each sample from an axis will only consist of data from 64 fibres instead of the 640 fibres on a complete axis. However, if the beam were to spread to greater than 64 fibres or a spurious second signal was present, then the system may fail to identify the true centroid of the laser beam. The second method considered (Figure 9. 1b)), examines the fibres sequentially from one side of an axis in the same way as the first technique. When the first non-zero fibre reading is detected its position would be stored in the FIFO. The fibre outputs are then examined from the other side of the axis until the first non-zero fibre reading is detected. Again this position is stored on the FIFO. This method identifies the two edges of the spread beam and would not miss any illuminated fibres. Consequently, the width of the beam could be determined using two 11-bit numbers that are transferred to the PC. This data could be transferred in 3.2ms. Although, dropouts and spurious points lying between the two outer most fibre signals could not be identified, abnormally large beam spreads could be rejected. This final solution is preferred and it is envisaged that it would not require an excessive alteration to the existing design relative to the other options mentioned in this section.

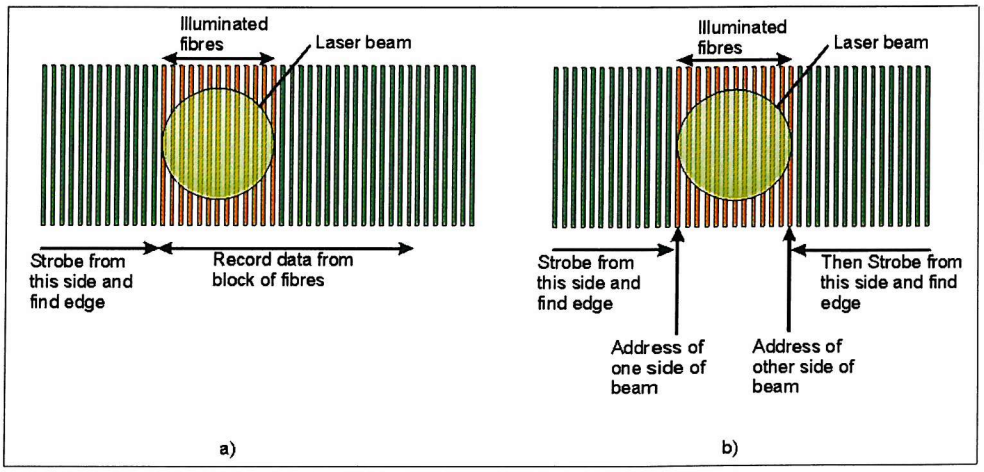

Figure 9. 1. Two possible methods that could be used to measure a larger beam diameter. Either, a) the first fibre of the beam can be detected and then a predefined block of data recorded after that point or b) the two edges of the beam can be identified.

9.1.2. Digital Slopemeter Integration for Ocean Deployment

Once the detector is successfully operating in the laboratory in its fully modified form, it is necessary to integrate the instrument with a structure to attach it to the bow of a research vessel as described in chapter 7. This structure should enable the detector to be deployed not only from the bow of the research vessel but also from a pontoon or pier. This will allow experience in deploying the detector, to be gained prior to a relatively expensive sea trial. This structure must ensure that the underwater laser scanning system is mounted rigidly to the detector. For the initial deployments of the instrument at sea it is proposed that a simple rigid structure is used to attach it to the research vessel. This will be sufficient to deploy the instrument in coastal waters although, if it is to be deployed in open waters it would be preferable if the instrument could be lifted from the water. This would allow the instrument to be moved safely at speed to the area of the ocean where it is going to be operated.

The objective of this instrument was to investigate small-scale surface roughness to aid the investigation of the sea surface structure that is observed by imaging radar. This is in addition to furthering the understanding of the processes involved in radar backscatter from the ocean surface. Therefore, it is important to relate the wave slopes measured to space and time co-ordinates. The timing of the measurements is recorded using the PCs internal clock, which is carefully set. In order to relate the measurements to a position in space the following instrumentation will be deployed:

- **A tiltmeter** to provide a measure of the inclination of the instrument relative to the horizontal. These inclinations are removed from the wave slope measurements made to generate wave slope values that are relative to the horizontal. It is expected that this correction will be small until the wavelengths become comparable to the length of the research vessel. In these conditions vessel may begin to pitch considerably.

- **Differential Global Positioning System** to provide the longitude and latitude measurements of the instrument to within a few meters accuracy. This provides the track of the vessel over seabed. It also allows the position of the instrument to be related to charts of the area, which in turn can be related to radar image of the area.

- **A simple impeller** to record the speed at which water flows past the instrument. This would be mounted near to the submersible scanner system. This measurement can be used to determined the error in the wave slope profile caused by the Doppler shift.

- **A magnetometer** to give the direction in which the detector points. This allows the absolute direction of each scan line to be determined.

This is the basic complement of instruments required during a deployment of the Digital Slopemeter at sea. In addition to these instruments it is also desirable to make synchronous measurements of the parameters that may effect the ocean roughness. Consequently, it is proposed that the following instruments will be deployed to provide information about the environment around the sea surface:

- **An anemometer** will measure the wind speed at a height of 5m above the sea surface. This can be used to indicate the wind speed required to generate a particular wave slope profile.
- **An echo sounder** will determine the depth of the seabed below the measurement area. By combining this data with the track of the vessel, a seabed profile can be generated.
- **A current-meter** will provide an accurate measurement of the current while the wave slope measurements are being made. This can be used in conjunction with the echo sounder data to determine how the flow of the water over the bottom topography affects the surface roughness.

The combination of the measurements made with these instruments in coincidence with radar images of the surface can be used to increases the understanding of radar backscatter. This is in addition to increasing the understanding of the processes taking place on the sea surface with relation to the wind, bottom topography and currents.

9.1.3. Future Development of the Digital Slopemeter

Finally, after the initial deployments of the detector, it would be desirable for the submersible scanner system to be modified to allow raster scan of the surface. This would generate a 2-dimensional wave slope profile of the surface allowing a two dimensional spectrum of the sea surface to be generated. This would enable a comprehensive study of the directionality of the wave field to be made. However, faster scanning units such as acousto-optic or rotating polygon mirror scanning devices would be required. Initially, it may be possible to use the present scanning system to gain further directional information about the sea surface. Possibly even an average two directional wave spectrum could be generated by rotating the cross scan pattern relative to the instruments axis in successive scans as shown in Figure 9. 2. However, further research is required before this can be confirmed as a useful technique.

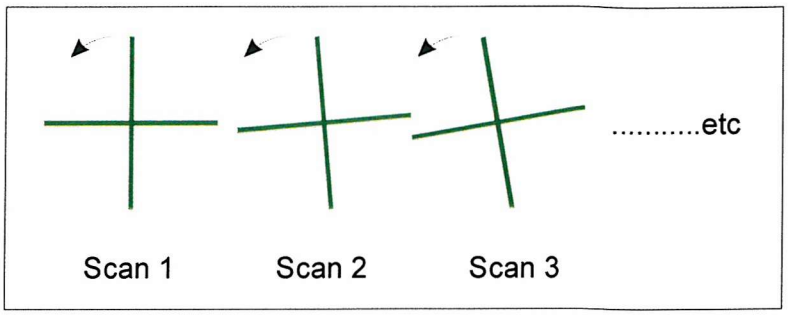

Figure 9. 2. A rotational scan pattern.

9.2. Conclusions

The objective of this work was to develop an instrument to measure the sea surface roughness to provide information about its profile. The Digital Slopemeter was designed to address the problems that have been encounter with past laser slopemeters. It has been designed to measure the sea surface wave slope profile using a laser scanning system, which will allow a wavenumber spectrum to be generated. The wave slopes from waves with lengths between 10 and 224mm can be measured with this instrument. The design of the Digital Slopemeter allows it to be deployed from the bow of a research vessel in moderate seas. However, the nature of its design would not prevent the instrument being used with much larger waves by scaling it up in size.

It has been shown that the instrument built has met the resolution, range and speed specifications that were laid out in chapter 4. Chapter 9 has suggested a permanent seaworthy modification to the readout electronic, which will allow the laser beam to be detected even when in has expanded to greater than 11.2mm, which the original detector was designed to measure. This modification permits the PC to determine the centroid of the beam with a minimum additional processing time. It is hoped that this instrument will generate convincingly accurate and reliable data sets, to allow a comprehensive study of the sea surface to be made in way that has not been achieved before.

Appendix A
The divergence of light from a small lens

Optical fibres can be used to scan the laser beam over the sea surface, as discussed in section 4.4.1. A lens can be used at the output of the optical fibre to generate a beam of collimated laser light. Unfortunately, the light from a finite diameter fibre can never be perfectly collimated in this way. The reason for this is best explained by considering Figure A. 1. The divergence of light from the optical axis of a lens after passing through the focal plane, a distance, d_c, from the focal point is given by the equation,

$$\tan\phi_d = \frac{d_c}{f} \qquad \text{(A. 1)}$$

where f is the focal length of the lens as shown in Figure A. 1. This indicates that the larger the focal length of the lens, the smaller the divergence of the beam. However, it is necessary to use a lens with a short focal length so that it may be placed close to the fibre. This will ensure that the all the light emitted from the end of the fibre is incident on the lens. A 3mm diameter spherical lens has a focal length of 1.65mm [Newport Products, 1996]. The divergence of the light emerging from a lens illuminated by a 50μm fibre, is 15mrad. This lens would produce a 30mm beam diameter at a distance of 1m. The use of a beam of this diameter would greatly reduce the resolution of the detector.

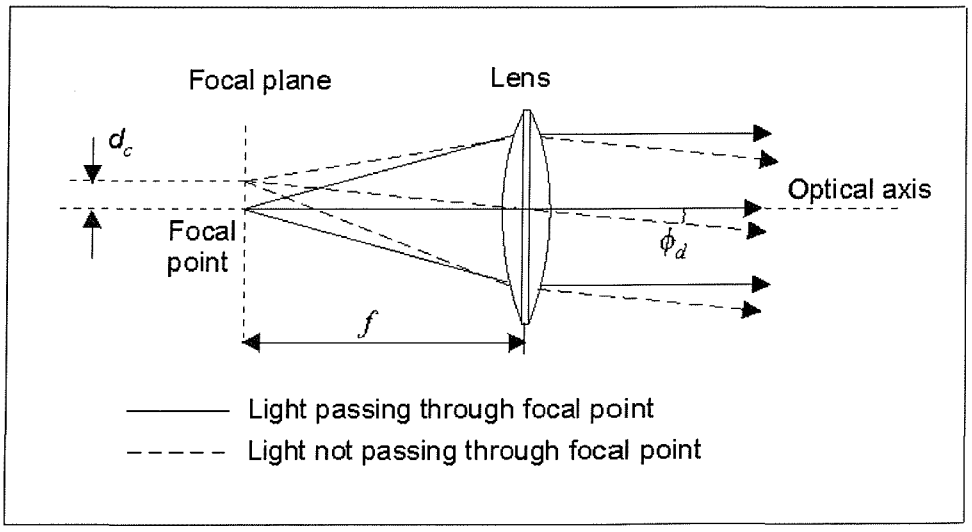

Figure A. 1. The collimation of light emanating from the focal plane of a lens.

The divergence of the beam can be reduced by using a gradient index micro (GRIN) lenses. These lenses have a refractive index that decreases gradually away from the central axis of lens. This causes the light passing through the lens to gradually change direction. Ray tracing can be used to calculate the path of light through the lens (these equations are given in the SELFOC Products Guide). The divergence of the light emerging from a 3mm diameter lens that is illuminated by a fibre with a core diameter of 50μm, is ~ 8.5 mrad. This would produce a beam of 17mm at 1m, which is still unsatisfactory.

The solution to this is to reduce the diameter of the core of the fibre which consequently reduces d_c. For example, a 20μm fibre illuminating a grin lens would generate a 2mm beam at 1m. For a fibre with this core diameter the amount of light that can be launched into it is greatly reduced.

The deciding factor in determining whether this system was feasible was the precision required to machine a mount to hold the lenses in position. The light emerging from each lens in the array, must be parallel. For example, two beams of light each with an diameter of 2mm placed 3.5mm apart will overlap 1m away if they are both offset by 1mrad towards each other. Both the inclination of the lens and the position of the fibre in front of the lens will effect the direction of the beam. It is extremely, difficult to position such a lens precisely in the limited space available. Therefore, an alternative approach to this is considered in sections 4.4.2 and 4.4.3.1

Appendix B
The Efficiency of a Wavelength Shifting Fibre

The wavelength shifting fibres that are used in the detector are double clad and absorb light of wavelength 532nm. This light is then emitted from the dye within the fibre isotropically as shown in Figure B. 1. Light will become trapped within the fibre when θ_{air} is greater than 90° and total internal reflection occurs. Using Snell's Law $n_{core}\sin\theta_{core} = n_{air}\sin\theta_{air}$ this will occur when,

$$\theta_{core} \leq \sin^{-1}\left(\frac{n_{air}}{n_{core}}\right) \qquad \text{(B1)}$$

The dye in the fibre re-emits light isotropically into a sphere. All the light that is emitted into the cone angle $\phi = \frac{\pi}{2} - \theta_{core}$ will be trapped in the fibre. The fraction of light that is trapped can be calculated by determining the fraction of the area of the sphere into which the light is being emitted. This can be achieved by first integrating over the area of the cone with the cone angle ϕ,

$$\text{Cone Angle, } \Omega = \int_{Cone\_angle} d\Omega = \int_0^{2\pi} d\theta \int_0^{\phi} \sin\phi \; d\phi$$

$$= 2\pi(1-\cos\phi) \qquad \text{(B2)}$$

Then by dividing the result of equation B2 by the total number of steradians being illuminated which is 4π to give the resultant fraction of light that is trapped as:

$$f_{TE} = \frac{1}{2}\left[1 - \cos\left(\frac{\pi}{2} - \theta_{core}\right)\right] \qquad \text{(B3)}$$

For the fibre specification given in Table B. 1 of n_{core} = 1.49 and with $n_{air} \sim 1$ using equation B.1, $\theta_{core} \sim 42°$. Therefore, the trapping efficiency, f_{TE} given by equation B3, is ~ 16.4%. A glass light-guide containing Ethanol was mentioned in chapter 5. Glass has a refractive index of 1.5 and Ethanol has a refractive index of 1.359 [Robert et al., 1980]. No light will, therefore, be trapped by the glass-Ethanol interface. However, light will be trapped at the glass-air interface. The efficiency of this light guide can be calculated using, n_{core} = 1.359 and with $n_{air} \sim 1$. Using equation B1 to B3, this efficiency is 13.2%.

The trapping efficiency can then be used to calculate the power emitted at the end of the fibre, P_E using the equation [Hecht 1987],

$$P_E = P_{TIR} e^{-\frac{l}{l_A}} \tag{B4}$$

where $e^{-\frac{l}{l_A}}$ allows for the reduction of light at a length l down a fibre with an attenuation length of l_A, and where the light energy trapped in the fibre, P_{TIR}, is given by $f_{TE} f_A P_I$. The value f_A is the fraction of incident light energy (P_I) absorbed by the dye. These equation where used in the model described in Section 5.4.3 to calculate the light output at the end of each fibre when a 50mW laser beam passes through the digital Slopemeter detector.

MANUFACTURER	BICRON	**1ST CLADDING**	
CORE		Material	Acrylic
Material	Polystyrene	Refractive index, $n_{cladding1}$	1.49
Refractive index, n_{core}	1.60	Cladding thickness	3% of fibre diameter
Density	1.05	Trapping efficiency, f_{TE}	3.44%
Wavelength shifting dye	BCF-99-06A		
Operating temperature	-20°C to +50°C	**2ND CLADDING**	
Attenuation length, l_A	>3.5m	Second cladding material	Fluor-Acrylic
		Refractive index, $n_{cladding2}$	1.42
		Second cladding thickness	1% of fibre diameter
		Trapping efficiency, f_{TE}	5.6%

Table B. 1. A summary of the properties of the wavelength shifting fibres produced by BIRCON.

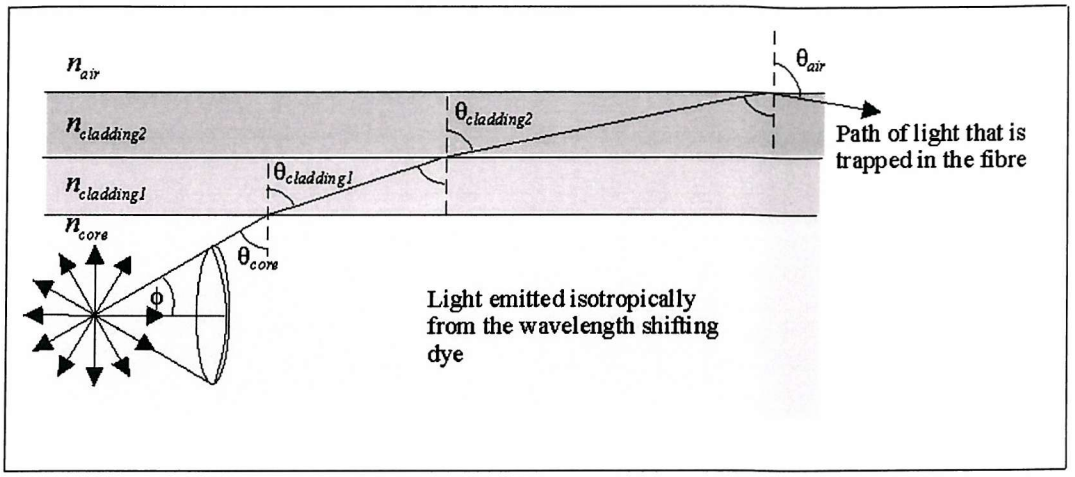

Figure B. 1. The path of light within a wavelength shifting fibre that has been trapped after being emitted by the dye.

Appendix C
Detector PCB Photographs

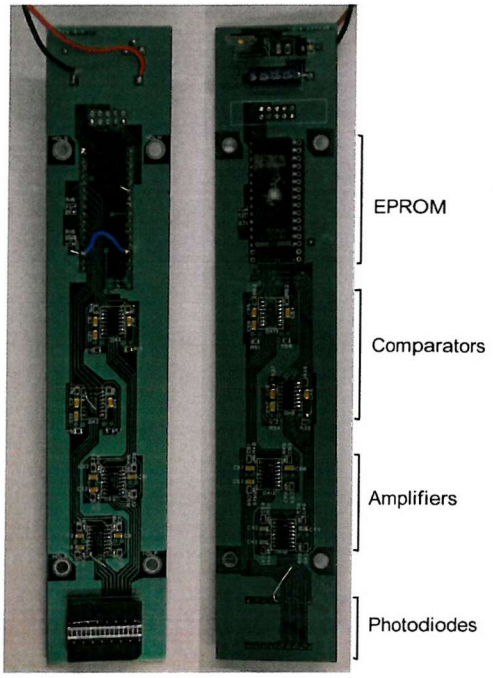

Figure C. 1. Initial test PCB for the Front End Electronics circuit. Front and back views.

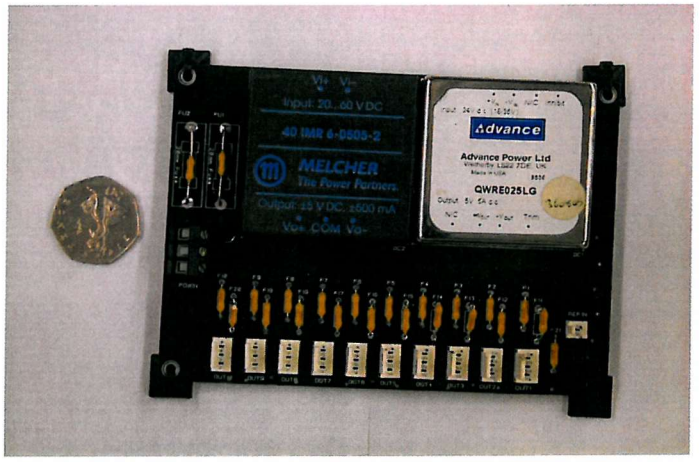

Figure C. 2. Power PCB. The detector requires four of these PCBs, one for each detector axis. This supplies 5V, 10V and a reference signal to ten Front End PCBs.

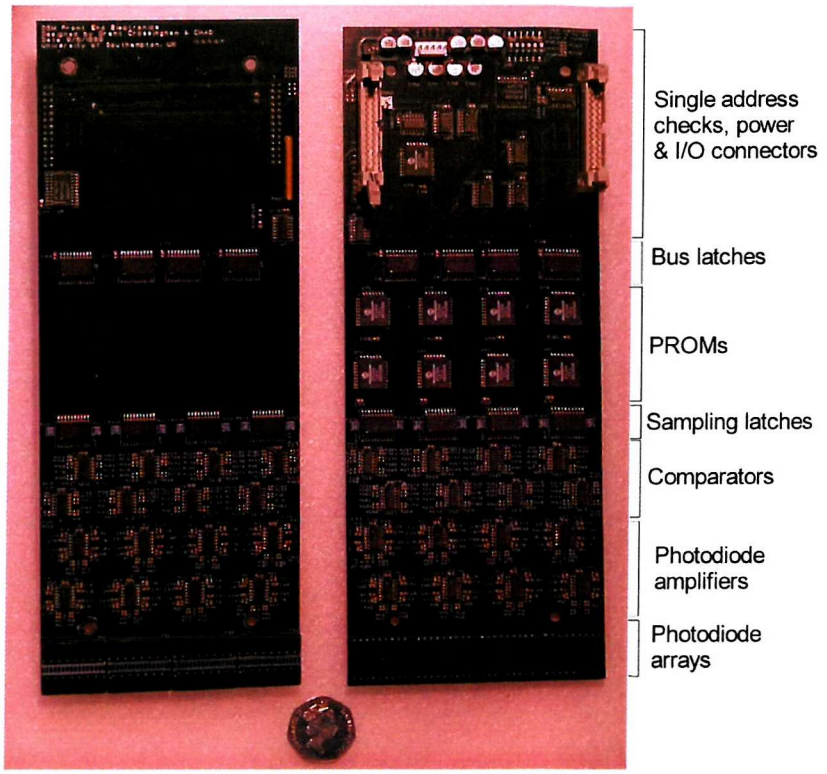

Figure C. 3. The Front End Electronics PCBs. Front and back views. Detector requires 40 of these PCBs, ten per axis.

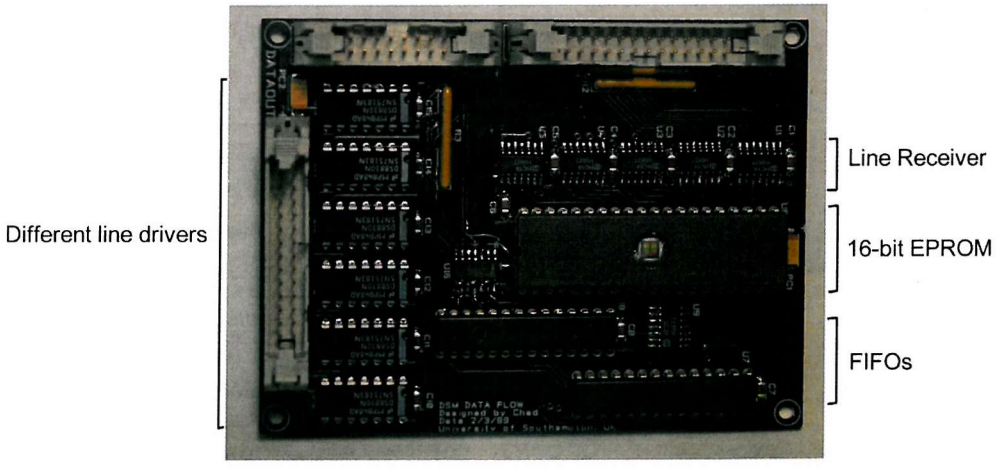

Figure C. 4. Data Flow PCB. The detector requires four of these PCBs, one for each detector axis. This receives data from the Front End Electronics PCBs and transfers it to the PC.

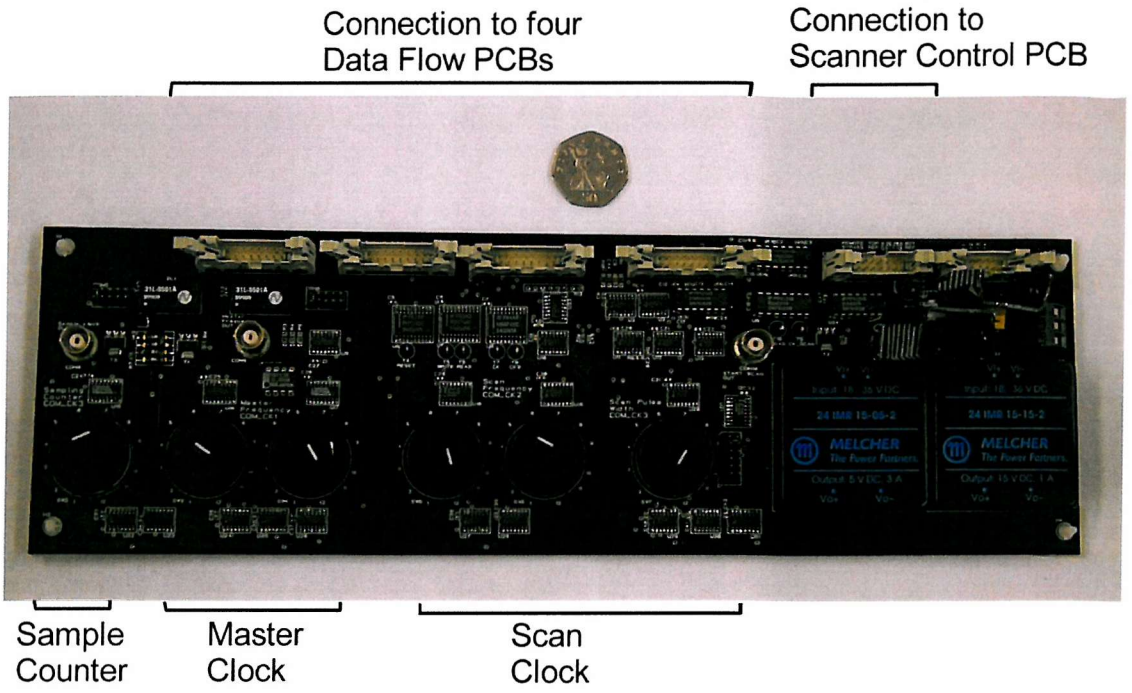

Figure C. 5. Command Board. This controls the timing of the whole instrument. The detector requires one of these PCBs.

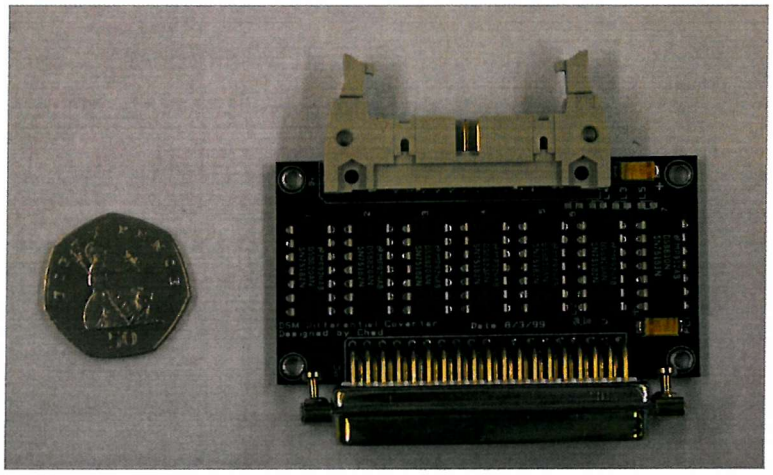

Figure C. 6. Differential line receiver PCB. This receives the beam position data from a Data Flow PCB. The detector requires four of these PCBs.

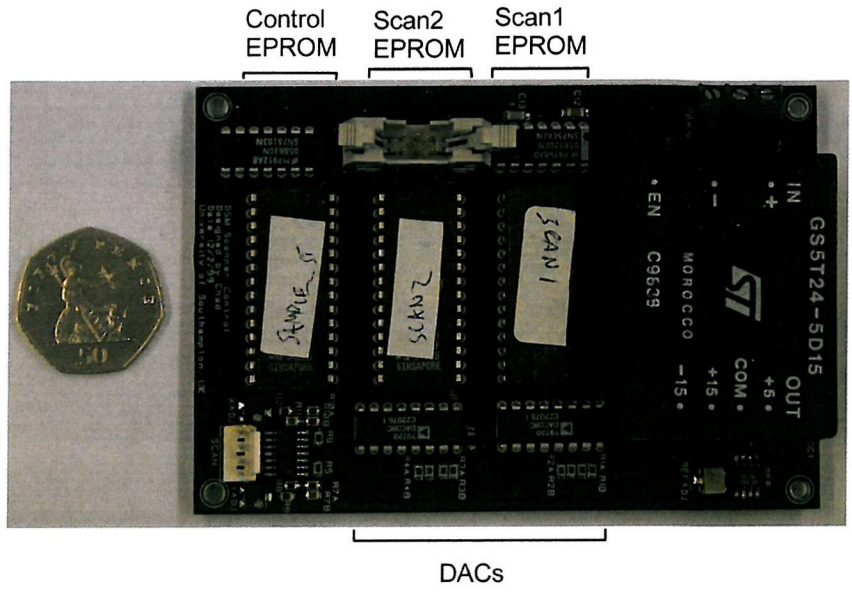

Figure C. 7. Scanner Control PCB. This controls the x and y scanners. The detector requires one of these PCBs

Appendix D
Beam Spread Calculations

When a laser passes through a curved surface every photon within the beam is refracted depending on the slope of that surface. Ideally the laser would be a point source so that the entire beam will pass through the same surface slope. However, the laser beam has a finite diameter and may therefore encounter a varying slope. This will cause different part of the laser beam to be refracted differently. This will cause the laser beams cross section to vary after passing through the surface. It is unclear whether the slopes present on the ocean surface will cause the beam to change shape significantly. Therefore, an investigation into how different size sinusoidal waves will spread the laser beam was carried out and is described in chapter 8. The sinusoidal wave used is described by,

$$W(x) = A_{\max} \cos kx \qquad \text{(D1)}$$

where A_{max} is the wave amplitude, k is the wave number given by $k = 2\pi/\lambda$ and x is the position along the wave. As the laser beam passed through the wave the difference in wave slopes between the rays within the beam will cause the beam to spread. The spread of the beam can be determined by calculating where each ray within the beam, intersects the detector layer. The majority of the time the outer most rays will intersect the detector layer with the greatest distance between them. However, this will not be the case as the beam passes the points of inflexion of the wave (points N, M, O and P). Here it is possible that the greatest difference in refracted rays is between an outer ray and a ray within the beam. Therefore, the position of each refracted ray, on the detector layer a distance h from the sea surface, was calculated. The spread of the laser beam was then the maximum distance between two rays incident on the detector layer. The geometry used to calculate the beam spread is shown in Figure D. 1. To calculate the spread of the laser beam given by $r_1 + r_2$ the slope of the wave through which each ray passes was first determined. The slope of the wave is the differential of equation D1, and is related to the wave slope angle in the following way:

$$\frac{dW(x)}{dx} = -kA_{\max} \sin kx = \tan\theta_s \qquad \text{(D2)}$$

where θ_s is the wave slope angle. To calculate the beam slopes θ_{b1} and θ_{b2} from the wave slope equation 3.2 is used. This equation is,

$$\theta_b = \sin^{-1}\left(\frac{n_a}{n_w}\sin\theta_s\right) - \theta_s \qquad \text{(D3)}$$

From this calculated beam slope, the position that each rays intersects the detector layer can be calculated using the following equation,

$$r_n = h\tan(\theta_b) - r_b \qquad \text{(D4)}$$

where r_n is the position of a particular ray in the beam. The two most extreme positions can then be used to calculate the beam spread. The position of the beam on the wave can then be moved and the beam spread calculated for all points on the wave. By varying the amplitude and wavelength of the sinusoidal waves, and the diameter of the beam, the plots in chapter 8 where generated.

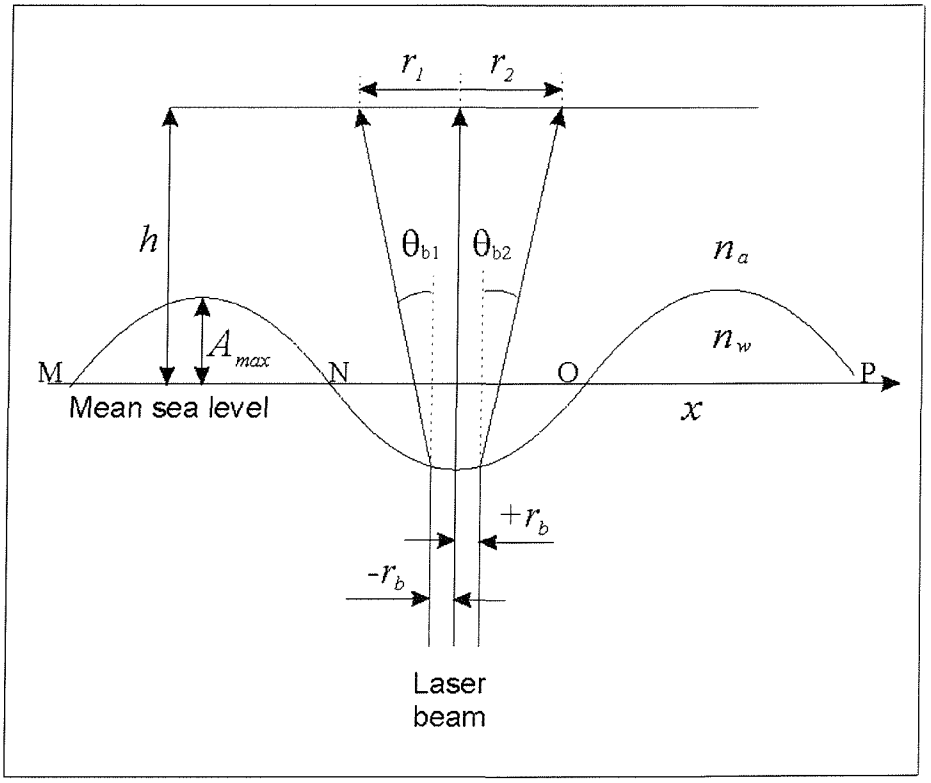

Figure D. 1. Geometry showing the spreading of a laser beam as it passes through a sinusoidal wave.

References

ADLink Technology Inc. 1998, 'NuDAQ, Data Acquisition Products, PCI-7200 PCI-Bus 32 Digital I/O',

Allmendinger E. E. 1990, 'Submersible vehicle systems design', Society of Naval Architects and Marine Engineers, Jersey City, N.J.

Amplicon 1997, 'Amplicon Liveline Catalogue, 1997', Amplicon Liveline Limited, Centenary Industrial Estate, Hollingdean Road, Brighton, East Sussex BN2 4AW, England.

ASF ERS-1 SAR: ' Image 20994200 Image description', Alaska SAR Facility - User Services, Geophysical Institute, University of Alaska Fairbanks, PO Box 757320, Fairbanks, AK 99775-7320 (web page)

Atakturk S. S. and **Katsaros K. B., 1987**, ' Instrinsic Frequency Spectra of Short Gravity-Capillary Waves Obtained From Temporal Measurements of Wave Height on a Lake', J. Geo. Res., Vol. 92, No. C5, P5131-5141.

Barber N and **Doyle D., 1956,** 'A Method of Recording the Direction of Travel of Ocean Swell', Deep Sea Res., Vol. 3, P206-213.

Bernd J. and **Schultz H., 1992**, 'Calibration and Accuracy of Optical Slope Measurements for Short Wind Waves', Optics of the Air-Sea Interface, Vol.1749, P222-233.

BICRON, 1991, 'BCF-91A "Green" Plactic WLS Fiber', Bicorn Corporation, 12345 Kinsman Road, Newbury, Ohio, United States.

Bowden K. F., 1983, 'Physical Oceanography of Coastal Waters', Ellis Horwood Limited, P90.

Cambridge Technology Inc., 'High Performance Optical Scanners, Model 6800, specification sheet', UK suppliers - Laser 2000, Wooton Grange, East Hunsbury, Northampton, NN4 0UA, England.

Churnside J. H., Hanson S. G., Wilson J. J., 1995 'Determination of Ocean Wave Spectra from Images of Backscattered Incoherent Light', Applied Optics, Vol. 34, No.6, P962-968.

Cote L. F., Davis J. O., Marks W., McGough R. F., Mehr W. J., Pierson Jr., Ropek J. F., Stephenson G. and **Vetter R. C., 1960**, 'The Directional Spectrum of a Wind Generated Sea as Determined from Data Obtained by the Stereo wave Observation Project' N. Y. Univ., New York, Meteorological Papers, Vol. 2, No. 6, P88

Cox C. and **Munk W., 1954**, 'Statistics of the Sea Surface Derived from Sun Glitter', J. Mar. Res., Vol. 13, P198-227.

Cox C., 1958, 'Measurements of Slopes of High-Frequency Wind Waves', J. Mar. Res., Vol. 16 , P199-224.

Crossingham G. J. 1996, 'TLS Prototype Development Plan', Internal document, Department of Physics, University of Southampton.

De Leonibus P. S., 1963, 'Power Spectra of Surface Wave Heights Estimated From Recordings Made From a Submerged Hovering Submarine', Ocean Wave Spectra, Prentice-Hall Inc., EngleWood Cliffs, N. J., P243-249.

Dobson E. B., 1970, 'Brief Reports – Measurements of the Fine Structure of the Sea', J. Geo. Res., Vol 75, No. 15, P2853-2856.

Farmer H. G., 1963, 'A Data Acquistion and Reduction System for Wave Measurements', Ocean Wave Spectra, Prentice-Hall Inc., EngleWood Cliffs, N. J., P227-233.

Ghataure H. S. and **Ramsden D., 1992,** 'Water Slopemeter Progress Report (Instrumentation)', Report from University of Southampton to the DRA, Contract 2040/509/RAE.

Gommenginger C., **Robinson I., Willoughby B. J.** and **V Taylor, 1998**, 'Experimental evidence during C-STAR of ocean roughness modulation over bathymety and its impact on sythetic aperature radar imagery in the coastal zone.' Fifth International Conference on Remote Sensing for Marine and Coastal Environments.

Hamamatsu, 1995, 'Large- Area PSD Series (Long-Area 1D PSD and 2D PSD)', Hamamatsu Photonics UK Limited, Lough Point, 2 Gladbeck Way, Windmill Hill, Enfield, Middlesex EN2 7JA, England.

Hamamatsu, 1996, '16-element Si Photodiode Arrays S5668 Series', Hamamatsu Photonics UK Limited, Lough Point, 2 Gladbeck Way, Windmill Hill, Enfield, Middlesex EN2 7JA, England.

Hecht E. 1987, 'Optics – Second Edition', Addision-Wesley Publishing Company, P110.

Hwang P. A. and **Shemdin O. H., 1988,** 'The Dependence of Sea Surface Slope on Atmospheric Stability and Swell Conditions', J. Geo. Res., Vol. 93, No. C11, P13903-13912.

Jähne B. and **Riemer K. S., 1990,** 'Two-Dimensional Wave Number Spectra of Small-Scale Water Surface Waves', J. Geo. Res., Vol. 95, No. C7, P11531-11546.

Jähne B., Waas S. and **Klinke J., 1992,** 'A Critical Review of Optical Techniques for Short Ocean Wave Measurements', SPIE Vol. 1749 Optics of the Air-Sea Interface, P204-215.

Jones W. L. Schoreder L. C. Boggs D. H. Bracalente E. M. Brown R. A. Dome G. J. Pierson W. J. and **Wentz F. J. 1982,** 'The SEASAT-A Satellite Scatterometer: The Geophysical Evaluation of Remote Sensed Wind Vectors Over the Ocean', J. Geo. Res., Vol. 87, No. C5, P3297-3317.

Keller W. C. and **Gotswols B. L., 1983,** 'Two-Dimensional Optical Measurements of Wave Slope', Applied Optics, Vol. 22, No. 22, P3476-3478.

Kinsman B., 1965, 'Ocean Waves, Their Generation and Propagation on the Ocean Surface', Prentice-Hall, Inc., Englewood Cliffs, N.J.

Lambda Research Corp., 1995, 'Guerapv, User Manual', Lambda Research Corporation, 80 Taylor Street, P.O. Box 1400, Littleton, MA 01460-4400.

Lange P. A., Jahne B., Tschiersch J., and **Ilmberger I., 1982,** 'Comparison Between an Amplitude-Measuring Wire and a Slope-Measuring Laser Water Wave Gauge', Rev. Sci. Inst., Vol 53, P651-655.

Laser 2000, 1996, 'Diode Pumped CrystaLaser', Laser 2000 (UK) Ltd,Britannia House, Denford Road, Ringstead.

Laser Scanning Products, 'Resonant Scanners, Series TRS, specification sheet', UK suppliers - Lasermet Vibrometers Ltd., Five Oaks, Sway Road, Brockenhurst, Hants, SO42 7RX, England.

Lincolin Laser Co., 'Polygonal Mirrors, specification sheet', UK suppliers - Laser Lines limited, Beaumont Close, Banbury, Oxon, OX16 7TQ, England.

Lincolin Laser Co., 'Scanner Motors, specification sheet', UK suppliers - Laser Lines limited, Beaumont Close, Banbury, Oxon, OX16 7TQ, England.

Lee C. G-Y., 1995, 'Design of a Towed Laser Slopemeter System for the Measurement of Short Scale Sea Waves', Ph.D. Thesis, University of Southampton, Southampton, U.K.

Lee P.H.Y., Barter J.D., Beach K.L., Hindman C.L., Lake B.M., Rungaldier H., Schatzman J.C., Shelton J.C., Wagner R.N., Williums A.B., Yee R. and **Yuen H.C., 1992,** 'Recent advances in ocean surface characterisation by a scanning laser slope gauge', Opt. Air-Sea Interface, SPIE Vol. 1749, P234-244.

Li Q., Zhao M., Tang S., Sun S. and **Wu J., 1993,** 'Two-Dimensional Scanning Laser Slope Gauge: Measurements of Ocean-Ripple Structure', Applied Optics, Vol. 32, No. 24, P4590-4596.

Liu H. T., Katsaros K. B., and **Weissman M.A. 1982,** 'Dynamic Response of Thin-Wire Wave-gauges', J. Phys. Geo. Res., Vol. 87, No. C8, P5686-5698.

Lobemeier P., 1981, 'A wire Probe for Measuring High Frequency Sea Waves', J. Phys. E: Sci. Instrum., Vol.14, P1407-1410.

Longuett-Higgins M.S., Cartwright D.E. and **Smith N. D., 1963,** 'Observations of the Directional Spectrum of Sea Waves Using the Motion of a Floating Buoy', Ocean Wave Spectra, Prentice-Hall Inc., EngleWood Cliffs, N. J., P111-136.

Longuett-Higgins M.S. and **Smith N. D. , 1983,** 'Measurement of Breaking Waves by a Surface Jump Meter', J. Geo. Res., Vol 88, No. C14, P9823-9831.

Macovsky M. S. and **Mechlin G. F., 1963,** 'A Proposed Technique for Obtaining Directional Wave Spectra by an Array of Inverted Fathometers', Ocean Wave Spectra, Prentice-Hall Inc., EngleWood Cliffs, N. J., P235-241.

Macdonald F. C. 1963, 'Radar Sea Return and Ocean Wave Spectra', Ocean Wave Spectra, Prentice-Hall Inc., EngleWood Cliffs, N. J., P251-257.

Martinsen R.J. and **Bock E.J. 1992,** 'Optical Measurements of Ripples using a Scanning Laser Slope Gauge Part I: Instrumentation and Preliminary Results', Optics of the Air-Sea Interface, SPIE Vol. 1749, P258-271.

McConnell A. 1981, 'Historical Instruments in Oceanography', Her Majesty's Stationary Office, Government Bookshops.

McGoldrick L.F. 1971, 'A Sensitive Linear Capacitance-to-Voltage Converter, with Application to Surface Wave Measurements', Rev. Sci. Instru., Vol. 42, No. 3, P359.

Melles Griot, 1994, 'Laser Instruments Guide', Melles Griot, Brookmount Court, Kirkwood Roa, Cambridge, CB4 2PF, England, P D6-3.

Melsheimer C. and **Gade M. 1998,** 'Rain Cells Over the sea Monitored by Synthetic Aperture and Weather Radars: A Comparison.' Proceedings OCEANS'98 IEEE Conference & Exhibition.

Moses W.W. Beuville E. and **Ho M.H. 1996,** 'Winner-Take- All IC for Determining the Crystal of Interaction in PET Detectors', IEEE Transactions on Nuclear Science, Vol. 43, No. 3, P1615-1618.

NEOS, 1995, 'Acousto-Optic Products Catalog', UK suppliers - Elliot Scientific Ltd., Gladstone Place, 36-38 Upper Marlborough Road, St. Albans, Herts, AL1 3US, England.

NE Technology, 'Scintillation Materials', NE Technology Limited, Bath Road, Beenham, Reading, Berkshire, England, RG7 5PR

Palm C. S., Anderson R. C. and **Reece A. M. 1977,** 'Laser Probe for Measuring 2-D Wave Slope Spectra of Ocean Capillary Waves', Applied Optics, Vol. 16, No. 4, P1074 -1081.

Pedersen J.P., Bauna T., Seljelv L.G., Landmark F., Enoksen R.T., Andersen J.H., 'Earth Observation - a Cost-effective Improvement for Oil Spill Monitoring' Tromsø Satellite Station, Tromsø, Norway, (web page).

Pickard G. L. and Emery W. J, 1990, 'Descriptive Physical Oceanography: An Introduction', Fifth Enlarged Edition, Pergamon Press, P26.

Pitt E.G. and Fortnum B. C. H. 1980, 'Progress in Wave Climate Studies at the institute of Oceanographic Sciences', Sea Climatology, Conference Interationale Pais, 3-4 October 1979, Technip, P191-205.

Prettyman C.E. and **Cermak M. D. 1969,** 'Time Variation of the Rough Ocean Surface and its Effect on an Incident Laser Beam', IEEE Trans. Geo. Elec., Vol. GE-7, No. 4, P 235-243.

Robert C.W. and **Melvin J.A., 1980,** 'CRC Handbook of Chemistry and Physics, 61st edition 1980-1981', CRC Press Inc., PE390.

Robinson I. 1985, 'Satellite Oceanography, an introduction for oceanographers and remote sensing scientists', Ellis Horwood Limited, P344.

Russell T. L. 1963, 'A Step-type Recording Wave Gage', Ocean Wave Spectra, Prentice-Hall Inc., EngleWood Cliffs, N. J., P251-257.

Scott J. C., 1974, 'Optical Probe for Measuring water Wave Slopes', J. Phys E: Scientific Instruments, Vol 7, P747-749.

Shaw J.A. and **Churnside J.H., 1996,** 'Ocean Ripple Statistics Measured with a Scanning-Glint Sensor', IEEE IGARSS 96, Vol. 2, P1328-1330.

Shemdin O. H. and **Hwang P. A., 1988,** 'Comparison of Measured and Predicted Sea Surface Spectra of Short Waves', J. Geo. Res., Vol. 93, No. C11, P13883-13890.

Shemdin O. H., Tran H. M. and Wu S. C., 1988, 'Directional Measurements of Short Ocean Waves With Stereophotography', J. Geo. Res., Vol. 93, No. C11, P13891-13901.

Stilwell D., 1969, 'Directional Energy Spectra of the Sea from Photographs', J. Geo. Res., Vol. 74, No. 8, P1974-1986.

Stolte S., 1994, 'Short-Wave Measurements by a Fixed Tower-Based and Drifting Buoy System', IEEE J. Oce. Eng., Vol. 19, No 1., P10-22.

Sturm G.V. and **Sorrell F.Y., 1973,** 'Optical Wave Measurement Technique and Experimental Comparison with Conventional Wave Height Probes', Applied Optics, Vol. 12, No. 8, P1928-1933.

Tang S. and **Shemdin O. H., 1983,** 'Measurements of High Frequencey Waves Using a Wave Follower', J. Geo. Res., Vol. 88, No. C14, P9832-9840.

Taylor V. J., 1996, 'Towed Laser Slopemeter Full Preliminary Data Analysis Report', DRA Report, DRA/CIS(CIS2/WP96012/1.0.

Thomas S. L. Seller P. and **Sharp P. H. 1995,** 'HX2: A 16-Channel Charge Amplifier IC for the Read-out of X-ray Detectors', IEEE Trans. Nucl. Sci., Vol 42, No 4, P830-834

Tober G., Anderson R. C. and **Shemdin O. H., 1973,** 'Laser Instrument for Detectoring Water Ripple Slopes', Applied Optics, Vol. 12, No. 4, P788-794.

Thomson-CSF Semiconducteurs Specifiques, 'CCD Products', Thomson Electronic Components Ltd., Unit 4, Cartel Business Centre, Stroudley Road, Basingstoke, Hants., RG24 OUG.

Tucker M.J., 1956, 'A Shipbourne Wave Recorder', Trans. Instn. Naval Arch., Vol. 98, No. 3, P236-246.

Tucker M.J., 1963, 'Recent Measurements and Analysis Techniques Developed at the National Institute of Oceanography', Ocean Wave Spectra, Prentice-Hall Inc., EngleWood Cliffs, N. J., P219-226.

Verboom G. 1980, 'The Interest of the Oil Industry for Physical Oceanography and Marine Meteorological Matters', Sea Climatology, Conference Internationale, Paris, 3-4 Octobre, 1979, P397-411.

Vesecky J. F. and **Stewart R. H. 1982,** 'The Observation of Ocean Surface Phenomena Using Imagery From the SEASAT Synthetic Aperture Radar: An Assessment', J. Geo. Res., Vol. 87, No. C5, P3397-3430.

Waas S. and **Jähne B., 1992,** 'Combined Slope-Height Measurements of Short Wind Waves: First Results from Field and Laboratory Measurements', Opt. Air-Sea Inter., Vol. 1749, P295-306.

Willoughby B. J., 1998, 'The Assessment of a Towed Laser Slopemeter for Measuring Short Scale Sea Surface Wave Slopes', Ph.D. Thesis, University of Southampton, Southampton, UK.

Wu J., 1971, 'Slope and Curvature Distributions of Wind-Disturbed Water Surface', J. Opt. Soc. Amer., Vol. 61, No. 7, P852-858.